UNIVERSITY OF CALIFORNIA SAN DIEGO

A survey of highly siderophile elements and incompatible trace elements in chondrites, and the implications for planetary feedstocks

A thesis submitted in partial satisfaction of the

requirements for the degree Master of Science

in

Earth Sciences

by

Nicole D. Phelan

Committee in charge:

Professor James M.D. Day, Chair
Professor Jeffery Gee
Professor Richard Norris

2018

The thesis of Nicole D. Phelan is approved, and it is acceptable in quality and form for publication on microfilm and electronically:

(Chair)

University of California San Diego

2018

DEDICATION

For the countless hours that went into creating this thesis, there were thousands of hours dedicated to me from family, friends and colleagues that led to the completion of the document you see before you today. To begin, I want to thank my parents for all the phone calls throughout college, your words and hard work inspire me to continue through any struggle I face. Although you tell me much of my strength comes "from within," the truth of the matter remains, that you both were and still very much are my role models of which I aspire to nearly every day.

A significant thank you is in order to the Scripps Isotope Geochemistry Lab group. First, thank you James for trusting me with so many special samples and having faith in my abilities to undertake such a large project on such a short timescale. Secondly, thank you to Ruan, I think as a lab manager, your job goes underappreciated much of the time. Your help in the early mornings and late at night when everyone else had gone home and I was still running samples meant a great deal to me, thank you. To the other lab members (especially Carrie and Jen), thank you for all taking my questions, helping me with various tasks and showing me that criticism can be one of the greatest tools for success if taken/used the right way. I would be lying if I didn't say I felt lost and confused for a good portion of this program, but you all helped to keep me motivated and on track.

The list is far too long for each individual friend I owe a thank you to, but below are a few individuals who stand out. The late night calls while you are driving home from work (Ali), the cards the last few weeks I was finishing my thesis (Maddy), the supportive texts and food/coffee that was bought for me (Aman, Aaron, Kathy, Amy, Mel, Grant, J-Bae…), the support you showed the few times I got to come home (Nikki, Kenna, Evan); all of it helped me reach this point. And to Lem, despite you not taking credit for the support you showed throughout my masters, this page would not be complete without your name on it. Thank you, from the bottom of my heart for everything you all do for me.

Finally, this thesis is dedicated to my grandma Mary Lou and great Aunt Sally, without whom I may not have had the opportunity to attend such a renowned college. Your belief in me and my future pushes me every day and while you may no longer be here in person, your love will always remain a part of me. Thank you for everything you have done for me and our family.

TABLE OF CONTENTS

LIST OF FIGURES

LIST OF TABLES

ABSTRACT OF THE THESIS

A survey of highly siderophile elements and incompatible trace elements in chondrites, and the implications for planetary feedstocks

by

Nicole D. Phelan

Master of Science in Earth Sciences

University of California San Diego, 2018

Dr. James M.D. Day, Chair

This study aims to better characterize highly siderophile element (HSE; Re, Os, Ir, Ru, Pt and Pd) and incompatible trace element abundances in meteorite sample from the carbonaceous, ordinary and enstatite chondrite classes to better understand their origins and histories. The sample suite of thirty-two chondrites was analyzed for bulk sample major- and trace-element compositions, oxygen isotope systematics, HSE abundances, and Re-Os isotope systematics. Mineral chemical compositions were also obtained for the Chelyabinsk ordinary chondrite meteorite that fell on Februrary 15th, 2013. The HSE abundances and Os isotope systematics measured in this study are useful tracers for nebular formation conditions, secondary parent body processing and terrestrial alteration. The HSE data paired with the Re-Os isotope systematics and major- and trace-element data allows for a distinction of these processes and their effects on different chondrite classes and individual samples. All Northwest Africa (NWA) chondrite meteorites measured in this study show mobility of the HSE, Re and Os, from terrestrial alteration. The absolute abundances of the HSE vary considerably between and within the

chondritic classes. However, some of these variations are shown to reflect heterogeneities within sample aliquots. HSE ratios (e.g., (Os, Ru, Pt, Pd, Re)/Ir) were therefore used as a means to distinguish nebular formation conditions for the chondrite classes. Mineral phases measured in Chelyabinsk give insights to parent body processing and its effects on sample mineral chemistry. Trace-element data on various phases suggest formation from ordinary chondrite precursors in the Chelyabinsk parent body, followed by equilibration, likely induced from shock metamorphism. Collectively, these results reveal significant differences in the degrees of terrestrial alteration, parent-body process and initial compositions within chondrite classes.

1. Introduction

Meteorites offer unique insights into the chronology of our Solar System, as well as fundamental understanding of how planetary bodies formed and evolved (e.g., Day, 2015). For simplicity, the Earth and other celestial bodies that we observe today, can be considered the products of three fundamental processes (White, 2015). The nucleosynthetic process, responsible for creating the elements, the accretion or formation of planetesimals, and the "intra-" and "inter-body" interactions that took place after their initial accretion. These complex processes eventually led to the construction of the major planetary bodies, such as Earth.

Nuclear Synthesis, which creates elements, is believed to have first started through the Big Bang Theory (Coc, 2009). Supported by observations and theoretical calculations, the Big Bang theory is considered the "birth" of the universe and centers around the concept that the universe is continually and rapidly expanding after a massive energy burst from a singularity nearly 14 billion years ago (e.g., Hubble & Humason, 1931; Penzias & Wilson, 1965; Olive et al., 2000; Lemaitre, 1931). Within seconds to minutes of the "Big Bang," while the universe was still extremely hot and dense, the lightest elements of H, He and Li are thought to have formed (Burles et al. 2001); He and Li are still being produced today through nuclear fusion in stars such as our own. As temperatures dropped in the universe, molecular clouds started forming from the gravitational attraction between tiny particles. Eventually, some molecular clouds formed dense enough regions that the cloud collapsed in on itself. During this collapse, the adiabatic temperature of the cloud increased. Gravitational potential energy was converted to the kinetic energy of the individual gas particles moving inward. Particles began crashing into one another, converting the kinetic energy into thermal energy, ultimately initiating the process of fusion within central stars (Bennett et al., 2007). The fusion process within stars, in a general sense, creates elements that are heavier than H, He and Li, but lighter than ^{62}Ni (e.g. Hoyle 1954, Käppeler 2007). When a star "dies," there is the potential, depending on the star type and size, that it will have a catastrophic ending with a supernova explosion. This high energy event is one of the various physical processes

that creates elements heavier than Ni (e.g. Seeger et al. 1965; Bethe 1996; Langanke et al., 2011).

Nucleosynthesis can be further broken down into various "processes," namely, the s-, r- and p- process. These processes create heavier isotopes, or variants of a single chemical element that differs by neutron number, through neutron or proton addition. Both the s- and r-process occur through neutron addition. The s-process, known as the "slow" neutron capture process, is thought to occur in massive stars with a significant neutron flux and is responsible from creating elements such as copper, silver, gold and zirconium (e.g. Chaisson & McMillan, 1999; Busso et al., 1999). For isotopes heavier than ^{209}Bi, the s-process will no longer work as a process to create heavier isotopes. Currently, it is thought that heavier isotopes at this stage, must be created from supernovae with the r-process, or "rapid neutron capture." The "layers" of the star, containing the heavier elements are thought to be blown off during the supernova explosion, providing the raw material of heavy elements to distant hydrogen cloud where new stars will eventually be formed (e.g. Chaisson & McMillan, 1999; Arnould & Takahashi, 1999; Meyer, 1994). Finally, the p-process, also known as "proton addition," is responsible for creating the rarer, proton-rich heavy isotopes that cannot be made through neutron capture (e.g. Arnould & Goriely, 2003; Meyer, 1994). The p-process is more poorly understood than the r- or s-process. The "sites" at which the p-process occurs and on what timescale is still debated, however, arguments have been made that it could occur in supernova (e.g. Meyer,1994; Woosley & Howard, 1978) or even in the hydrostatic oxygen burning phase of a star's life (e.g. Arnould, 1976). These processes described above are responsible for further complicating the compositions of the universe and our Solar System. Understanding the origins of various isotopes can help yield more information on processes occurring during the formation of our Solar System. This will be described in further detail in the following paragraphs.

The second process to discuss in Solar System history is the accretion of planetesimals. Astronomical observations and physical models have been used to understand the start of our Solar System. Through these studies, it has been shown that around 4.65 billion years ago,

the Solar System began from the collapse of a dense molecular cloud core made up of gas and dust (Yokoyama et al. 2016, Boss 2003) originating from diverse stellar environments, as described above. In the surrounding area of the newly formed Sun, particles began to accrete to one another, eventually forming planetesimals. Depending on the timing and area in which material was accreting, planetesimals likely varied in elemental and isotopic compositions (e.g. Keil, 1968; Meibom et al., 2001; Weisberg et al., 2001; Weisberg et al., 2006). Figure 1 shows the solar photosphere abundance versus chondritic elemental abundance (Anders &

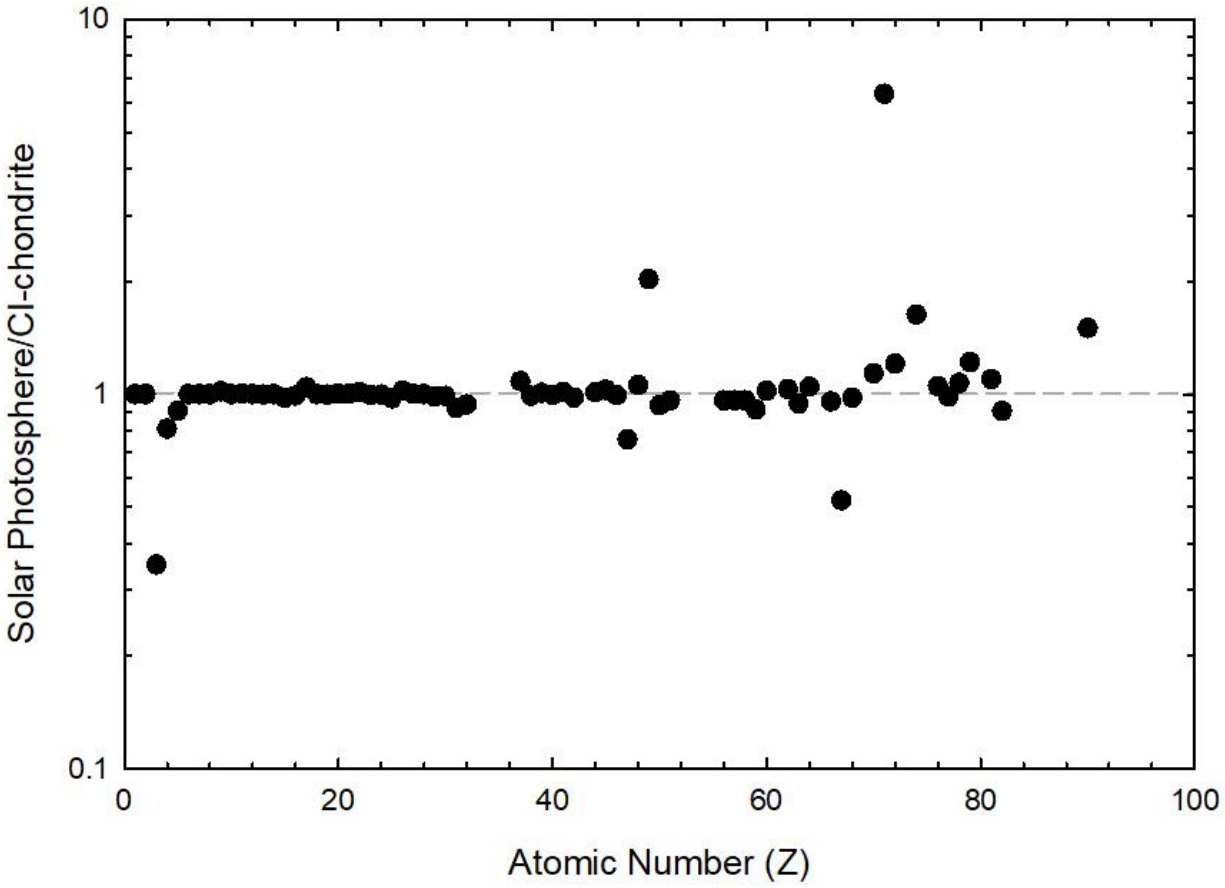

Figure 1. Comparison of solar photosphere and chondritic abundance of the elements. Plot uses log scale. Figure is modified from Anders & Grevesse, 1989. Data is from Anders & Grevesse, 1989.

Grevesse, 1989). With exception to some elements, chondrites generally show a similar composition to that of the solar photosphere. This leads to the interpretation that chondrites represent the bulk composition of the Solar System, having collateral implications to Earth's formation history.

As chondrites and planets formed from the same solar nebula as the Sun, it is expected that the bulk Solar System abundance (solar photosphere abundances) would be representative of abundances of elements in Earth. However, previous studies have shown that terrestrial materials have different isotopic compositions to that of the bulk Solar System (e.g. Boyet and Carlson, 2005). After reassessment, other studies have shown that Earth's composition is, in fact, chondritic and therefore representative of the bulk solar composition (e.g. Burkhardt et al., 2016; Bouvier and Boyet, 2016). Despite opposing findings, it is important to realize that it is likely that variations of isotopic and elemental compositions are affected during the accretion of the planetesimals and eventual planets, as well as during intra- and inter body interactions that occur after initial accretion. Understanding these processes then becomes an important part in understanding why we see the compositions we do today on our own planet and may potentially yield information on the existence of "missing reservoirs" (Day 2016) for some elements and isotopes.

Finally, "intra-" and "inter-body" interactions within and between accreted planetesimals further affected - and still affects - the compositions of materials throughout the Solar System. Intra-body interactions include melting events and differentiation, while inter-body interactions include high energy events, such as collisions between bodies (Corder, 2015). Examples of intra-body interactions include radiogenic heating, aqueous alteration and temperature and pressure variation with depth (e.g. Bogard, 2011). Shock metamorphism is an example of inter-body interactions, heat generated upon impact of one body against another will cause melting events (e.g. Bogert et al., 2003).

For this study, the focus is placed on undifferentiated chondrites, with special attention to the Chelyabinsk meteorite that fell on February 15th, 2013. Chondrites are important as chemically primitive and relatively unprocessed material from the early Solar System (Archer, 2014). Understanding the timing of their formation and the sources from which they are derived can yield important information about the formation of our Solar System as a whole. Various

geochemical characteristics of chondrites are analyzed in this study (mineral chemistry, oxygen isotopes, trace- and major-element abundances etc.) however, the emphasis of this thesis will be on the highly siderophile elements (HSE) and osmium isotopes.

The HSE (Re, Os, Ir, Ru, Pt, Rh, Pd and Au) provide insight into the sources of planetary materials in conjunction with the processing that led to the differentiated bodies that we observe today. The HSE include the Re-Os isotope system, a long-lived chronometer useful for constraining the timing of HSE formation and inter-element partitioning. The HSE are also important for understanding Earth history. The HSE partition into metal phases during metal-silicate equilibration, so they are expected to be sequestered into Earth's core. However, HSE abundances in the silicate Earth are much higher than predicted by metal-silicate partitioning experiments (Day et al., 2016b). These observations can be explained by a delivery of chondritic material to Earth after core formation.

This work examines chondrites from the three major classes (carbonaceous, ordinary and enstatite) to gain further understanding of the variability of the HSE between and within the classes. This variability is believed to be due, in part, to the diluting effect of the incorporation of variable amounts of volatile elements, but also to an inhomogeneous distribution of the HSE-bearing metal and sulphide phases (Day et al., 2016b). However, the degree and scale of the HSE abundance variability remains an open question. Having an improved understanding of the HSE variability between chondritic groups can yield information, not only, on the formation and secondary processes occurring in the earlier Solar System, but also what late accretionary material may have provided to create the terrestrial composition today.

2. Samples

A suite of thirty-two undifferentiated chondrites were examined in this study. Of these, fourteen are ordinary chondrites, fourteen are carbonaceous chondrites, and four are enstatite chondrites. Due to constraints of available mass, not all measurements could be performed on all samples. Thirty chondrites were measured for Re-Os isotopic compositions and highly siderophile element abundances, twenty-four were measured for trace and major element compositions and eight were measured for triple O isotope systematics. A polished thin section of the Chelyabinsk meteorite fall was used to determine major and trace-element mineral chemistry for the sample. Non-analytical characteristics of chondrites from this study are listed in Table 1.

Chondrites are, generally, ultramafic in composition and consist of components, such as chondrules, calcium-aluminum inclusions (CAIs) and matrix material. Chondrules, igneous particles that crystallize within minutes to hours, are the most abundant components of chondrites (Scott & Krot, 2007). CAIs are refractory inclusions produced through high-

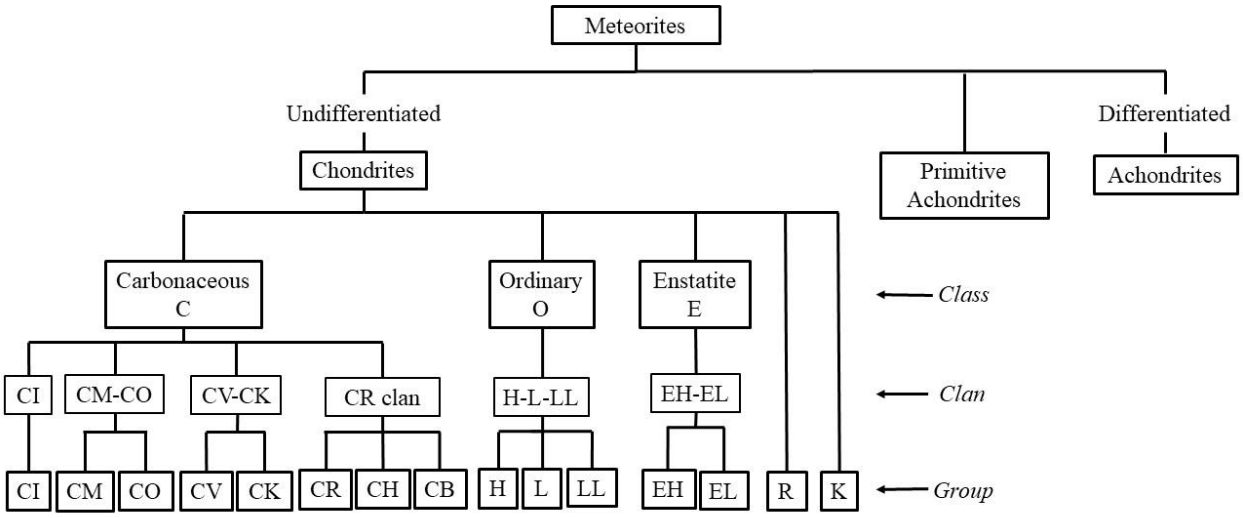

Figure 2. Diagram of meteorite classifications, showing major meteorite classes, clans and groups. Diagram after Weisberg et al. (2006).

temperature processes (e.g. condensation, evaporation). Chondrite matrices are diverse in their mineralogies, but are characterized by their fine-grained nature that fills the interstices between the various components, such as mentioned above (Scott & Krot, 2007). Collectively, meteorite

samples are classified under a class, then clan, then group (Figure 2 after Weisberg et al. (2006)) They are then further categorized by petrologic type, which is denoted by a number after the group letters. A description of some petrologic type characteristics can be found in Table 2, after Van Schmus & Wood, (1967).

Finally, chondrites can be classified as "falls" or "finds"; the latter referring to samples which have spent an unknown length of time on Earth's surface. In contrast, falls are samples which were collected almost immediately after their impact on Earth. The suite of samples analyzed in this study include both falls and finds.

2.1 Carbonaceous Chondrites

The class of carbonaceous chondrites are categorized by Mg/Si ratios that are similar to that of the solar value and oxygen isotope compositions that typically plot below the terrestrial fractionation line (TFL), where the TFL is representative of Earth's oxygen isotope composition (figure 3). From a petrologic point-of-view, separate clans within the carbonaceous class have varying chondrule sizes and matrix abundance within the sample (Weisberg et al., 2006). Within the suite of chondrites used in the study, Carbonaceous-Ivuna (CI), Mighei (CM), Karoonda (CK), Vigorano (CV) and Bencubbin (CB) types were analyzed.

CI chondrites are characterized as all belonging to petrologic type 1 (table 2), being the least melted or metamorphosed of all chondrites. The CI clan consists of hydrated chondrites, with matrices of fine-grained phyllosilicates and minor amounts of magnetite, sulfides, sulfates and carbonates (e.g., McSween and Richardson, 1977; Endress et al., 1996; Leshin et al., 1997; Weisberg et al., 2006). Chondrules and calcium-aluminum inclusions (CAIs) in CI chondrites are argued to either be composed of all matrix components or consumed, having their primary textures destroyed, during extensive hydrothermal alteration (Weisberg et al. 2006).

CM chondrites, or "Mighei-like" chondrites, generally contain small (~300µm) chondrules and CAIs that have either been completely or partially replaced by phyllosilicates (Weisberg et al., 2006). Most CM chondrites fall under the petrologic type 2, however, aqueous alteration varies extensively through this group (e.g., Weisberg et al., 2006; McSween, 1979; Browning et al., 1996). Materials like those in CM chondrite are commonly found as clasts in other chondrite groups, therefore, it has been suggested that CM chondrites had a wide distribution in the early Solar System (Zolensky et al., 1996).

The CK chondrite group ("Karoonda-like") generally contain large chondrules (700-1000µm) and a high abundance on matrix. Most CK chondrites, like the one measured in this study are of petrologic type 4-6. The high content of fayalite in the olivnes (Fa_{29-33}) of CK chondrites indicate oxidization (Weisburg et al., 2006). Depletions in moderately volatile elements in CK chondrites are greater than those in CV or CO chondrites and their abundances of refractory-lithophile elements as are between those of CV and CO chondrites (Kallemeyn et al., 1991).

CV chondrites ("Vigarano-like") have high abundances of matrix and large CAIs. Their chondrules are also large (~1 mm) (Weisberg et al., 2006). CV chondrites are all characterized as petrologic type 3; however, the diversity in the group comes from the subdivisions of oxidized (CV_{ox}) and reduced (CV_{red}), which are based on the model metal/magnetite ratios and the metal and sulfide content of Ni within the sample (McSween, 1977; Weisberg et al., 2006). Furthermore, various studies have shown that mineralogical differences between subgroups of the CV grouping are likely the result of varying degrees of late-stage alteration (Krot et al., 1998, 1995, 2003) suggesting that these secondary characteristics were "superimposed" onto various members of the CV group (Weisberg et al., 2006).

The CB ("Bencubbin-like") chondrite group is vastly different from other carbonaceous chondrite groups due to their extremely high metal abundances (60-80 vol.%), their significant depletions in moderately volatile-lithophile elements, as well as their enrichment in heavy N

isotopes (Weisberg et al., 2001). The CB chondrite measured in this study, Gujba, falls into the CB_a subgroup. CB_a chondrites have ~60 vol% metal and chondrules that are that are typically centimeter-sized (Weisberg et al., 2006). This groups' unique depletions, enrichments and overall abundances have been a source of contention for many studies. Some studies have interpreted their compositions to be sourced from highly primitive nebular materials consisting of metal that condensed directly from the solar nebula (Meibom et al., 2001; Weisberg et al., 2001; Campbell et al., 2001; Petaev et al., 2001; Krot et al., 2002; Weisberg et al., 2006). Other studies have suggested that these chondrites formed from a vapor cloud created from an impact on a chondritic planetesimal (Campbell et al., 2002; Kallemeyn et al., 1978; Weisberg et al., 2006).

2.2 Ordinary Chondrites

Ordinary chondrites - the most common class of chondrites, or of any meteorite type - are characterized by a high abundance of chondrules and low matrix abundances (10-15 vol.%). (Weisburg et al., 2006). Ordinary chondrites are also distinguished through oxygen isotope compositions that plot above the terrestrial fractionation line (figure 3) and Mg/Si ratios that are below the solar abundance ratio. (The Metrological Society, Meteoritical Bulletin Database). Ordinary chondrites are separated into the groups H, L, and LL by the metal abundance and variations of chondrule size (Weisberg et al., 2006). L and LL groups are considered to have "Low-Iron" and "Low-Metal" abundances, whereas the H group is representative of "High-Iron" samples (Krot et al., 2003). Previous studies have shown that in olivine grains, Co concentrations of kamacite versus fayalite display a break between H and L ordinary chondrites, but not between the L and LL groups (Rubin, 1990). Various studies have also shown that siderophile element abundances can be used to show variances between the LL, L and H groups (Kallemeyn et al., 1989; Sears et al., 1991; Weisberg et al., 2006). For this study ordinary chondrites from each group (H, L & LL) were studied.

2.3 Enstatite Chondrites

Enstatite Chondrites are characterized by their uncommon metal, sulfide and nitride phases that are absent within other chondrite groups. Iron-poor silicates and Si-bearing metal and various other elements (Mn, Mg, Ca, Na, K) that typically behave as lithophile elements in most meteorite groups, potentially behave as chalcophile elements within the enstatite group (Wiesberg et al., 2006). These unique mineral chemistries are considered to be due to formation under highly reducing conditions (Keil, 1968). This group is also defined by its oxygen isotope compositions which plot on the terrestrial fractionation line; the only chondrite group which does so (Clayton et al., 1984). Measured oxygen isotopes for the various chondrite groups can be found in Figure 3.

This study examined only EL chondrites. EL enstatite chondrites are distinguished from EH chondrites due to the characteristic alabandite (MnS) content as well as lower amounts of Si in their metals (<1 wt.%) (Lin & El Goresy, 2002; Weisberg et al., 2006). Both EH and EL groups range in petrologic grade (EH3 to EH5 and EL3 to EL6). Compared to EH3 samples, EL3 chondrites have higher abundances of enstatite (~66 vol.% versus ~63 vol.%) and more Ni-rich and Si-poor metal compositions (Krot et al. 2007, Weisberg et al., 2006). However, in this study, only EL6 samples were measured.

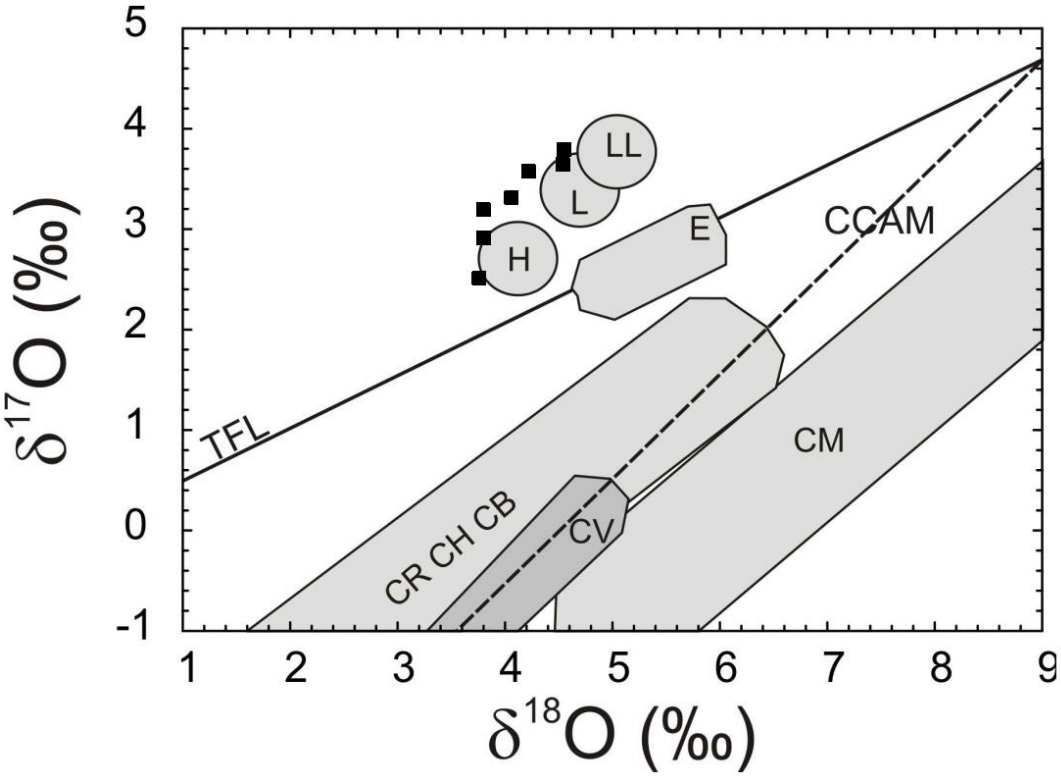

Figure 3. Oxygen isotope compositions of the various chondrite groups. Black squares represent ordinary chondrite measurements from this study, carbonaceous chondrites measurements from this study plot beyond the scale of this figure. TFL: Terrestrial fractionation line. CCAM: carbonaceous chondrite anhydrous mineral line. Figure compiled using data from Yurimoto et al. (2008), Clayton and Mayeda, (1999) and Clayton et al. (1984).

2.4 Ungrouped Carbonaceous Chondrites

There are various chondrites that fall at intermediate compositions between chondritic groups based on their characteristics and compositions. These samples are considered "ungrouped." In this study, two samples, Tagish Lake and NWA 5958, are considered as such. Tagish Lake has hydrously altered characteristics with two separate lithologies that have been altered to different extents (Zolensky et al., 2002). Tagish Lake has moderately volatile and volatile-lithophile elements abundances that fall between those in the CI and CM groups as well as similar siderophile and chalcophile abundances to CI and CM chondrites (Mittlefehldt, 2002; Friedrich et al., 2002).

NWA 5958 is classified as a C3.0 (Göpel et al., 2014). Recent studies have shown this sample to contain the lowest $\Delta^{17}O$ values of any carbonaceous chondrites measured so far (Bunch et al., 2011). The petrology of NWA 5958 shows well-preserved chondrules surrounded by multiple rims (Göpel et al., 2014). It has also been determined that the mesostasis of the sample has been affected by terrestrial weathering (Brunch et al., 2011).

3. Analytical Methods:

3.1 Electron probe micro-analysis (EPMA)

Thin sections of Chelyabinsk were prepared and polished at the University of Tennessee. Prior to analysis, a coating of carbon was added to prevent electrical charging from the electron beam. Major- and minor-element mineral compositions were measured using a *Cameca SX-100* electron probe micro analyzer at the University of Tennessee. Analyses were made using a beam size of 1µm and an accelerating potential of 15 keV. Standards were used in the calibration of the instrument as well as throughout the analysis to confirm data quality. See Day et al. (2015) for further detail on methods and techniques used in analysis.

3.2 Laser Ablation Inductively Coupled Plasma Mass Spectrometry (LA-ICP-MS)

Silicate, phosphate, sulfide and metal mineral phases of the polished thin section of Chelyabinsk were measured at the Scripps Isotope Geochemistry Laboratory using a *New Wave Research* UP213 laser ablation system coupled to a *Thermo Fisher Scientific* ICAP Qc ICP-MS. A 150 µm beam diameter was used for analysis spots with a laser repetition rate of 5 Hz. Within the 3 cm^3 ablation cell in which the analysis took place, He-gas was flushed to enhance the transport and production of a fine aerosol which was then mixed with an Ar carrier-gas (~1 L/min) before reaching the plasma. Data collection occurred over a period of ~60 s with a washout time of >120 s between each analysis. Time-resolved mode was used to account for mineral zoning, inclusions and possible underlying phases in the thin section. For further details on the methodology see Day et al. (2017).

3.3 Whole-rock sample preparation

Whole rock fragments of samples were powdered with limited force using a cleaned agate mortar and pestle. All tools used during preparation of samples were thoroughly cleaned with 18.2 Ω MQ water and a small amount of ultrapure quartz sand between each sample to avoid cross-contamination. Powders were then placed in small labeled vials (precleaned with 1N HCl and 18.2 Ω MQ water and dried), and left until sample weighing steps.

3.4 Trace and major element analysis

Samples (including blanks and terrestrial standards) were digested using Teflon Paar bombs or Teflon vials at the SIGL. Sample powders placed in Teflon Paar bombs were digested at 180°C in Optima grade HF (4 mL) and HNO_3 (1 mL) for ~72 hours in a processing oven. After this initial digestion step, samples were sequentially dried and then taken up in concentrated HNO_3 to remove fluorides (Day et al. 2017). For samples digested using the conventional 7 mL Teflon vials, HNO_3 (750 µL) and HF (3 mL) were added before setting the sealed vials on a hotplate at 150°C for 5 days. Samples were then sequentially dried down and then taken up in HNO_3 (1 mL) before being placed on the hotplate again for 24 hours at 140 °C. Finally, samples were dried down and placed aside until preparation for trace and major element analysis.

Sample stock solutions were prepared by adding 1 ml of Teflon distilled nitric acid (HNO_3), 1 ml of indium (In) spike and 3 ml of 18.2Ω MQ water to each dried down sample. Prepared stock solutions were then sealed and placed on a hot plate at 60°C for 3 days. On the day of analysis, 500µl of the prepared solution was added to clean centrifuge tubes. 10 ml of 2% nitric acid was then added to each of the centrifuge tubes to dilute the sample to measure the trace elements of interest. Trace element abundances were measured using a *ThermoScientific* iCAP Qc quadrupole inductively coupled mass spectrometer (iCAP-ICPMS Qc) in normal mode.

To measure major elements of interest, 1 ml of solution was aliquoted from each of the centrifuge tubes after trace elements analyses were completed. After discarding the remaining liquid in the centrifuge tube, the 1 ml was returned to the tube and 9 ml of 2% nitric acid was added to dilute the sample by a factor of 9. The centrifuge tubes containing the new dilutions were then measured using the iCAP-ICPMS Qc.

All major and trace element abundance measurements were corrected for diluent blank, drift using In, and the sample weight, before being corrected for abundances to the reference material BHVO-2. Additionally, the reference material BCR-2 and an equilibrated ordinary

chondrite were analyzed as “unknowns” to track potential instrument drift as well as gauge the accuracy and reproducibility of the measurements. The reproducibility of trace elements in the reference material BHVO-2 was generally better than 4 to 9% (RSD) excluding Pb (17%), Te (15%), Mo (24%), and Se (11%). For major elements the reproducibility of the reference material was better than 2 to 3% (RSD), except for P (7%).

3.5 Oxygen isotope analysis

Oxygen isotope analysis was conducted at the Institut de Physique du Globe-Paris following the methodology outlined in Day et al. (2015) and Rumble et al. (1997). Silicate grains were separated using alcohol in a tungsten-carbide mortar and pestle. Weathering products were removed from the sample materials using ultra-sonication for 240 s, at room temperature, within a dilute HCl solution, before being washed with ultrapure water and dried down. Nonmagnetic fractions were separated out and measured using laser fluorination. The standard, San Carlos olivine was measured before the chondrite samples to ensure accuracy and reproducibility of measurements. The standard, UWG-2 garnet from the Gore Mountain mine, Adirondack Mountains, New York (Valley et al., 1995) was measured after every two to four samples to check for instrument drift.

Near the end of the oxygen isotope analytical campaign, the glass apparatus that transfers sample material to the mass spectrometer failed. A fix was made to complete sample analysis, using an ultra-torr vacuum fitting. Ten runs were completed with this setup including runs on the samples Allende, Chelyabinsk (without fusion crust) and Murchison MTF 2005. Due to the issue of whether the measurements with this setup are reproducible, they have been discarded from the final data set. There is no publishable oxygen isotope data of the Murchison MTF 2005 sample due to the improvised fix, however, all the other samples were analyzed at least once before the incident (Corder, 2015).

Oxygen isotopes are typically expressed in δ units. These units are deviations in per mil (‰) in $^{17}O/^{16}O$ and $^{18}O/^{16}O$ ratios from the standard mean ocean water (SMOW) (Yurimoto et al. 2008): $\delta^{17,18}O_{SMOW}=[(^{17,18}O/^{16}O)_{sample}/(^{17,18}O/^{16}O)_{SMOW}-1] \times 1000$, where $^{17}O/^{16}O_{SMOW} = 0.0003829$ and $^{18}O/^{16}O_{SMOW} = 0.0020052$ (McKeegan & Leshin, 2001). The $\Delta^{17}O$ value was then calculated from the δ values. This value represents deviations from the terrestrial fractionation line (TFL) in per mil using the equation: $\Delta^{17}O_{SMOW} = \delta^{17}O_{SMOW} - 0.5241 \times \delta^{18}O_{SMOW}$ (Criss & Farquhar, 2008). The $\delta^{18}O$ values were normalized to the UWG-2 garnet with δ18O= <0.03‰. 2 SD (‰) uncertainties of the two standards were ± 0.09 for $\delta^{17}O$, ± 0.17 for $\delta^{18}O$ and -0.004 ± 0.018 for $\Delta^{17}O$ (2σ, n = 18). Uncertainties for the remainder of the individual sample measurements were <0.07‰ for $\delta^{17}O$, excluding an individual run of Peace River and Kunashak and <0.04‰ for $\delta^{18}O$ excluding an individual run for Murchison.

3.6 Highly siderophile element analysis

For highly siderophile element abundance and osmium isotope analysis, borosilicate Carius tubes were used for sample digestion (Carius, 1865). Powdered samples were transferred into Carius tubes with an appropriate amount of isotopically enriched spike (^{99}Ru, ^{106}Pd, ^{185}Re, ^{190}Os, ^{191}Ir, ^{194}Pt) and ~6 mL of Teflon distilled 12N HCl (2.5 mL) and 15.7N of HNO_3 (3.5 mL) purged of Os and Teflon distilled, before sealing the Carius tubes and placing them in metal jackets. Samples were digested for 72 hours at ~240°C in an oven.

The HSE were separated from bulk samples using a solvent extraction and anion exchange column procedure outlined in Day et al. (2016a). Osmium was separated from the other HSE in samples using solvent extraction in CCl_4 and then back extraction into HBr (Cohen and Waters, 1996). The fraction of HCl-HNO_3 solution remaining from the samples was then dried down and re-dissolved in 1M HCl. Once samples were equilibrated, cleaned Bio-Rad AGI X8 (100-200 mesh) exchange resin was used to separate the fractions of Re-Pt-Ir-Ru in ~8 mL of 15.7N TD HNO_3 and the Pd fraction in ~7 mL of warm 12M HCl. Each of these fractions were then dried down before analysis using a *Cetac* Aridus II Desolvating Nebulizer coupled to a *ThermoScientific* iCAPq C ICP-MS at the SIGL.

Total analytical blanks (TABs) had HSE concentrations lower than those of the samples by a factor of ~10,000 on average with 1SD (0.000125) and 2SD (0.00025).

3.7 Osmium isotope analysis

Osmium was separated from the other HSE through solvent extraction into CCl_4 and back-extraction into HBr. These samples were then further purified using micro-distillation of the Os into HBr from a dichromate solution in H_2SO_4 (see Roy-Barman, 1993). Purified Os cuts were then measured using negative ions on the Thermo Scientific Triton TIMS at the SIGL.

Total analytical blanks (TAB) for Os isotope analysis measured $^{187}Os/^{188}Os$ ratios of 0.183 (0.006σ) for TAB 1, 0.250 (0.009σ) for TAB 2 and 0.40 (0.01σ) for TAB 3.

4. Results

4.1 Mineral compositions of the Chelyabinsk chondrite meteorite fall

4.1.1 Major element mineral chemistry

Major mineral phases present in the Chelyabinsk polished thin section that we analyzed include olivine grains with a relatively constant forsterite content ($Fo_{71.0\pm0.4}$; n = 128), Na-rich plagioclase ($An_{11\pm2}Ab_{83\pm4}$; n = 60), low-Ca pyroxenes ($Wo_{1.4\pm0.3}En_{74.6\pm0.4}Fs_{24\pm0.4}$; n = 156), high-Ca pyroxenes ($Wo_{45.1\pm0.9}En_{46.4\pm0.5}Fs_{8.5\pm0.9}$; n=55), Cr-Spinel (Cr# = 79.5, where Cr# = Cr/(Cr+Al) × 100; n = 35), Cl-rich apatite (5.35 ± 0.40 wt.%; n = 79), and MgO-rich merrillite (3.61 ± 0.07 wt. %; n = 32). A single orthoclase grain of $Or_{84}An_{7}Ab_{9}$ (n = 1) was measured, and ilmenite (n = 6), troilite (n = 12), kamacite (n = 1) and taenite (n = 2) all occur in the sections. The major element mineral chemistry for Chelyabinsk can be found in Table 4.

4.1.2 Trace element mineral chemistry

Various components and mineral phases were measured for trace element abundances in Chelyabinsk using LA-ICP-MS, including, fusion crust (n = 4), chondrule fragments (n = 4), individual grains of olivine (n = 4), low Ca-pyroxene (n = 8), plagioclase (n = 1) and a phosphate (n = 1) in the matrices. The trace element mineral data can be found in Table 5. Figure 4 shows the incompatible trace element patterns and rare earth elements patterns (REE) for the different mineral phases found in Chelyabinsk.

The phosphate shows, overall, the greatest enrichment in incompatible trace elements relative to CI-chondrite Orgueil, however, there are relative depletions of Rb, Nb and Zr within this phase. The phosphate grain's REE pattern (Figure 4b.) show a depletion in Eu relative to the other REE, which agrees with previous studies of REE patterns in chondrite phosphates (Jones et al., 2014) although the phosphate is far more enriched in all the REE than samples measured within that previous study.

Plagioclase shows the second greatest enrichment of incompatible trace and rare earth elements of the phases and components measured. The plagioclase shows a relative depletion in the most incompatible elements, with increasing abundance in the less incompatible elements. The plagioclase REE pattern has a slight enrichment in Eu, which again, is consistent with previous studies of ordinary chondrite mineral phases (Allen & Mason, 1973) although the measurement from my study shows an enriched by a factor of ~10.

The chondrule measurements show a significant enrichment in U and smaller enrichments in Th, Nb, Ta, Zr and Hf compared to the rest of the incompatible trace elements measured in the sample. The REE pattern for the chondrule is relatively flat. Mesostases in type 1 chondrules measured in Jacquet et al. (2015) displayed similar patterns as observed in this study.

Both the low-Ca pyroxene and the fusion crust have similar incompatible trace element and REE patterns. The only elements from the two patterns that show a notable difference are Th and Eu (Figure 4). Both components show a minor decrease in abundance of elements from Nb to Nd and an increase in abundance from Dy to Lu (Figure 4a.). The low-Ca pyroxene from this study follows similar REE trends as seen in low-Ca pyroxene chondrules from Jacquet et al. (2015), although the phase from this study is, again, enriched by a factor of ~10.

Lastly, the olivine is shown to be the most depleted in incompatible trace elements and the REE of all the components and phases measured in Chelyabinsk. Relative to other incompatible trace elements in the sample, the olivine is enriched in Nb, Ta and Zr. Previous studies have shown a slight, but visibly distinct, trend in abundance of REE from La to Lu, however, no visible trend is distinguishable in the data collected in this study (Jacquet et al., 2015). For the olivine measured in this study, REE La to Nd are enriched by a factor of ~10, while the remainder of the REE show comparable results to those of Jacquet et al. (2015).

REE patterns in the Chelyabinsk minerals reflect compatibility of the phases. Figure 4b shows a positive Eu anomaly in the plagioclase with a corresponding negative Eu anomaly in the phosphate. The REE pattern of the fusion crust displays evidence for little incorporation of phosphates and plagioclase. Finally, the bulk chondrule falls in the middle of the phases suggesting compositions of multiple mineral phases within chondrules of the sample (e.g. olivines, pyroxenes).

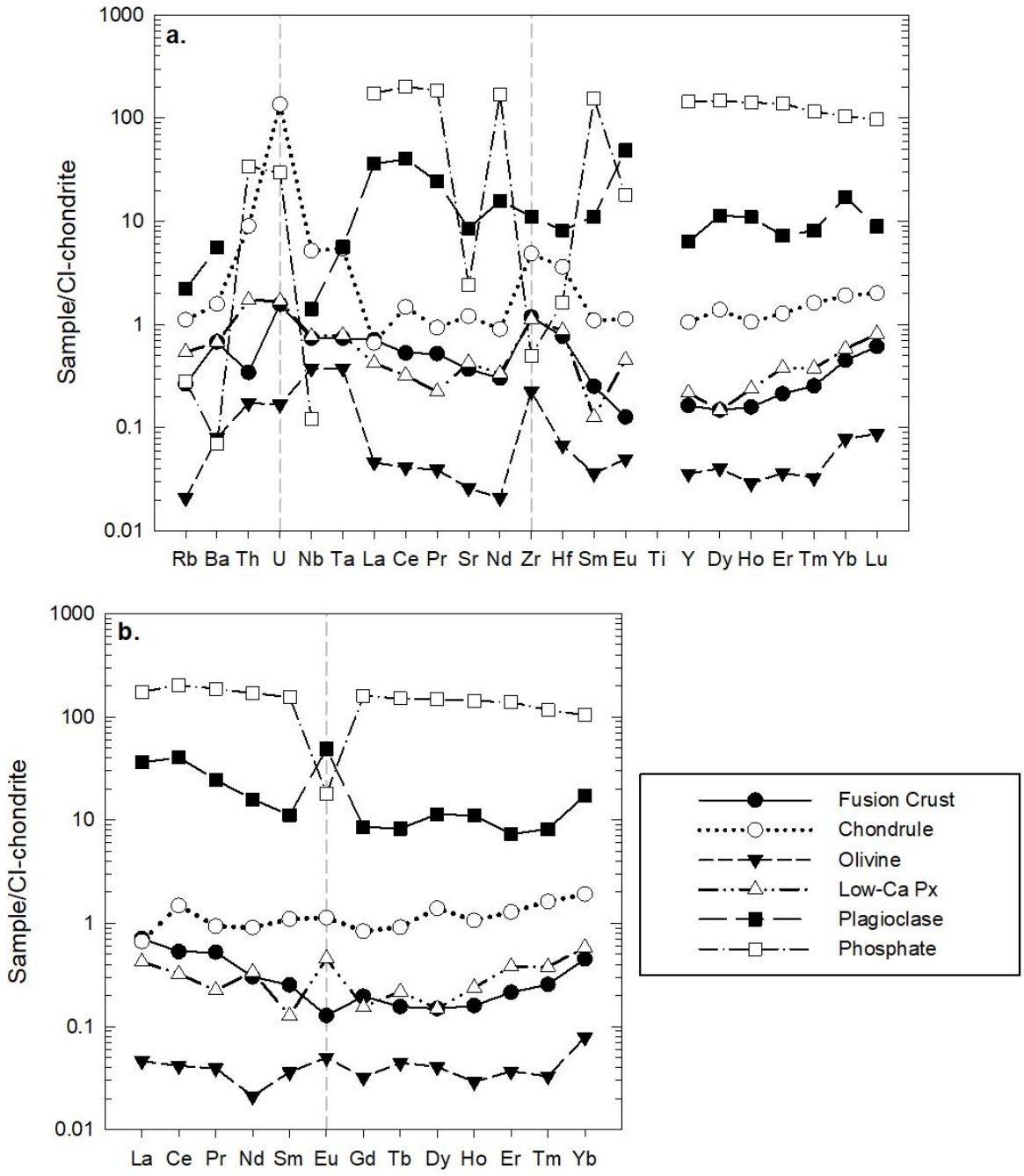

Figure 4. a. Incompatible trace element patterns in Chelyabinsk mineral phases, Fusion Crust (n = 4), Chondrule (n = 4), Olivine (n = 4), Low-Ca Pyroxene (Px) (n = 8), Plagioclase (n = 1) and Phosphate (n = 1). b. Rare earth element patterns for the same mineral phases mentioned above. All data is normalized to CI-chondrite Orgueil from Barrat et al. (2012).

4.1.3 Chelyabinsk HSE abundances

Chelyabinsk was measured for HSE abundances multiple times in this study in order to see potential variations that could exist between separate sample aliquots. As seen in Figure 5, abundances of the HSE between the Chelyabinsk sample without fusion crust differ, on average, by a factor of ~0.5, excluding Re and Pd concentrations, from HSE concentrations within the Chelyabinsk sample with fusion crust. This distinction indicates variations in absolute HSE abundances within separate aliquots and fragments of the Chelyabinsk meteorite. The bulk sample measurements of Chelyabinsk show similar HSE patterns, however the measurements differ by a factor of ~0.5. This difference shows, further, the variability among sample aliquots.

HSE abundances were also measured in Chelyabinsk metals using LA-ICP-MS (Table 3). From these data, it is shown that two groups of metals exist within the Chelyabinsk chondrite (Figure 6). Type-1 and Type 2 metals are similar in their HSE abundances, however, Type-2 shows a depletion in Pd and Au. Previous studies have shown that high Ni-metals tend to contain high Cu, Pd and Au relative to low-Ni metals while refractory platinum group elements (PGEs)

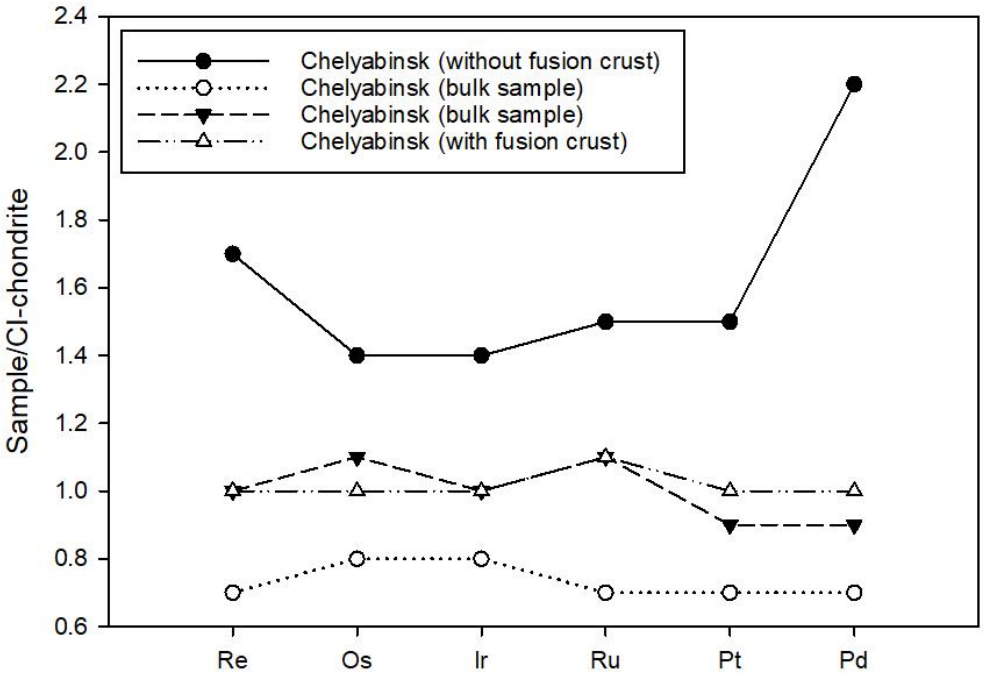

Figure 5. HSE abundances in various Chelyabinsk sample aliquots from this study. Samples normalized to Orgueil from Day et al. (2016b).

remain nearly unfractionated between high and low-Ni metal groups (Campbell and Humayun 2003).

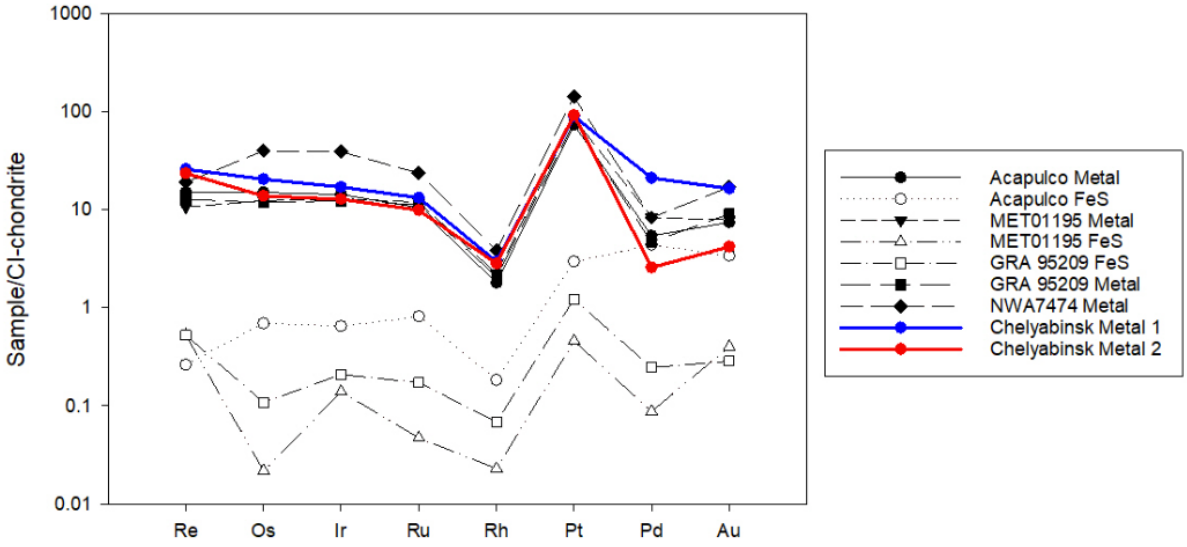

Figure 6. HSE abundances of Chelyabinsk metals, Type-1 (n = 5) in blue and Type-2 (n = 3) in red. Acapulco, MET01195, GRA95209 and NWA7474 metal and FeS abundances from Dhaliwal et al. (2017).

4.2 Bulk sample major element compositions

Major element compositions for bulk chondrite samples can be found in Table 6. The weight % of oxide components can be found in Table 7 along with Mg/Si, Al/Mg, Ca/Al and Fe/Mg ratios for the samples. Figure 7 shows the Mg/Si versus the Fe/Mg ratios for chondrites measured in this study. As seen in the figure, carbonaceous chondrites show a greater spread of Mg/Si ratios. The Allende (CV3), GRA0610 (CV3) and Maralinga (CV3) samples all fall further to the right on the plot than the C2 and CM2 samples, suggesting on average, that lower petrologic grades of carbonaceous chondrites have distinct Mg/Si ratios. The ordinary chondrites measured show variations in both Mg/Si and Fe/Mg ratios, however, there is greater variation in the Fe/Mg ratios. This makes sense given the groupings or ordinary chondrites are determined by metal content (LL, L, H). Pultusk (H5) shows the highest Fe/Mg (2.585) and Mg/Si (0.864) ratios of the ordinary chondrites. The enstatite chondrites show the least spread in Mg/Si data, however, their Fe/Mg ratios vary far more. Khaipur (EL6) has the highest Fe/Mg ratio (2.327) from the Enstatite group.

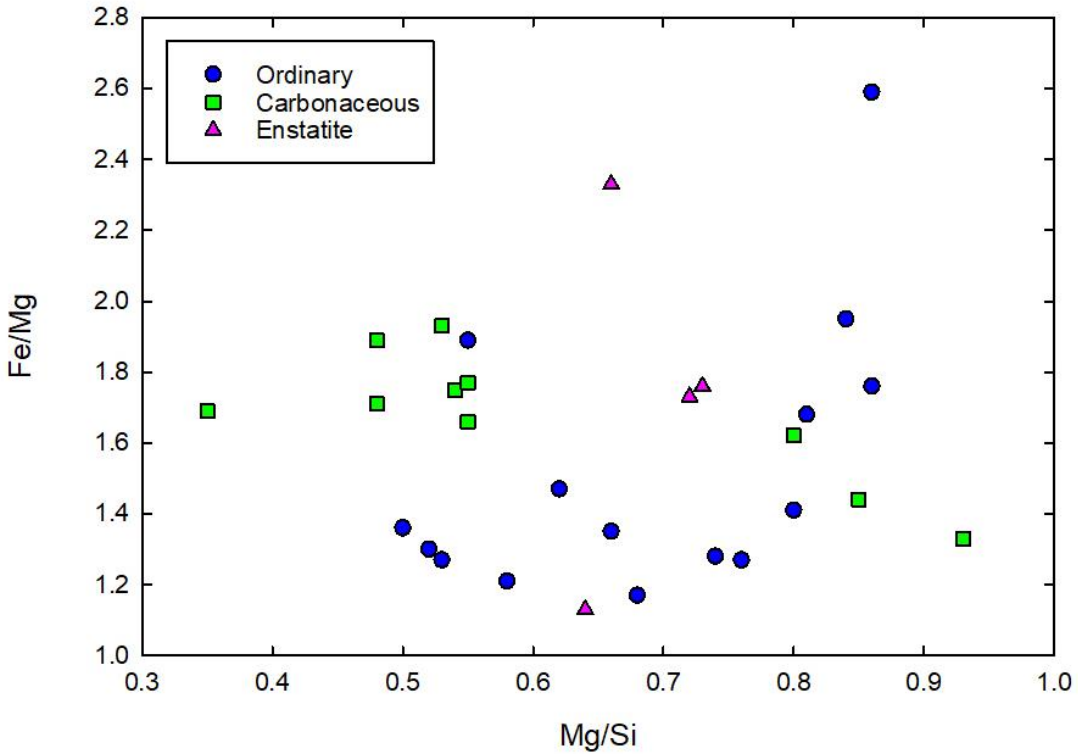

Figure 7. Mg/Si versus Fe/Mg ratios for chondrites in this study. Blue circles are ordinary chondrite ratios, green squares are carbonaceous chondrite ratios and pink triangles are enstatite chondrite ratios.

4.3 Bulk sample trace element chemistry

Trace elements and REE in the following sections have been normalized the Barrat et al. 2012. In general, there are anomalies for Zr, Hf and Th for multiple samples. These enrichments are likely due to incomplete dissolution of Zircons from the chondrite in the Barrat et al. 2012 study, which was used to normalize my data to. Therefore the enrichments seen in the figures are not necessarily representative of anomalies from samples within my dataset.

4.3.1 Incompatible trace elements in carbonaceous chondrites

The incompatible trace element patterns for the different groups of carbonaceous chondrites can be found in Figure 8. In general, most samples within each group (C2, CK4, CV3, CM2) show a depeletion in Rb while the remaining incompatible trace elements are slightly enriched relative to CI-chondrite Orgueil. For the $C2_{ung}$ chondrites, Tagish Lake and NWA 5958, both samples show a slight enrichment of Zr. NWA 5958 also shows enrichments in Ba, U and

Sr relative to CI-chondrite Orgueil. Excluding Rb, Maralinga ($CK4_{an}$) shows greater enrichments in the more incompatible elements (Ba-Zr), with the greatest enrichments in Ba, Ce and Sr. GRA 06101 (CV3) has enrichments in Th and Zr; similar to other carbonaceous chondrites, it also shows a depletion in Rb. Allende UCSD 142 (CV3) generally follows previous measurments (Allende – *Literature*), although it shows a relatively high enrichment of La and Ce. From the CM2 samples, Murray shows the most significant enrichment of incompatible elements of all the carbonaceous chondrites measured. Both Murchison samples show an enrichment in Th, however, the Murchison fragment shows far more variability in its measurments of incompatible elements. Enrichments also occur in Ba, U, Zr, Hf, Ti and Lu.

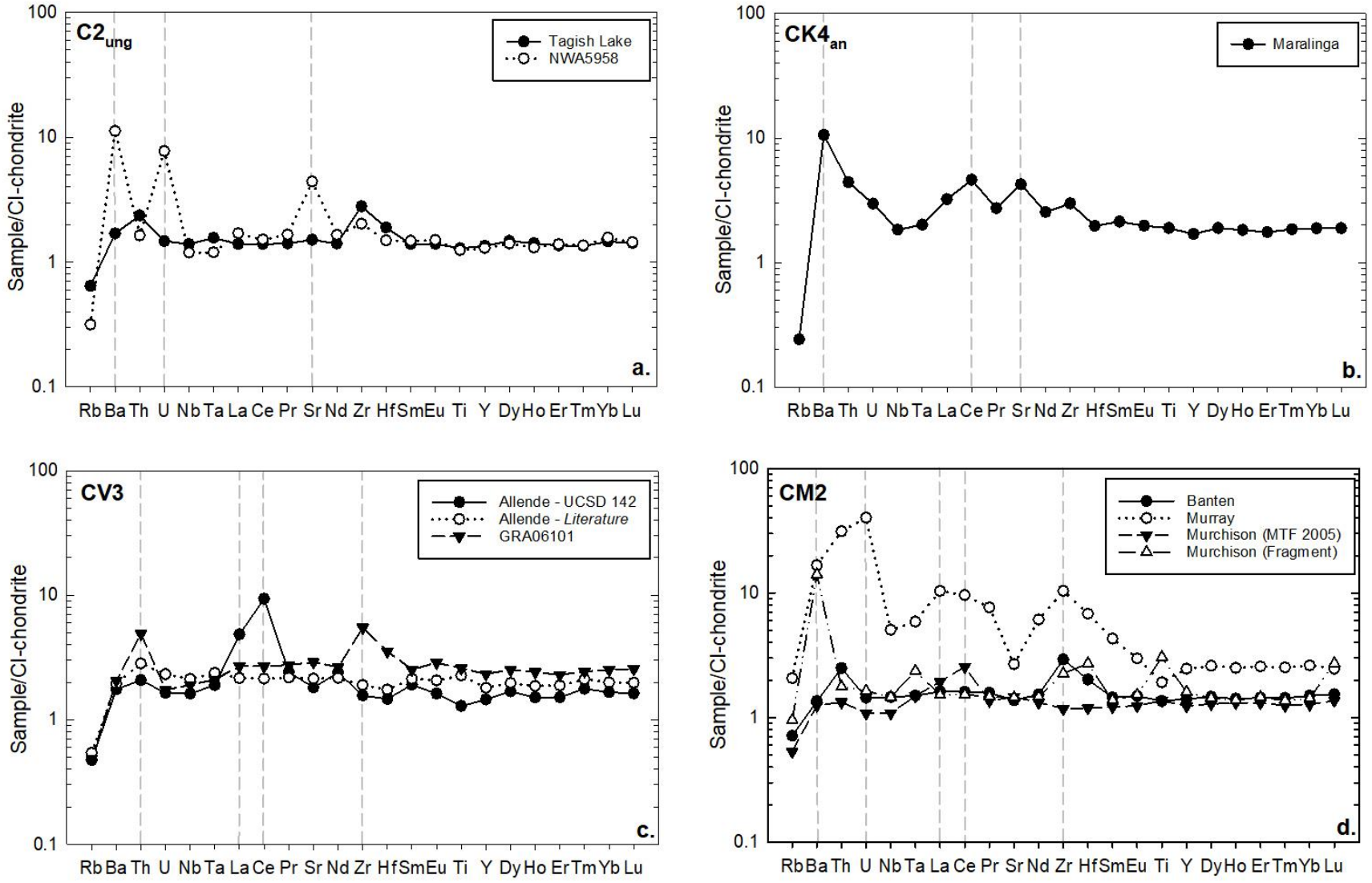

Figure 8. Incompatible trace elements in carbonaceous chondrites measured in this study. All samples in incompatible trace and rare earth element figures hereon after are normalized to CI-chondrite Orgueil from Barrat et al. (2012). (a). Incompatible trace elements in C2ung chondrites. (b). Incompatible trace elements in CK4an chondrites. (c). Incompatible trace elements in CV3 chondrites. (d). Incompatible trace elements in CM2 chondrites. Elements are ordered from most incompatible (Rb) on the left to least incompatible on the right.

4.3.2 Incompatible trace elements in ordinary chondrites

Incompatible trace element variabilty between different groups of ordinary chondrites are shown in Figure 9. The “High Iron” (H) ordinary chondrite group displays minor enrichments in all incompatible trace elements relative to CI-chondrite Orgueil (Figure 9a). All the high-iron samples in this study show additional enrichment in Zr. Richardton (H5), exhibits enrichments in Ti and Ta compared to the rest of the group. Fayateville (H4), shows additional enrichments in Ba, Th and U. Forest City (H5), as well as having the highest enrichment of Zr from the group, shows enrichment in Th. Figure 9b shows the “Low Iron” (L) and “Low Iron & Metal” (LL) groups trace element patterns. Five of the sample measurments from this grouping show a depletion in Rb relative to CI-chondrite Orguiel (Kunashak (L6), Larkman, and Air (L6)). A few unique sample patterns to note are those of NWA 869 (L3-6), Peace River (L6) and Saratov (L4). NWA 869 shows an extreme enrichment of Ba as well as a large enrichment of U and Sr. Peace River shows enrichments in Ba and Ta compared to the other samples in the group and Saratov shows minor enrichments in Th, Ta, and Zr, although other samples show similar patterns but not as great of an enrichment (e.g. Air (L6) & Kyle (L6)). Both the Chelyabink samples, one containing fusion crust and the other without, show similar patterns in their incompatible trace elements, however the Chelaybinsk sample without the fusion crust is slightly more enriched in the incompatible trace elements than the sample with fusion crust.

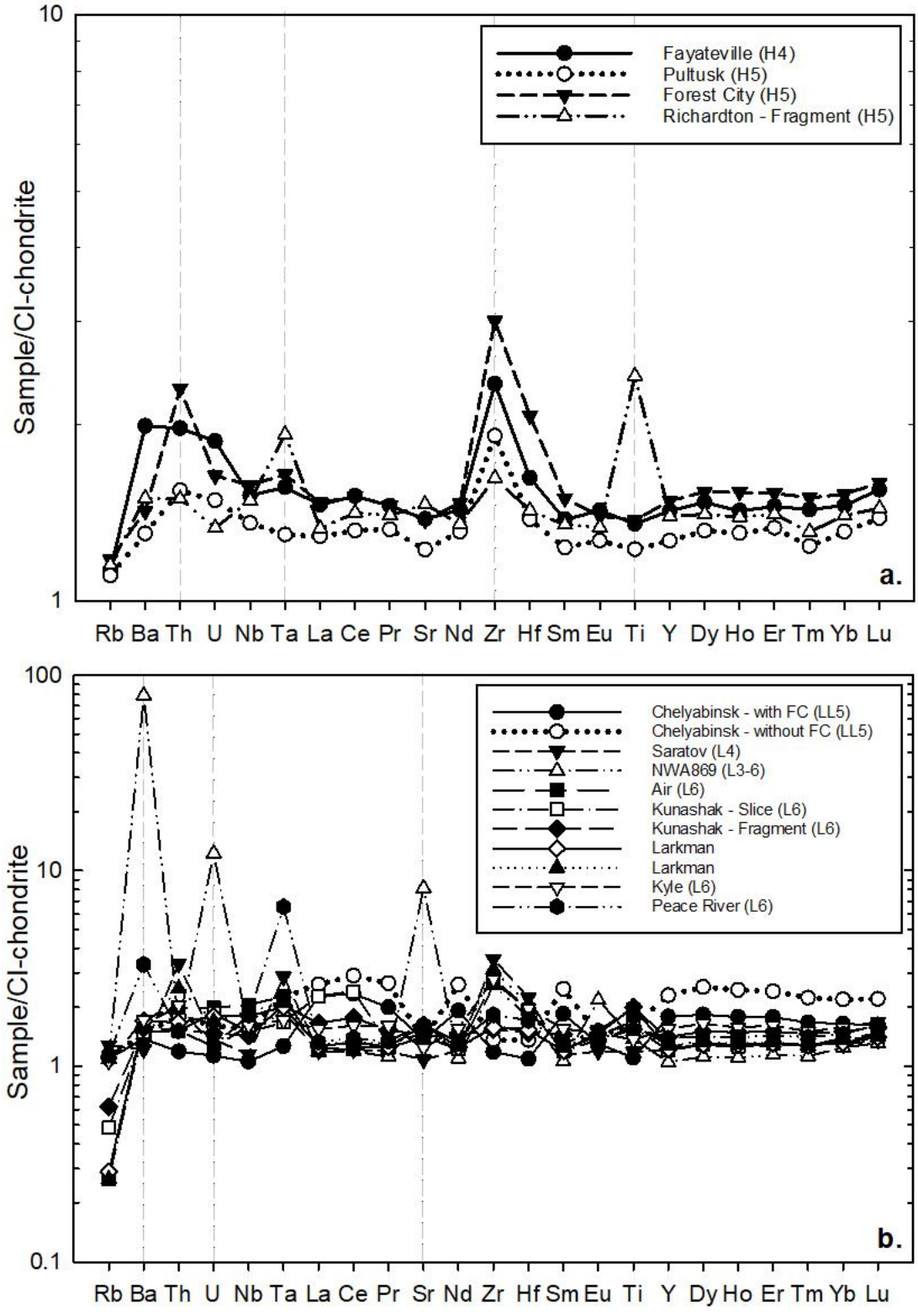

Figure 9. Incompatible trace elements in Ordinary Chondrites from this study. (a). Incompatible trace elements in "High Iron" ordinary chondrites. (b). Incompatible trace elements in “Low Iron” ordinary chondrites.

4.3.3 Incompatible trace elements in enstatite chondrites

Incompatble trace element patterns for Enstatite chondrites can be found in Figure 10. Enstatite chondrites from this study show depletions in most incompatible trace elements compared to CI-chondrite Orguiel. However, for the samples Atlanta and LON91400, there are slight enrichments in Th, Zr and Hf. Khaipur shows the most significant depletions in incompatible trace elements out of all the samples measured, although it does have a slight enrichment in Zr and Hf, following the pattern of the other samples in the group.

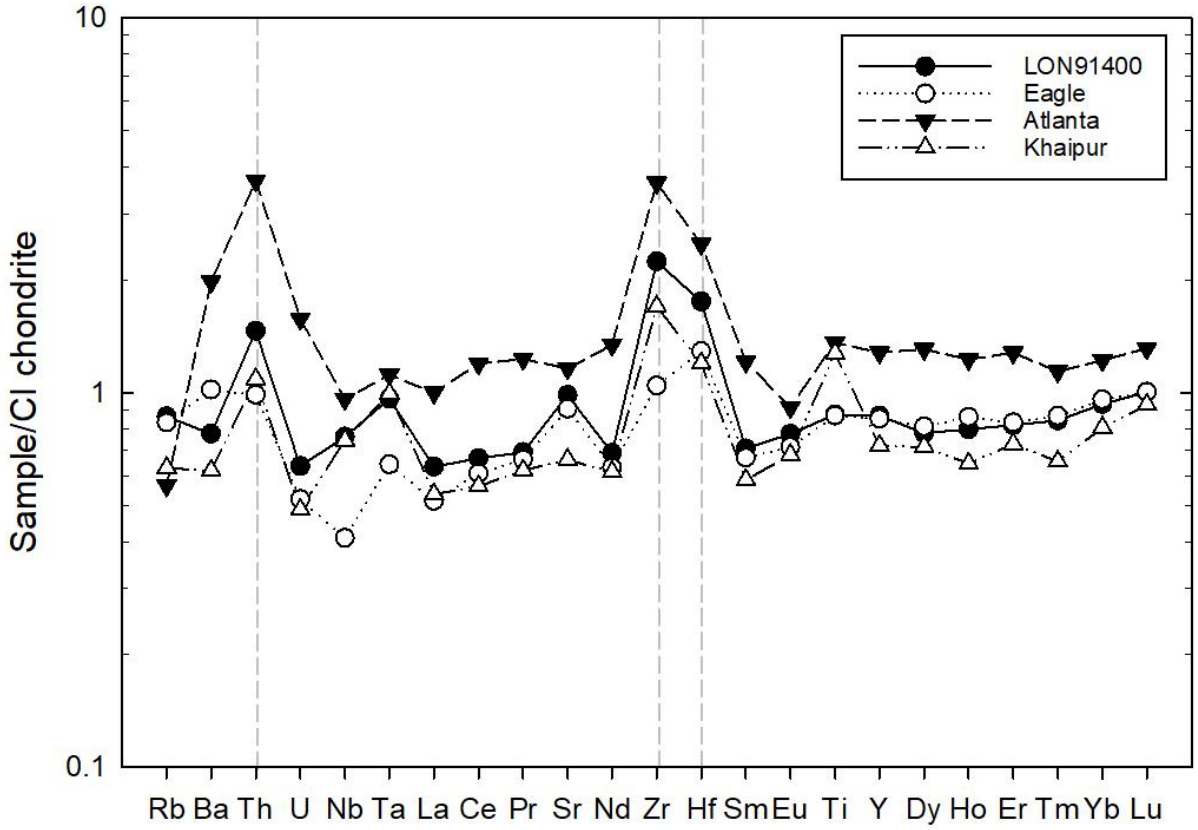

Figure 10. Incompatible trace elements in enstatite chondrites measured in this study.

4.3.4 Bulk sample rare earth element abundances

Rare earth element patterns in bulk-sample carbonaceous chondrites, in general, show no to only a slight enrichment compared to CI-chondrite Orgueil (Figure 11). Murray shows enrichment in all the REE compared to CI-chondrite, however it has a significant enrichment in

La, Ce, Pr, Nd, and Sm. Allende (UCSD 142) shows enrichment in La and a large spike in Ce before flattening out and following similar concentrations and patterns as the Allende literature measurements. Maralinga shows enrichment in La and Ce. GRA06101 shows a slight enrichment in Ce compared to the rest of the REE in the sample. Other than the few samples mentioned above, most carbonaceous chondrite REE patterns are flat, in agreement with a recent study (Braukmüller et al. 2018).

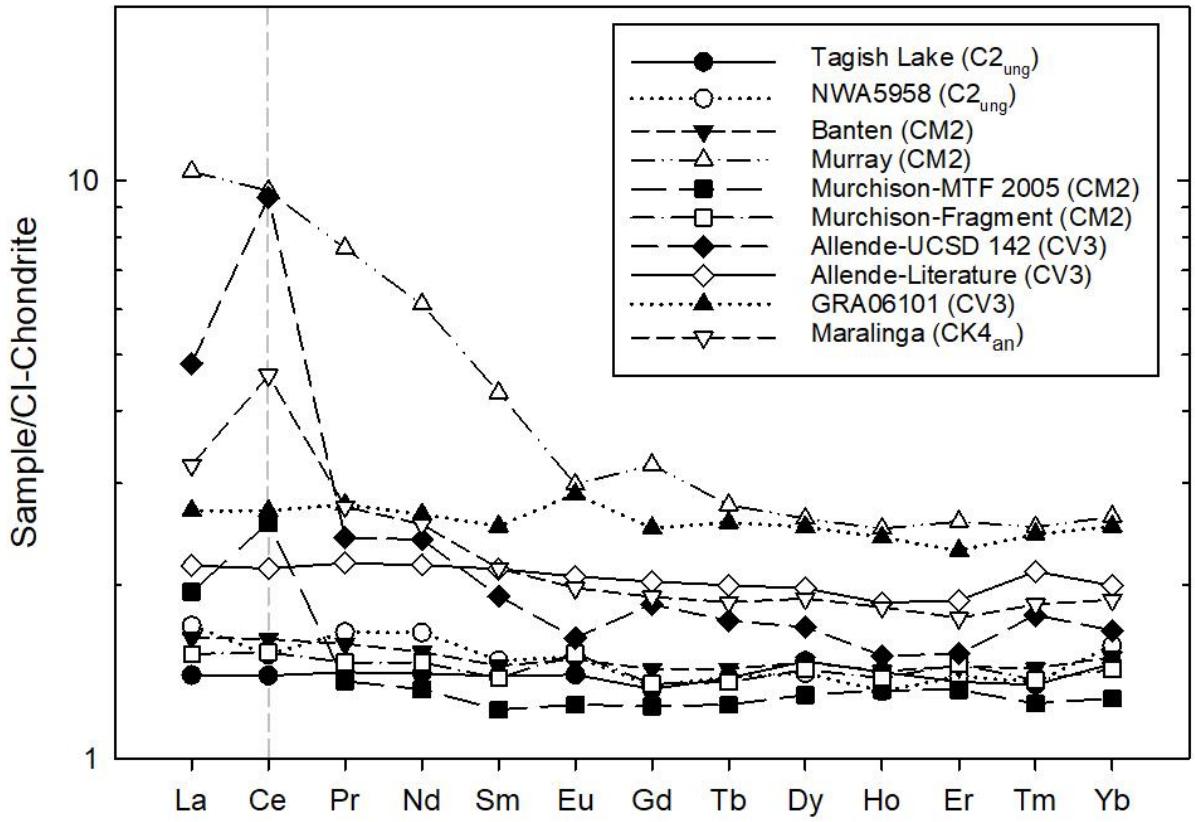

Figure 11. REE patterns for carbonaceous chondrites measured in this study.

For ordinary chondrites, the REE pattern generally shows slight enrichments in REE compared to CI-chondrite (Figure 12). Both Chelyabinsk (LL5) samples show larger enrichments in the REE within the suite. The Chelyabinsk sample excluding the fusion crust ("without FC") shows the most significant enrichment in the REE from the suite, excluding its large depletion in Eu. The Chelyabinsk sample with fusion crust ("with FC") incorporated into the powdered

sample has slightly lower REE with a similar depletion in Eu. The Kunashak slice (L6) has an enrichment in La and Ce. Some samples (e.g. Air (L6), Saratov (L4), Peace River (L6)) show a slight enrichment in Eu as well consistent with previous studies on LL and L ordinary chondrites (Friedrich et al. 2003), although NWA 869 (L3-6) shows a significant enrichment compared to other samples within the suite.

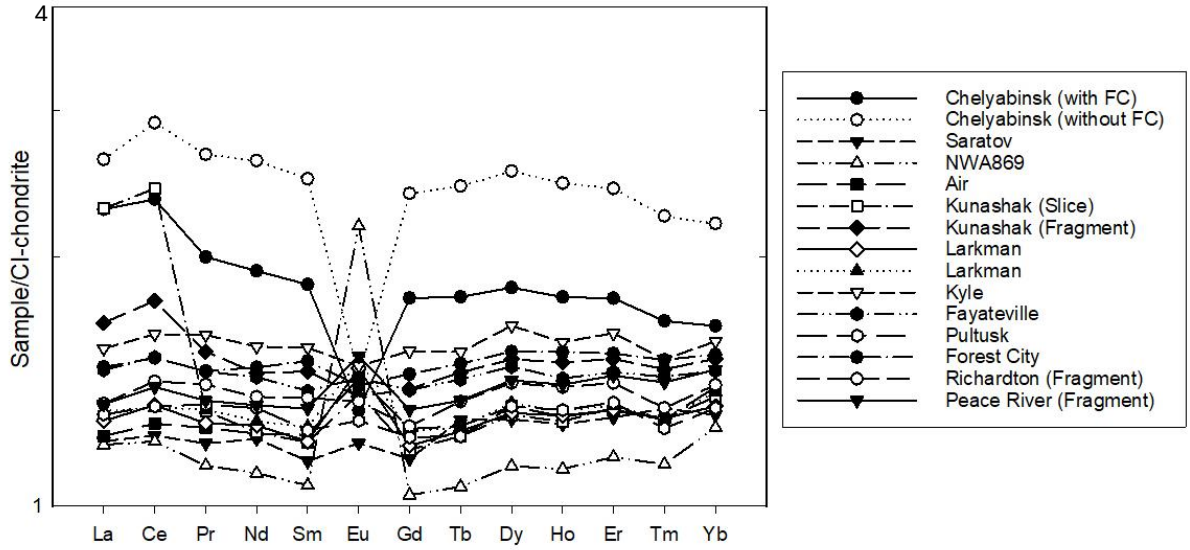

Figure 12. REE patterns for ordinary chondrites measured in this study.

Only four enstatite chondrite were measured in this study all of which are in the EL group. The REE patterns show an interesting trend for three of the four samples (Figure 13). LON91400, Eagle and Khairpu are all depleted in the REE compared to CI-chondrite however, they show an increase in abundance from La to Yb. These samples follow the "anomalous EL6 trend" described in Barrat et al. 2014 while also displaying a slight La depletion, in agreement with previous results (Barrat et al. 2014; Kallemeyn & Wasson 1986; Shinotsuka et al. 1995) Atlanta shows a slight enrichment in REE compared to CI-chondrite, though, it has a depletion in Eu.

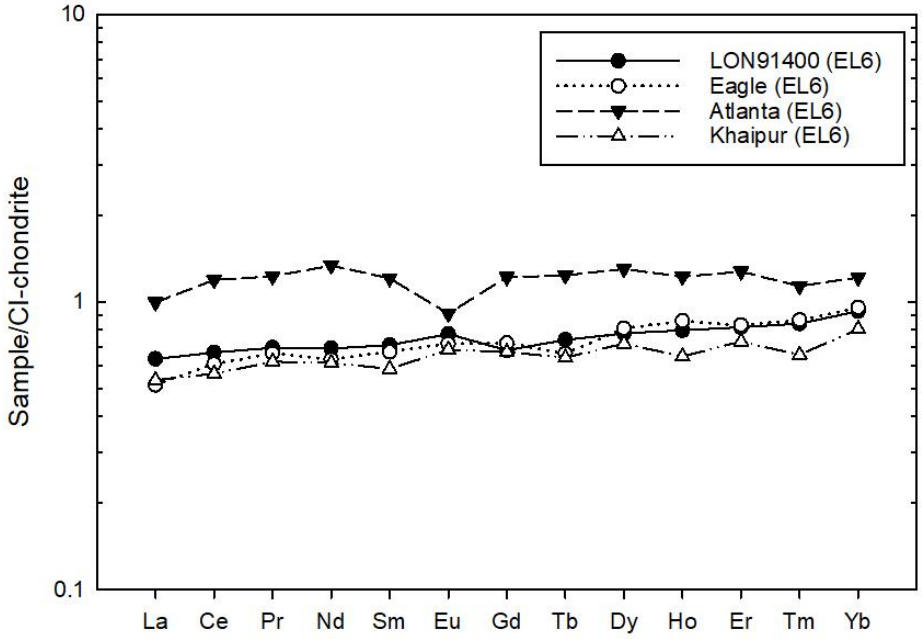

Figure 13. REE patterns for enstatite chondrites measured in this study.

4.4 Oxygen isotope compositions

Oxygen isotopes were measured on nine chondrites from the sample suite. Averaged measurements can be found in Table 8. For figures used in this study, comparisons are made to the terrestrial fractionation line (TFL), which has a slope of 0.5241. Deviations from the TFL are described using $\Delta^{17}O_{SMOW} = \delta^{17}O_{SMOW} - 0.5241 \times \delta^{18}O_{SMOW}$ (Criss & Farquhar, 2008). Figure 14 shows the relations between $\delta^{18}O$, $\delta^{17}O$ and $\Delta^{17}O$.

In figure 14a. regression lines were plotted using the SigmaPlot curve fitting function. The regression line for ordinary chondrites measured in previous studies (OC_1) differs to that of the ordinary chondrites measured in this study (OC_2) (Yurimoto et al. 2008, Clayton and Mayeda, 1999). From this study, Peace River (L6), NWA 869 (L3-6) and Chelyabinsk (LL5) all fall along both regression lines (OC_1, OC_2) however, Richardton (H5), Kunashak (L6) and the Larkman samples show a slight depletion in both $\delta^{18}O$ and $\delta^{17}O$ relative to the measurements

from Yurimoto et al., 2008, offsetting the regression lines of the two separate sample sets. The data collected from this study on the carbonaceous chondrites, Allende and Murchison, falls along the regression line from data collected in Yurimoto et al., 2008. Murchison, however, showed variable measurements between the two studies; the $\delta^{18}O = 1.41$ and $\delta^{17}O = -3.52$ from this study and $\delta^{18}O = 7.3$ and $\delta^{17}O = 1.196$ from Yurimoto et al., 2008 giving a $\Delta^{17}O$ value different by a factor of ~2 (Figure 14b.).

Considering that these measurements are "bulk sample" oxygen isotopic compositions, it is important to note that oxygen heterogeneities are a result of materials (i.e. chondrules and CAIs) forming at different times and experiencing variable conditions in the solar nebula and alteration events on their parent bodies (Krot et al., 1998). Despite efforts to 'homogenize' a bulk sample, secondary and altered phases will potentially be incorporated in variable amounts, yielding the variable results.

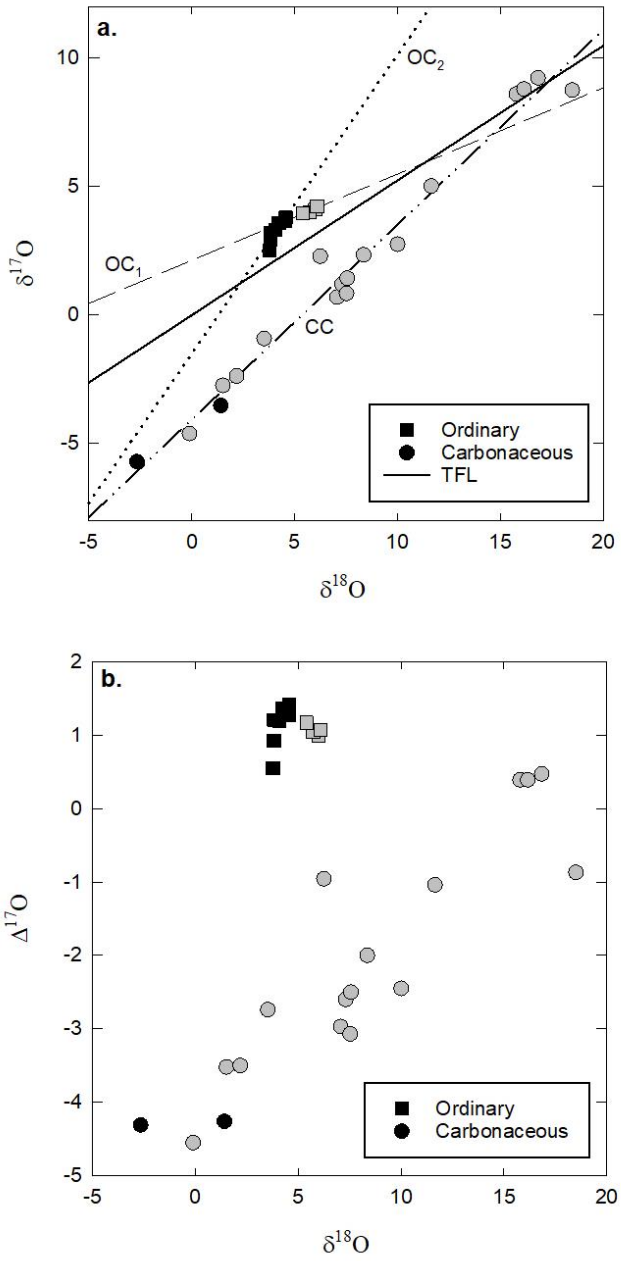

Figure 14. (a). $\delta^{17}O$ vs $\delta^{18}O$ in per mil (‰). OC_1-ordinary chondrite regression line from Yurimoto et al. (2008). OC_2 –ordinary chondrite regression line for data from this study. CC-carbonaceous chondrite regression line. TFL-Terrestrial Fractionation Line (slope: 0.5241). (b). $\Delta^{17}O$ vs $\delta^{18}O$ in per mil (‰). All grey symbols (a. & b.) are from Yurimoto et al. (2008) and Clayton and Mayeda, (1999).

4.5 Highly siderophile element (HSE) abundances

HSE blank-corrected abundances are reported in Table 9, along with previous HSE data collected for Allende (Fischer-Gödde et al. 2010, Becker et al. 2006, Brandon et al. 2005a,

Walker et al. 2002, Horan et al. 2003, Jochum 1996, Tagle & Berlin 2008, Takajashi et al. 1978, Jarosewich et al. 1987, Swindle et al. 1998).

Before discussing HSE results further, it is important to note how powdered sample aliquots have the potential to give variable results. As mentioned in the analytical methods section 3.3, whole rock samples were prepared by powdering the sample with limited force to homogenize the sample to give a more representative measurement. For phases, such as metal, this limited force will be unable to powder the phase completely and therefore may leave clumps or fragments, which will then cause measurements that are not always representative of the sample as a whole. Too much powdering, and the metals smear and are lost. This will be seen in the following sections (e.g. for Gujba).

4.5.1 Bulk sample HSE abundance variations

An in-depth discussion for Re and Os abundances and ratios within bulk samples can be found in section 4.7. It is important to note that the long-term Re/Os ratios of a sample can be examined through the long lived Re-Os isotopic system, assuming any alteration or disturbances to the system have occurred relatively recently, whereas, for other HSE ratios, such a check is not possible (Walker et al. 2002, Horan et al. 2003). In general, HSE absolute abundances within individual aliquots of samples can vary due to inclusions of metal and calcium aluminum inclusions (CAIs) or uneven distributions of various mineral phases. Figure 15 shows the HSE abundances of duplicate analyses of chondrite samples from this study. Some duplicate analyses show small variability, while others show more significant differences. From this figure and past studies (Horan et al. 2003, Fisher-Gödde et al. 2010, Morgan et al. 1985, McDonald et al. 2001, Walker et al. 2002) it becomes apparent that HSE ratios are more reproducible than absolute abundances.

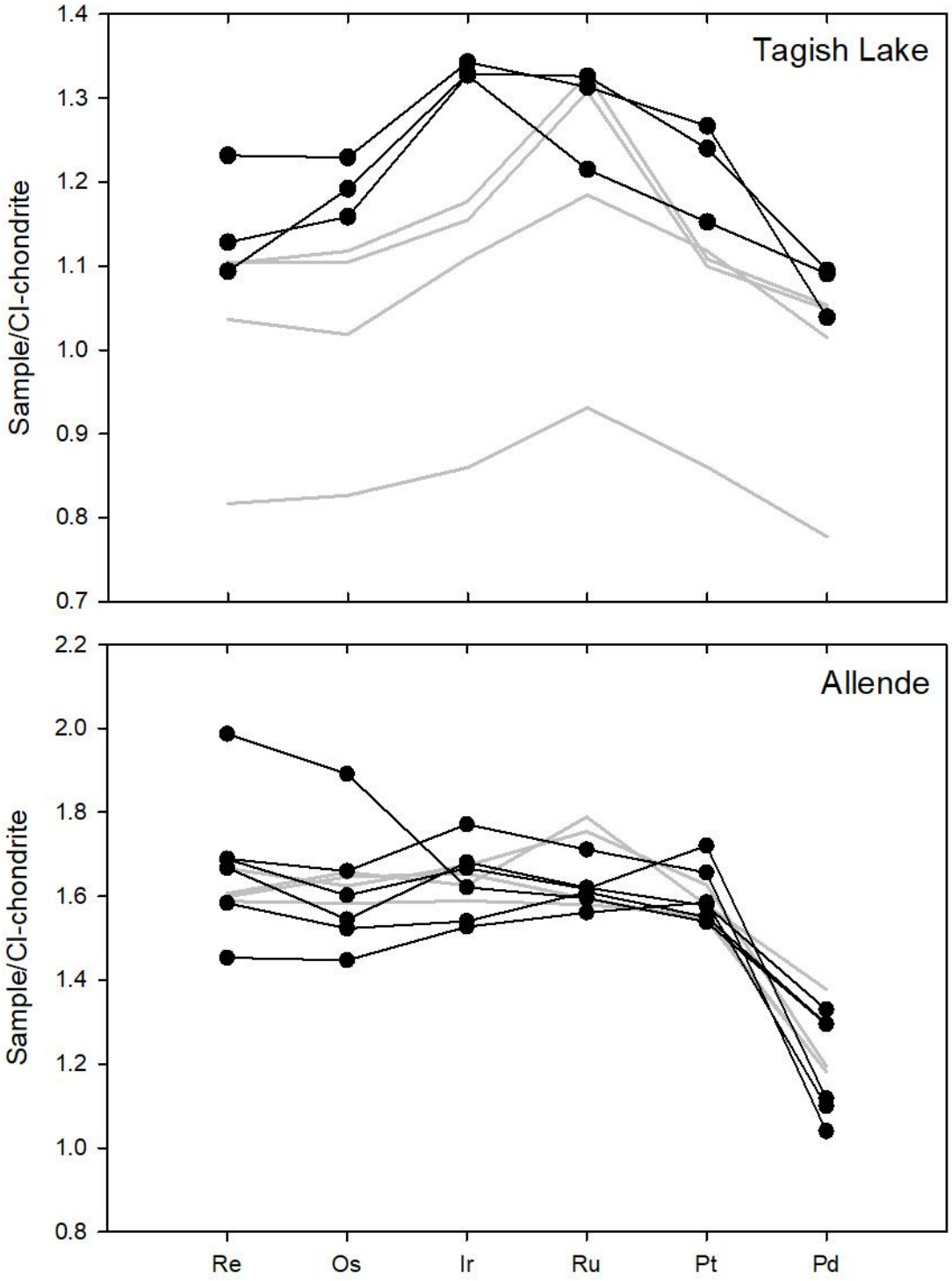

Figure 15. Black lines and black circles show HSE abundances measured in duplicates from this study on Tagish Lake and Allende. Grey lines are measurements from Brandon et al., 2005a, Fisher-Godde et al., (2010), Becker et al., (2006) and Walker et al., (2002). All samples are normalized to CI-chondrite Orgueil from Day et al. (2016b).

Figure 17 gives a comparison of HSE absolute abundance data from this study to previous studies (Horan et al. 2003, Fischer-Gödde et al. 2010). Overall, abundance data from this study are consistent with the published data, barring a few samples. Ordinary chondrites show the greatest spread of HSE abundances (~0.6-2.3 × CI-chondrite) compared to carbonaceous or enstatite. Most HSE abundances measured in the various chondrite classes are higher relative to CI-chondrite Orgueil, which they are normalized to. This is argued to be a dilution effect due to the presence of higher volatile components within CI-chondrites (Day et al. 2016b). Other effects to consider that modify primary HSE abundances are late impact processes (Day et al. 2016b, Norman and Mittlefehldt 2002). Potential incorporation of impact melts into powered samples from this and previous studies could yield varying HSE absolute abundances.

Absolute HSE abundances in ordinary chondrites increase with metal abundances LL<L<H. Similar to previous studies, data from this study on ordinary chondrites showed no correlation between the petrologic type and HSE abundance (Figure 16B.), suggesting that thermal metamorphism has no control on HSE abundances in the parent bodies of ordinary chondrites (Fisher-Gödde et al. 2010, Kallemeyn et al. 1989, Day et al. 2016b).

Carbonaceous chondrites from this study generally show increasing HSE abundances between the groups CI < CM2 < CV3. Maralinga (CK4-an) shows a significant depletion of Pd and NWA 5958 shows a depletion in Pt and an enrichment in Pd. Generally, most carbonaceous chondrites show a minor depletion of Pd relative to other HSE and CI-like HSE abundance patterns excluding the few mentioned above. Gujba has been excluded from multiple figures displaying the HSE due to its abnormally high HSE content, likely cause by the high metal content in the powdered sample from anomalously high metal. There is a trend for both Os and Pd in association with petrologic type seen in Figure 16A. Os shows a stronger correlation with its increasing abundance relative to increasing petrologic grade than that of Pd.

Only four enstatite chondrites were measured for HSE abundances in this study, all of which are from the EL6 group. Khairpur shows the largest enrichment in HSE abundances from

the enstatite chondrite suite compared to CI-chondrite, most notably in its Re abundance (Figure 17). Eagle, Atlanta and LON91400 show similar HSE abundances to previous studies (Horan et al. 2003, Fischer-Gödde 2010), although Eagle is enriched in Ir and Pd comparatively. Excluding Khairpur, the enstatite chondrites show a limited HSE abundance spread (including the literature data). Similar to the ordinary chondrites, the enstatite chondrites do not have strong trends associated with petrologic type (Figure 16C.). However, when all chondrites are plotted for both Re and Pd abundances relative to petrologic grade, a slight trend becomes apparent as seen in Figure 16D. (Day et al., 2016b).

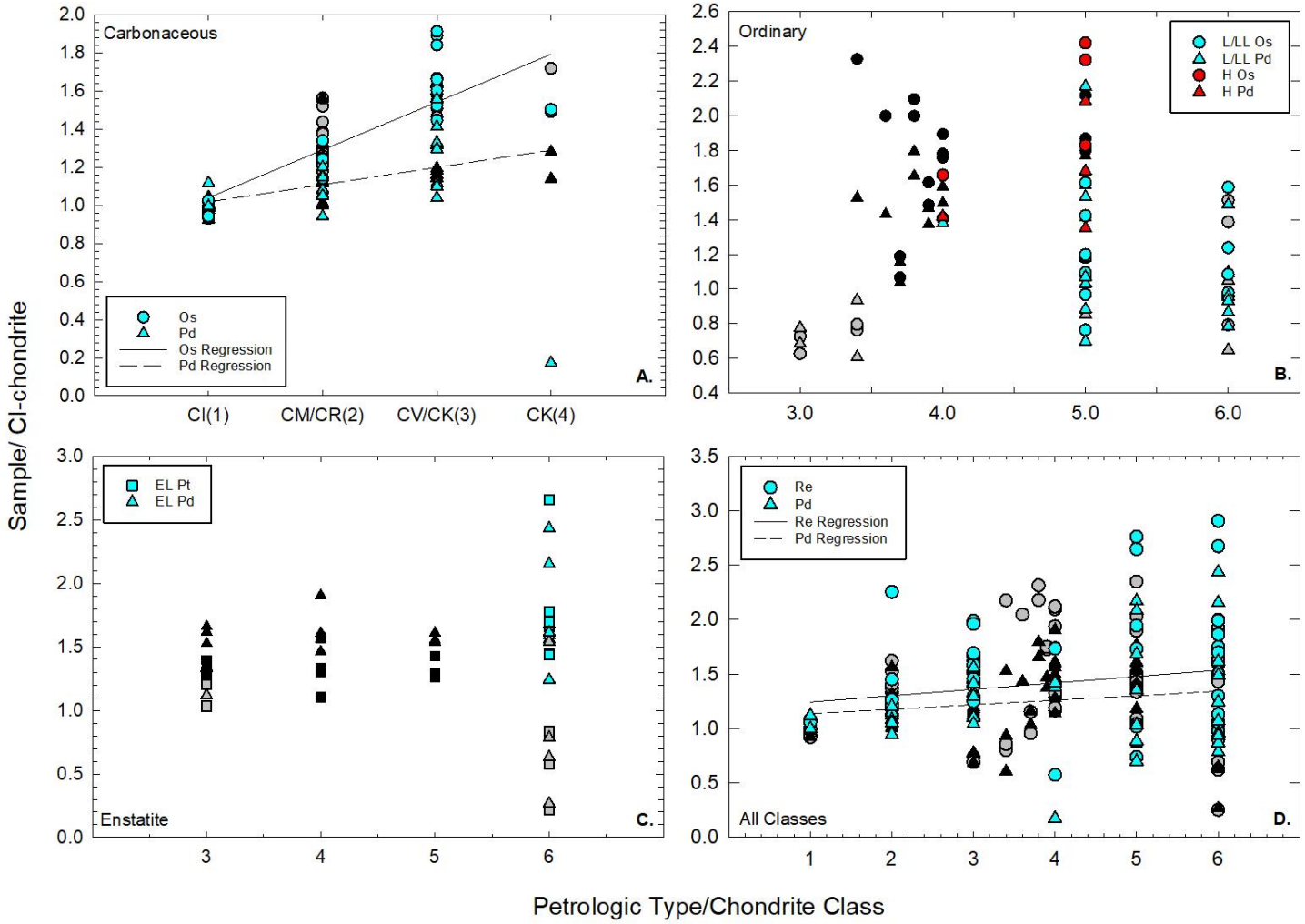

Figure 16. Plots of HSE abundances normalized to Orguiel[1] verses petrologic type in each class of chondrite (A.), (B.), (C.), and for all chondrite classes (D.). A. Blue symbols are representative of data from this study, grey circles are Os abundances from [1-4], black triangles are Pd abundances from [1-4]. B. Blue and red symbols are data from this study. Grey symbols are L/LL data from [1&4] and black symbols are H data from [1,2,4]; circles are Os data and triangles are Pd data. C. Blue symbols are data from this study, Grey squares are Pt data from [1&4] and grey triangles are Pd data from [1&4]. D. Samples from all chondrite classes. Blue symbols are from this study, grey circles are Re data from [1-4], black triangles are Pd data from [1-4]. [1]Walker et al., (2002); [2]Horan et al., (2003); [3]Brandon et al., (2005a); [4]Fisher-Gödde et al., (2010). Figure after Day et al., (2016b).

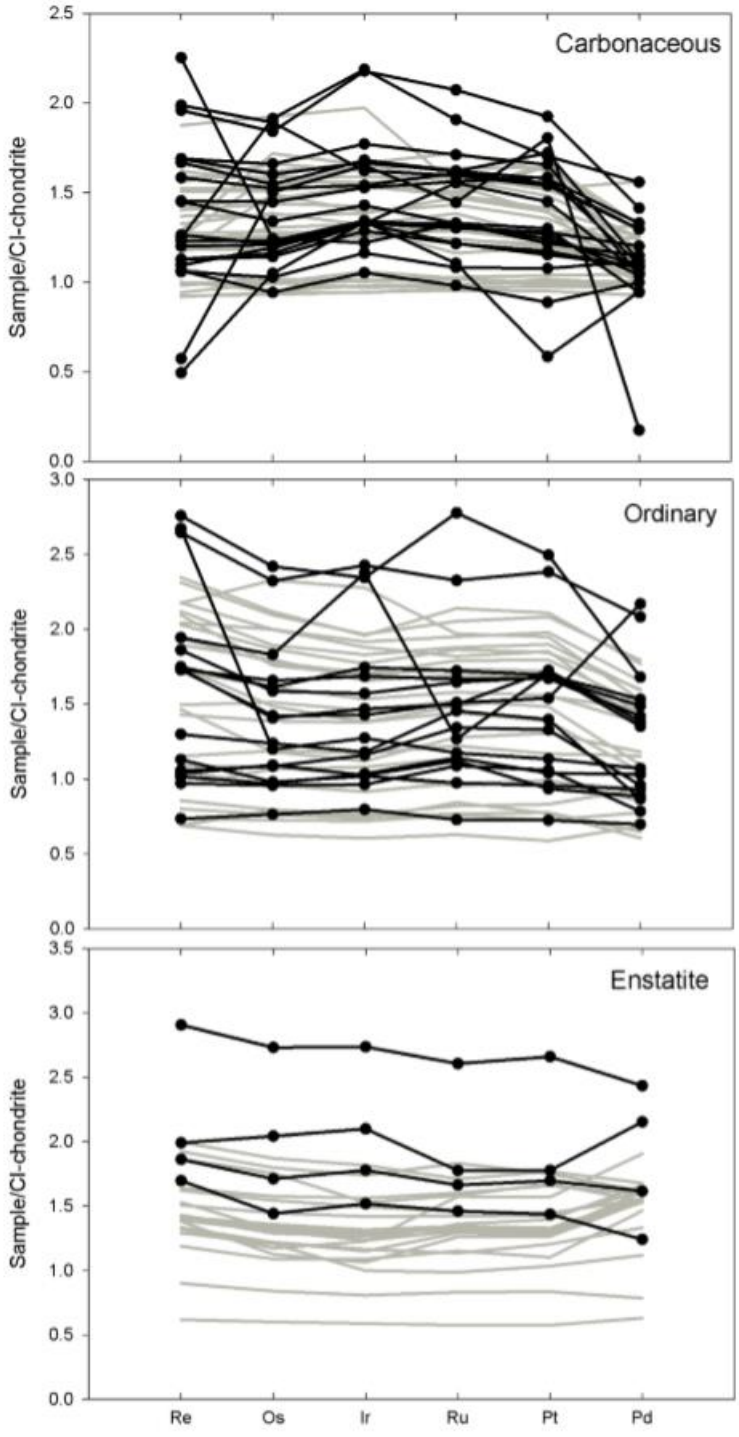

Figure 17. HSE abundance patterns between chondrite classes. Data from this study (excluding Gujba) are in black, data from Horan et al. (2003) and Fischer-Gödde et al. (2010) are in grey. Samples are normalized to CI-Chondrite Orgueil from Day et al. (2016b). Figure after Day et al. (2016b).

Figure 18, shows Re, Os, Ru, Pt and Pd (ppb) plots against Ir (ppb). The Os, Ru and Pt plots show significant correlation between the ordinary and enstatite classes as well as a close correlation to carbonaceous chondrites. Each plot shows a regression line of data from a chondrite class. These regression lines were plotted using the Sigmaplot curve fitting function. For ordinary and enstatite chondrites, the slopes of Re-Ir, Os-Ir, Ru-Ir and Pt-Ir are close to, or

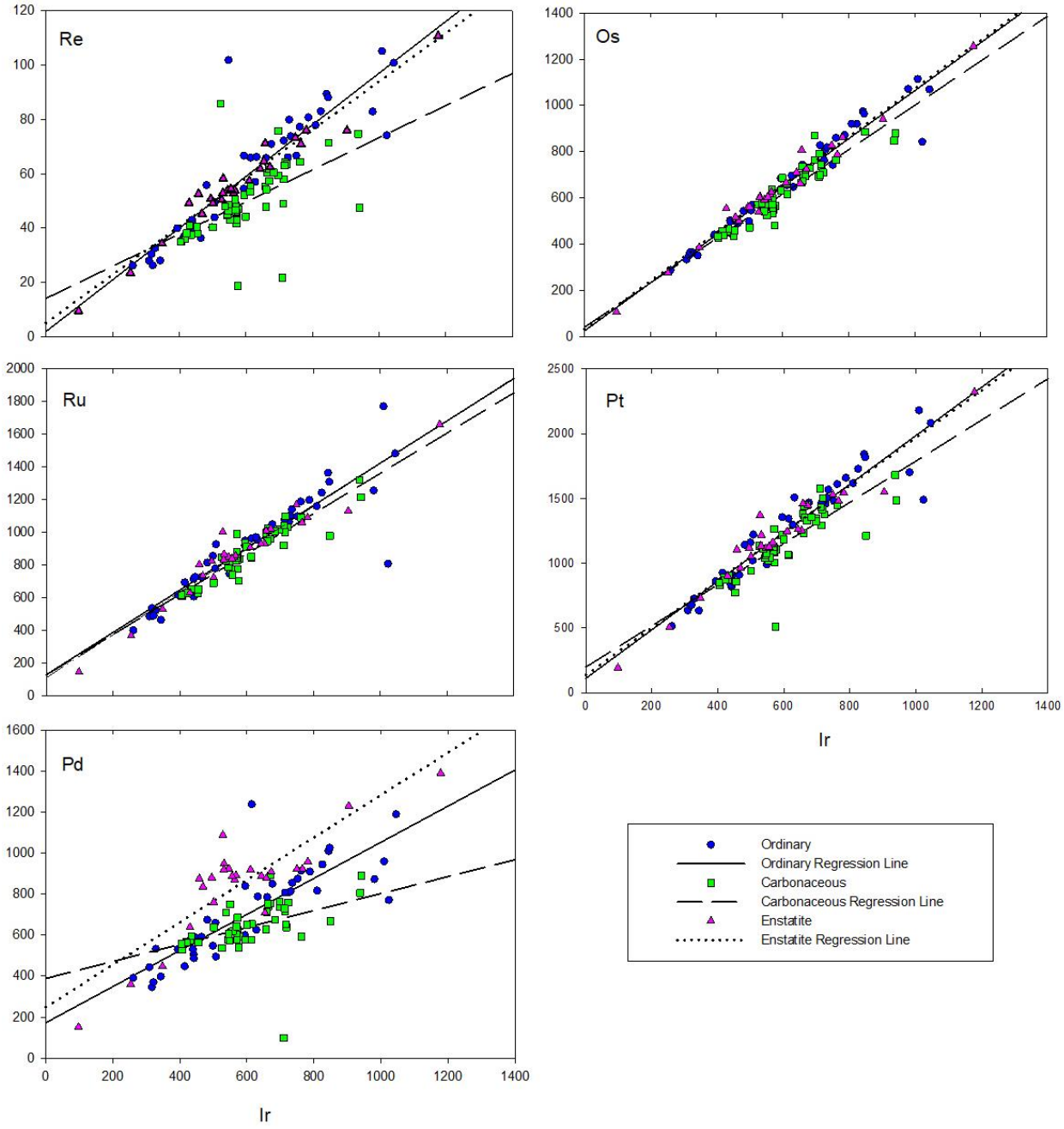

Figure 18. Highly siderophile element interelement variations, relative to Ir, between chondrite classes. Data includes measurements from this study, Horan et al. (2003) and Fischer-Gödde et al. (2010). Regression lines plotted using SigmaPlot fitted line tool.

essentially the

same. For carbonaceous chondrites, the slopes of Re-Ir and Pd-Ir are significantly shallower while the slopes of Os-Ir, Ru-Ir, and Pt-Ir are only slightly shallower. These results agree with previous studies (Fischer-Gödde et al., 2010).

4.6 Rhenium-osmium isotope systematics

New data collected for Re and Os abundances, $^{187}Re/^{188}Os$ and $^{187}Os/^{188}Os$ including calculated $^{187}Os/^{188}Os_i$ at 4568 Ma are listed in Table 9. In this study, concentrations for Re spanned from 18.82 ng g^{-1} to 295 ng g^{-1} and concentrations of Os spanned from 351 ng g^{-1} to 3337 ng g^{-1}, where Chelyabinsk (LL5) and NWA 5958 (C2) are the lowest in Os and Re respectively and Gujba (CBa) was the highest for both Re and Os concentrations. It is likely that the reason for Gujba's anomalously high concentrations of Re, Os and other HSE is due to a large incorporation of metal fractions in the measured sample. As is seen in previous studies (Walker et al. 2002), ordinary chondrites tend to have the highest concentrations of Re and Os, most likely due to the greater proportions of metal within sample aliquots (Figure 19) Considering Figure 19 further, carbonaceous chondrites do not vary as highly in Os concentrations as ordinary or enstatite chondrites do, however, carbonaceous chondrites show more offset in Re concentrations than the ordinary or enstatite chondrites.

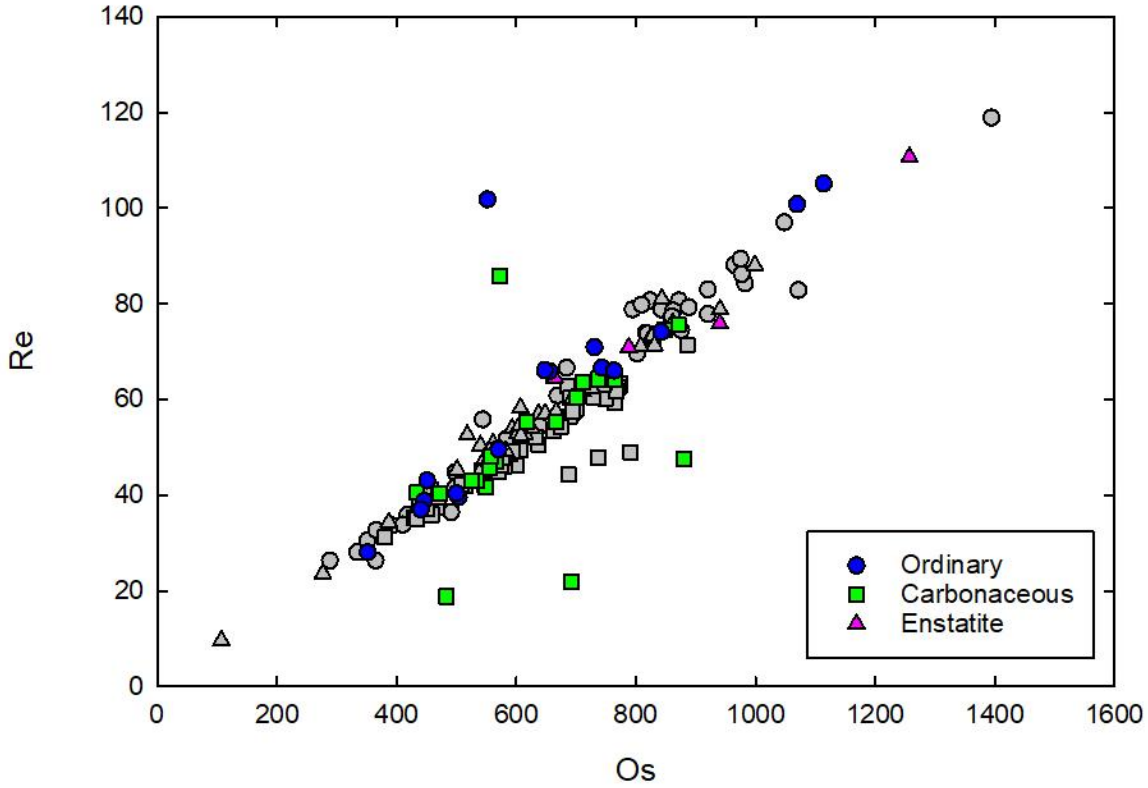

Figure 19. Plot of Re versus Os in ppb for ordinary, carbonaceous and enstatite chondrites (excluding Gujba). Colored symbols are from this study. Grey symbols are data from Horan et al. 2003, Fischer-Gödde et al. (2010), Walker et al., (2002), Brandon et al., (2005a), Walker et al., (2018).

$^{187}Re/^{188}Os$ ratios also show some variation between the chondrite classes as described in previous studies (Figure 20; Walker et al., 2002, Brandon et al., 2005a, M. Fischer-Godde et al., 2009). For ordinary chondrites in this study, the $^{187}Re/^{188}Os$ ratios span from 0.378 (Chelyabinsk LL5) to 0.889 (NWA869 L3-6). Excluding NWA869, the range for ordinary chondrites tapers to 0.378-0.493, close to the average ratio from Walker et al. (2002) of 0.422±0.025. Carbonaceous chondrites show a range from 0.152 (Maralinga CK4-an) to 0.722 (Murchison CM2), excluding the two samples mentioned prior, NWA 4502 (0.260), and NWA 5958 (0.188), the range from carbonaceous chondrites narrows to 0.366-0.450. The average for carbonaceous chondrites in Walker et al., 2002 was 0.389±0.021. The enstatite chondrites show a range from 0.389 (Eagle EL6) to 0.469 (Atlanta EL6); Walker et al. (2002) showed an average of 0.421±0.013 for enstatite chondrites. In general, the measurements from this sample set correlated closely to those of Walker et al. (2002), excluding the few mentioned above.

^{187}Re decays to ^{187}Os through β-decay with a half-life of ~42 Ga (Day et al., 2016b). This allows the ^{187}Re-^{187}Os system to be used in an isochron diagram. While these diagrams can be used as chronometers, it is important to consider the implications of Re/Os disturbances that may have occurred after the chondrites initial formation. ^{187}Os/^{188}Os ratios for Ivuna, Orgueil, Murray, Murchison, Allende, Vigarano, Forest City, and Atlanta are consistent with previous studies (Horan et al. 2003, Fischer-Gödde et al., 2010, Walker et al., 2002) and fall close to the 4.558 IIIA Iron Isochron (Figure 20). Chondrites to note that fall far off the isochron are NWA869 (L3-6), Murchison (SIGL-CM2), NWA5958 (C2) and Maralinga (CK4-an); suggestive of alteration effects and/or Re/Os disturbances after formation of the chondrite.

For carbonaceous chondrites the ^{187}Os/^{188}Os ratios range from 0.11351-0.12985, for ordinary the range is 0.12526-0.13312, and enstatite 0.12522-0.12808. The ranges for each class

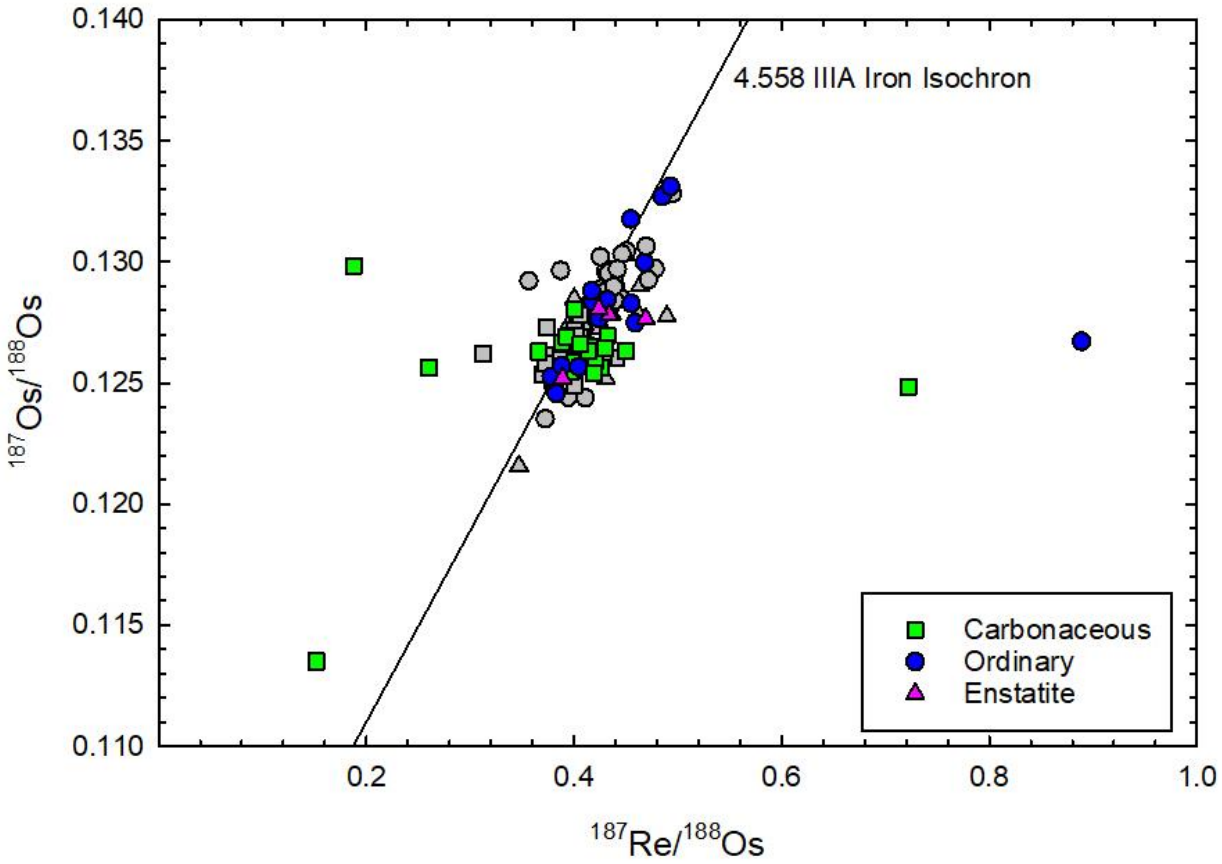

Figure 20. ^{187}Re/^{188}Os versus ^{187}Os/^{188}Os for bulk chondrite samples. Colored symbols show data from this study. Grey symbols represent data from Horan et al. 2003, Fischer-Gödde et al. (2010), Walker et al., (2002), Brandon et al., (2005) and Walker et al., (2018). The 4.558 IIIA iron isochron is from Smoliar et al. (1996).

vary; while the carbonaceous chondrites show the most significant range, when the lowest $^{187}Os/^{188}Os$ ratios are excluded (Maralinga CK4-an (from this study)), the ordinary chondrite

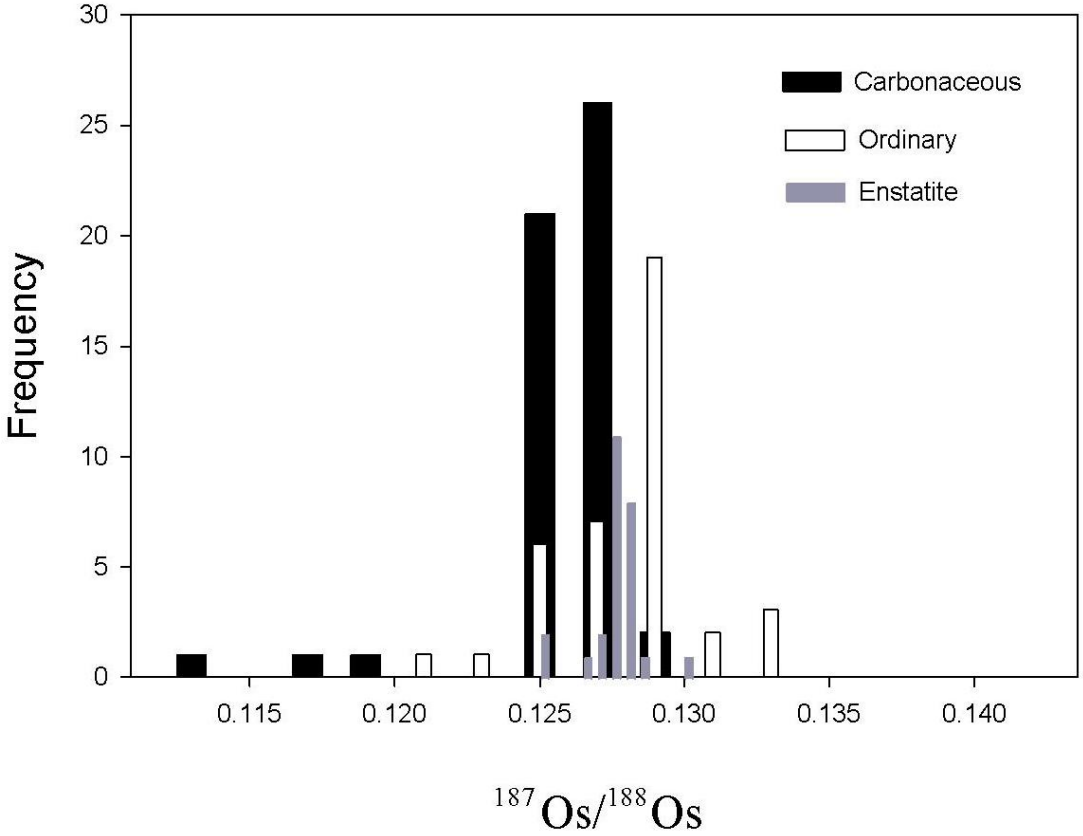

Figure 21. Histogram of $^{187}Os/^{188}Os$ ratios for chondrites from this study, Horan et al. 2003, Fischer-Gödde et al. (2010).

class shows the greatest variance between samples (Figure 21).

5. Discussion

5.1 A note on sample heterogeneities and effects of sample preparation

Although attempts were made to homogenize powdered sample aliquots to produce representative samples, variations in the amount and constituent materials of aliquots of chondrite samples were inevitable. This 'mode effect', where non-representative fractions of rock samples are measured, can have drawbacks, but can also be utilized to examine processes occurring with individual components (i.e., chondrules, matrix) of chondrites. Drawbacks include previous studies noting issues when comparing data on the same meteorites with other studies (e.g. Horan et al., 2003). As is made apparent in various figures from this study (e.g. figure 4 & 14) not all sample aliquots are representative of the "whole" chondrite sample. It is for this reason that I measured multiple elemental compositions, mineral phases and other components of chondrites to examine the role of these 'mode effects'. For example, the trace element data used in this study are a good "check" for various alteration processes (e.g., terrestrial alteration, section 5.2) that could be argued for within the HSE data, as compared to mode effects within samples.

5.2 Terrestrial alteration effects

Various chondrites within the sample suite show evidence for terrestrial alteration effects. For samples found in hot dessert environments (e.g., "NWA" samples), the terrestrial alteration effects can drastically modify the primary abundances of elements which can otherwise provide information on parent body processes (e.g., Hyde et al. 2014, Crozaz et al. 2003). Past studies have shown evidence of terrestrial alteration in chondrites to be consistent with increases in Ca, Ba, Sr, U, Pb and As abundances, as well as higher abundances of the light REE (LREE) compared to the heavy REE (HREE) (e.g., Hyde et al., 2014; Lee & Bland, 2004; Al-Kathiri et al., 2005). Deviations from the $^{187}Re/^{188}Os$ versus $^{187}Os/^{188}Os$ 4.558 IIIA Iron Isochron (Figure 19) are considered to be indicators of open-system behavior. Open-system behavior, leading to the mobility of Re and/or Os, is thought to have occurred within the last 2 billion years of the

chondrites initial accretion, and in some cases may have resulted from very recent terrestrial alteration (e.g. Day et al., 2016b; Archer et al., 2014).

All the NWA samples measured in this study show some evidence for terrestrial alteration. NWA 869 (L3-6) shows Re addition through its high Re abundance and high $^{187}Re/^{188}Os$ content (Table 9; Figure 19), indicating open-system behavior within the sample. Evidence of terrestrial alteration is corroborated through the samples high abundances of Sr and Ba (Figure 8b). NWA 5958 ($C2_{ung}$) shows Re loss through its Re abundance (Table 9), as well as an anomalously low $^{187}Re/^{188}Os$ ratio of 0.188. Again, NWA 5958 shows increases in Ba, U and Sr, suggestive of terrestrial weathering (Figure 7a). NWA 4502 (CV3) shows Re depletion similar to NWA 5958, however, because no trace element data was measured for this particular sample, the only conclusive information to be provided is that at some point in its history, the sample went through some amount of open-system behavior. As NWA 4502 is a find and not a fall, this would suggest, however, that terrestrial alteration is a likely explanation for the Re loss and low $^{187}Re/^{188}Os$ ratio seen (Figure 19).

Another sample which shows a Re disturbance is the Murchison – SIGL sample. For this sample there is a significant Re addition (Re – 85.8μg/g; $^{187}Re/^{188}Os$ – 0.722), however, because this sample is a fall it is difficult to explain where this Re addition came from. Anecdotal evidence is that some fragments of Murchison fell in farm-yard waste (J. Wasson pers comm to J. Day in 2014), but the cause of Re mobilization is unclear in this content. Alternatively, some fragments of the meteorite were collected sometime after the observed fall. No trace element data was collect for the sample aliquot that was measured for HSE abundances, however, trace element data was collected for the Murchison – MTF 2005 and the Murchison – Fragment. Both samples showed an enrichment in Ba. The Murchison fragment was enriched in all incompatible trace elements relative to the other CM2 chondrites measured, however, its greatest enrichments were in Ba, Th, U, La, Ce and Zr. The high Ba, U, La and Ce enrichments would be suggestive of terrestrial alteration, but again, this chondrite was a “fall”, so some residence time on Earth

must have occurred to explain these enrichments. Like previous studies, the enrichments seen in the Murchison sample are not reproducible for other Murchison powders analyzed and therefore it is unclear as to if the results are from heterogeneous distribution on the parent body, or are due to terrestrial weathering (Braukmüller et al., 2018).

Recent studies have shown that the effects of terrestrial alteration can occur quickly. The results from Walker et al. (2018) show that the sample interaction with rain caused redistribution of Re, as well as minor amounts of Os, within small pieces of the chondrite meteorite Sutter's Mill. The study found that Re is the most vulnerable HSE to terrestrial effects, especially rain, and should therefore be carefully examined, given that even chondrites with short-term histories on Earth's surface can be affected. This has potential implications to the Murchison sample studied here. The sample was not picked up immediately after the fall and could have therefore experienced some amount of dew or rain from the environment it was found in, however, more research will need to be conducted.

5.3 Carbonaceous chondrites

Carbonaceous chondrites from this study show, on average, ~8% lower Re/Os concentrations than those of ordinary or enstatite chondrites, agreeing well with previous studies (Horan et al., 2003). The lower average $^{187}Os/^{188}Os$ ratios of this class of meteorites would suggest that this difference is a long-term effect (e.g. Walker et al., 2002; Horan et al., 2003) caused during the formation of the meteorite group. An argument has been made that the fractionation is due to early, high-temperature fractionation in the solar nebula (e.g. Horan et al., 2003). This argument is corroborated by studies such as Sylvester et al. (1990) and (1993), where fremdlinge from CV3 chondrites showed sub-chondritic Re/Os ratios, measurements of which were then used in thermodynamic modeling, resulting in data consistent with solar nebula processing; as well as in Berg et al. (2009), where refractory metal alloys were recovered and measured for Os, W, Mo and Ru to display evidence for nebular condensation formation processes (Fischer-Gödde et al., 2010). Open-system behavior or short-term effects for some of the carbonaceous chondrites is described in section 5.2.

Maralinga ($CK4_{an}$) is a unique sample from the suite of carbonaceous chondrites in regard to its Re abundance and Re-Os isotopic compositions. Its significantly low Re (21.8 μg/g) and $^{187}Re/^{188}Os$ (0.152) ratio yield one of the lowest $^{187}Os/^{188}Os$ (0.11351) ratios ever measured for a chondrite meteorite. Maralinga has been described previously and is a petrologically anomalous sample. Petrologic observations have shown that Maralinga contains ~50% matrix, ~50% chondrules and 3% CAIs (Keller et al., 1992), this is starkly different to the mean CK chondritic values of ~75% matrix, ~15% chondrules and rare CAIs (0.5%) (Krot et al., 2004). Interestingly, Noguchi (1993) reported Maralinga to have the highest Ni contents in its olivine, pentlandite, ilmenite, magnetite and pyroxenes within the CK chondrites measured in the study. However, when considering all carbonaceous chondrites from our bulk sample major element analysis, Maralinga has one of the lowest Ni contents. This could be a results of processes invoked by various studies showing CK chondrites to containt only minor amounts of FeNi metal (Fischer-Godde et al., 2010). It has been shown that most of the metal in these samples has been oxidized, resulting in the formation of secondary phases like magnetitie, FeO-rich silicates and HSE-reich sulfides, tellurides and arsenides (e.g. Geiger and Bischoff, 1989; Kallemeyn et al., 1991; Choi and Wasson, 2003). The, overall, relative enrichment of trace elements in Maralinga could be suggestive of a low degree of parent body thermal metamorphism. This could be further argued from previous studies measurements of Maralinga's high Ni content in many of its minerals, suggesting un-equilibrated fine-grained phases in the matrix compared to those measured in other CK-chondrites (e.g. Geiger and Bischoff, 1989; Huber et al., 2006).

The HSE ratios for various classes of chondrites are shown in Figure 17. For carbonaceous chondrites, the trends seen in the Re and Pd versus Ir plots show a significant offset from those slopes of ordinary and enstatite chondrites. Mixing models from previous studies suggest that CI-like matrix compositions with CAI-like refractory rich components, processed under different nebular conditions could yield the bulk carbonaceous chondrite geochemical compositions (e.g. Fischer-Gödde et al., 2010; Wolf et al., 1980; Horan et al., 2003; Brandon et al., 2005b). Palladium, being one of the more volatile siderophile elements, shows that carbonaceous chondrites may have formed or were processed under different nebular

conditions than ordinary or enstatite chondrites (Figure 17, Pd versus Ir). The Re versus Ir plot for carbonaceous chondrites shows the mobility or Re through secondary processing (e.g. parent body processing, terrestrial alteration). Interestingly, this plot could suggest that Re is more mobile in carbonaceous chondrites than in ordinary or enstatite chondrites, potentially due to more unstable phases in the meteorites, which are vulnerable to alteration processes. More analysis would need to be conducted on the components of carbonaceous chondrites to test the model discussed above.

Most of the trace element data measured for the carbonaceous chondrites was used to determine terrestrial alteration effects of specific samples. In general, the trace element data for a majority of the carbonaceous chondrites are similar to CI-chondrite measurements. This would suggest that secondary processes, such as thermal metamorphism on the parent body, have only has minor effects on the bulk composition of carbonaceous chondrites (Braukmüller et al., 2018).

5.4 Ordinary chondrites

Generally, measurements of HSE in ordinary chondrites show decreasing HSE abundance from H > L > LL, which is consistent with increasing HSE partitioning into metal phases. The Re and Os concentrations of ordinary chondrites are generally higher than those of the other groups measured in this study, likely due to their higher metal content than other groups. New HSE data from this study agrees with previous conclusions that petrologic type (Figure 15) does not influence refractory elements in bulk rocks and therefore is unlikely that isochemical thermal metamorphism had a significant effect on these samples (e.g. Fischer-Gödde et al., 2010; Kallemeyn et al., 1989). As is suggested by Fischer-Gödde et al., 2010, the process that led to high or low metal abundances within ordinary chondrites did not pointedly fractionate the HSE from each other. It becomes possible then, that the HSE patterns seen in ordinary chondrites could have been established before the parent bodies of the ordinary chondrites were formed.

Similar to the carbonaceous chondrites, trace element data allowed the observation of terrestrial alteration in a few samples from the ordinary chondrite suite (e.g. NWA 869). It is important to note that the "high-iron" ordinary chondrites show less variation in incompatible trace elements, but this may just reflect the number of samples measured for high-iron ordinary chondrites compared to that of low-iron ordinary chondrites. The trace element data does not reflect an effect on the incompatible elements due to petrologic grade, similar to the results seen for the HSE.

The oxygen isotope data from this study yielded some interesting results. Figure 13 shows the $\delta^{17}O$ versus $\delta^{18}O$ values of samples from Yurimoto et al. (2008) and this study. The regression line for ordinary chondrites measured in this study is drastically different from that of Yurimoto et al. (2008). This could be due to the fact that not as many samples were measured in Yurimoto et al. (2008) and therefore, neither that nor this study are entirely representative of the oxygen isotopic systematics for ordinary chondrites. However, both studies showed a separation of trends between carbonaceous and ordinary chondrites. Oxygen isotopes are subjected to changes during aqueous alteration and thermal metamorphism on the parent bodies from which the chondrites are eventually derived (Yamanobe et al., 2018). Therefore, the oxygen isotopic data from this study reflects the different formation conditions and processing that has occurred between chondrite classes (e.g. carbonaceous and ordinary).

5.5 Enstatite chondrites

The HSE abundance data from the four enstatite chondrite meteorite samples measured in this study agreed relatively well with previous studies. Khairpur (EL6) showed anomalously high abundances compared to the other samples and previous measurements on various enstatite chondrites (Figure 16). The similar slopes seen in Figure 17 for the Os/Ir, Ru/Ir and Pt/Ir ratios for enstatite and ordinary chondrites would suggest similar histories for the components that hold the refractory elements within both of these classes (e.g. Fischer-Gödde et al., 2010; Y and Ho, Pack et al., 2007). The HSE abundances in EL chondrites measured from this study show similar compositions to both EL and EH chondrites from previous studies (e.g. Horan et al., 2003;

Fischer-Gödde et al., 2010). This would suggest that the HSE fractionation processes that occurred in EL chondrites were likely occurring in EH chondrites as well.

Generally, EL6 chondrites are considered be strongly affected by brecciation and/or impact melting (e.g. Rubin et al., 2009; Barrat et al., 2014). Trace element data from previous studies have shown negative Sm and Yb anomalies, thought to be a nebular signature, in EH3 and EL3 residues, however, as with these previous studies, no such anomaly is seen in the EL6 sample, indicating that such signatures may have been erased through metamorphism or impact melting processes (e.g. Barrat et al., 2014). While previous studies have suggested that all EL chondrites belong to the same metamorphic sequence, the lack of diversity among our sample suite for enstatite chondrites does not allow us to consider this idea further. Rubin et al. (2009), suggested that EL6 chondrites could be compositional residues of EL3 chondrites after the extraction of plagioclase- and oldhamite-bearing melt. Ca-depletion in EL6 chondrites is necessary for this model, but even so, it is difficult to prove (Barrat et al., 2014). Given the measurements included here, further proof of this idea is beyond the scope of this study.

5.6 Chelyabinsk in context

Analysis of individual mineral and chondrule components of the Chelyabinsk ordinary chondrite meteorite fall has yielded important information on the sample – and the components of chondrites - that could otherwise be overlooked through bulk sample analysis in isolation. Considering the various mineral phases of this chondrite yields information not only on the formational environment of its metals, but also its parent body processes.

The HSE abundances of the various components of the Chelyabinsk chondrite give information on the mobility of these elements during accretionary and parent body processing. Two types of metals were measured in the Chelyabinsk chondrite. The type-1 metal contained higher concentrations of Pd and Au, previous studies show that high-Ni metals in chondrites contain higher Pd and Au relative to low-Ni metals while the remaining PGEs remain nearly unfractionated between the two groups (Campbell & Humayun, 2003) Furthermore, previous

studies show that this pattern of HSE is the same as ones observed in kamacite/taenite partitioning in ordinary chondrites and iron meteorites (e.g. Narayan and Goldstein, 1985; Campbell and Humayun, 1999). The refractory HSE are nearly the same for both metals suggesting equilibration, likely between the kamacite and taenite. Slow cooling allows these metal phases to equilibrate, but in such a case, the Ni contents of both phases would have increased (Campbell & Humayun, 2003). Further research into the petrology of these metal phases would be required in order to understand the Ni-content and distribution in the phases.

5.7 Implications for siderophile and volatile element distributions in planetary feedstock materials

The history of planets, such as Earth, can be discussed through the information provided by chondrites. Considering that HSE partition into metal phases during metal-silicate equilibration, it is expected that these elements would be sequestered to the Earth's core. However, measured HSE abundances in silicate Earth are higher than predicted by metal-silicate partitioning experiments (e.g., Day et al. 2016b; Mann et al. 2012). These elevated abundances of the HSE in the bulk silicate Earth are thought to have occurred through late accretion of primitive material after core formation (e.g., Kimura et al., 1974; Chou, 1978; Becker et al., 2006; Hopp & Kleine, 2018). It has been argued that during late accretion, approximately ~0.5 wt% of chondritic material was added to the bulk silicate Earth (Walker et al., 2015). However, the nature of the chondritic material and whether it was carbonaceous, ordinary, enstatite, or something entirely distinct, is debated.

Studies such as Walker et al. (2002) and Meisel et al. (1996) suggest, based on Os isotopes and HSE abundances that enstatite or ordinary chondrite compositions are likely the late accretionary material. Platinum-osmium and rhenium-osmium isotope data support similar compositions (e.g., Brandon et al., 2005; Day et al., 2017). Whereas other studies, again based on Os isotopes and HSE abundances, suggest a carbonaceous chondrite-like material with chemically evolved metal components, such as those seen in some iron meteorites are the source of late accretionary material (Fischer-Gödde & Becker, 2012). To further compound this debate, data on lunar impact melt breccias imply an entirely different population of impactors from

modern chondrites striking the Moon at 3.8 Ga (e.g., Puchtel et al., 2008). Having a better understanding of the type of late accretionary material that was likely added to Earth is important to understanding, not only the later-stages of planetary formation, but could also to link the source of Earth's water and highly volatile element compositions (Wang & Becker, 2013).

Ordinary chondrites represent approximately 80% of the observed modern chondritic falls (Kallemeyn et al., 1989) and are thought to originate from the inner portion of the asteroid belt (Rubin, 2013). Scientists in Sweden have discovered dozens of ordinary chondrites within 470 Ma rocks, suggesting that ordinary chondrites have been falling to Earth for more than 10% of the planet's history (Schmitz et al., 2016). Furthermore, recent studies have revealed that the chondritic $\delta^{102/99}$Ru of Earth's mantle suggests that the $^{187}Os/^{188}Os$ difference between carbonaceous chondrites and the mantle cannot be compensated through admixture of a differentiated metal component, as the elevated $\delta^{102/99}$Ru of this component would result in a higher-than-chondritic $\delta^{102/99}$Ru value in the present-day bulk-silicate Earth (Hopp & Kleine, 2018). It would therefore seem, that the ordinary chondrite class is one of the most significant sources for HSE abundances in the bulk silicate Earth. The new data from this study support similarities between ordinary chondrites and bulk silicate Earth.

Carbonaceous chondrites, on the other hand make up approximately 5% of chondritic falls (Kallemeyn and Wasson, 1981). The high abundance of organic compounds often found in this class would suggest an origin further from the sun than that of the ordinary chondrites (Rubin, 2013). Given the hypothesized regions of the Solar System that these chondrites are sourced from, it is less likely that these two groups contributed significantly to late-accretion addition of the HSE. Marty, (2012) demonstrated through stable and noble gas isotopes that the source of Earth's volatiles is likely chondritic. Furthermore, the study noted that the fractionation of water and carbon incorporated in the Earth verses the higher noble gas concentrations in the atmosphere, is representative of active exchanges of volatile elements between the mantle and the surface of the Earth. This high water and carbon concentration of bulk Earth would suggest that the accretion of volatile elements from wet planetesimals occurred during the main Earth forming event, rather than a contribution of late-accretionary material (Marty, 2012).

Enstatite chondrites make up approximately 2% of the chondritic falls (Rubin, 2013). These rare chondrites are thought to be sourced from the orbit of Mars, considerably closer to the sun than other chondritic groups (e.g. Kallemeyn and Wasson, 1986; Rubin, 2013). Given the rarity of these samples, it would be difficult to argue for this group to be a significant contributor to late accretionary material, such as that described for ordinary chondrites.

5.8 Future work

Despite the size of this sample set, expanding the suite further to include more samples from various groups (e.g. CK, LL, EL, EH) would help close gaps left in the interpretation of the data collected. Furthermore, measuring more samples from groups already included would allow a more representative perspective on the geochemical and petrological characteristics of a group as a whole (e.g. LL). Making thin sections of more samples included in this suite would be a good step in obtaining important data on how various elements are fractionated into different phases of chondrites. This would be an important step in developing ideas as to how bulk sample compositions are attained.

Much of the time analysis on chondrites is constricted by the material available. While whole-rock major- and trace-element analysis is not always possible if there is limited material, this study demonstrates the benefits to doing such analysis. The complementary trace-element data allows conformation of processes effecting HSE such as Re & Os (e.g. terrestrial alteration).

Special attention to the study of Maralinga, Murchison and Khairpur would be a good step to understanding what makes these samples anomalous to others within their group. Obtaining thin sections of all three of these samples would be a good initial step in further developing their measured characteristics.

6. Conclusions

Chondrites are fundamental in understanding the history of our Solar System. Understanding the variations among the major classes of chondrites allow us to understand the various formational conditions these unique samples accreted from. Furthermore, understanding the various processing that occurred on the parent bodies of chondrites gives us insights into, not only their development as complex geochemical samples, but the development of our own planet.

This study has made clear the issue of heterogeneities within sample aliquots. Sample sizes and sample preparation give rise to aliquots that may not necessarily be representative of a bulk chondrite. While this issue is not easy to resolve, based on the availability of material and the preparation techniques, it is important to be recognized as an aspect of this kind of study.

The use of chemical analysis, laser ablation and thermal ionization mass-spectrometry has provided this thesis with a significant data set from which information about the histories of these samples can be revealed. The Re-Os isotopic systematics and complementary trace-element data yield clear evidence of terrestrial alteration for samples such as NWA869, NWA5958 and NWA4502. HSE ratios and oxygen isotopes provided evidence for formational environments and parent body processes that produce distinct geochemical characteristics for both the carbonaceous and ordinary chondrite classes. Even further, the close attention paid to the Chelyabinsk meteorite fall, through chemical and laser ablation analysis of the mineral phases, gives further detail of parent body processes, such as evidence for shock metamorphism, occurring after its initial accretion.

Although future efforts will need to be undertaken in order to gain further insights into the various processes hypothesized in the discussion sections, this study has significantly enriched the data thus far collected on various chondrite samples from different classes.

References

Al-Kathiri A., Hofmann B.A., Jull A.J.T., Gnos E., 2005. Weathering of meteorites from Oman: Correlation of chemical and mineralogical weathering proxies with ^{14}C terrestrial ages and the influence of soil chemistry. *Meteoritics and Planetary Science*, v. 40, 1215-1239.

Allen Jr. R.O. and Mason B., 1973. Minor and trace elements in some meteoritic minerals. *Geochimica et Cosmochimica Acta*, v. 37, 1435-1456.

Anders E., and Grevesse N., 1989. Abundances of the elements: Meteoritic and solar. *Geochimica et Cosmochimica Acta*, v. 53, 197-214

Archer G.J., Ash R.D., Bullock E.S., Walker R.J., 2014. Highly siderophile elements and ^{187}Re-^{187}Os isotopic systematics of the Allende meteorite: evidence for primary nebular processes and late-stage alteration. *Geochimica et Cosmochimica Acta*, v. 131, 402-414.

Arnould M., 1976. Possibility of synthesis of proton-rich nuclei in highly evolved stars. II. *Astronomy and Astrophysics*, v. 46, 117-125.

Arnould M. and Takahashi K., 1999. Nuclear astrophysics. *Reports on Progress in Physics*, v. 62, 395.

Arnould M. and Goriely S., 2003. The p-process of stellar nucleosynthesis: astrophysics and nuclear physics status. *Physics Reports*, v. 384, 1-84.

Barrat J.A., Zanda B., Jambon A., Bollinger C., 2014. The lithophile trace elements in enstatite chondrites. *Geochimica et Cosmochimica Acta*, v. 128, 71-94

Barrat J.A., Zanda B., Moynier F., Bollinger C., Liorzou C., Bayon G., 2012. Geochemistry of CI chondrites: Major and trace elements, and Cu and Zn Isotopes. *Geochimica et Cosmochimica Acta, v. 83*, 79-92.

Becker H., Horan M.F., Walker R.J., Gao S., Lorand J.-P., Rudnick R.L., 2006. Highly siderophile element composition of the Earth's primitive upper mantle: Constraints from new data on peridotite massifs and xenoliths. *Geochimica et Cosmochimica Acta*, v. 70, 4528-4550.

Bennett J., Donahue M., Schneirder N., Voit M., *The Cosmic Perspective*. 4th ed. San Francisco: Pearson Education, Inc., 2007.

Berg T., Marosits J., Maul J., Schönhense G., Hoppe P., Ott U., Palme H., 2009. Evidence for nebular condensation of sub-micron refractory metal alloys. *Lunar and Planetary Science Conference* 2009, 1585.

Bethe H.A., 1996. Supernova theory. *Nuclear Physics A*, v. 606, I 1-2, 95-117.

Bogard D.D., 2011. K-Ar ages of meteorites: Clues to parent-body thermal histories. *Chemie der Erde – Geochemistry*, v. 71, 207-226.

Bogert C.H., Schultz P.H., and Spray J.G., 2003. Impact-induced frictional melting in ordinary chondrites: A mechanism for deformation, darkening, and vein formation. *Meteoritics and Planetary Science*, v. 38. 1521-1531.

Bouvier A. and Boyet M., 2016. Primative Solar System materials and Earth share a common initial ^{142}Nd abundance. *Nature*, v. 537, 399-402.

Boyet M., and Carlson R.W., 2005. ^{142}Nd Evidence for Early (>4.53 Ga) Global Differentiation of the Silicate Earth. *Science*, v. 309, 576-581.

Brandon A.D., Humayun M., Puchtel I.S. and Zolensky M.E., 2005a. Re-Os isotopic systematics and platinum group element composition of the Tagish Lake carbonaceous chondrite. *Geochimica et Cosmochimica Acta, v. 69,* 1619-1631.

Brandon A.D., Humayun M., Puchtel I.S., Leya I., Zolensky M., 2005b. Osmium isotope evidence for an s-process carrier in primitive chondrites. *Science*, v. 309, 1233-1236.

Braukmüller N., Wombacher F., Hezel D.C., Escoube R., Münker, 2018. The chemical composition of carbonaceous chondrites: implication for volatile element depletion, complementarity and alteration. *Geochimica et Cosmochimica Acta (2018),* doi: https://doi.org/10.1016/j.gca.2018.07.023

Brearley A.J. & Jones R.H., 1998. Chondritic meteorites. In *Planetary Materials* (J.J. Papike ed.), 3-1 to 3-398. *Reviews in Minerology*, v. 36, Mineralogical Society of America.

Browning L.B., Mcsween H.Y. Jr., and Zolensky M.E., 1996. Correlated alteration effects in CM carbonaceous chondrites. *Geochimica et Cosmochimica Acta,* 60, 2621-2633.

Bunch T.E., Irving A.J., Wittke J.H., Rumble D., Hupe G., 2011. Petrology and extreme oxygen isotopic composition of type 3.00 carbonaceous chondrite Northwest Africa 5958: a unique, primitive ^{16}O-rich early Solar System sample. *Lunar and Planetary Science* XXXXII. Lunar and Planetary Institute, Houston. #1683 (abstract).

Burkhardt C., Borg L.E., Brennecka G.A., Shollenberger Q.R., Dauphas N., Kleine T., 2016. A nucleosynthetic origin for the Earth's anomalous ^{142}Nd composition. *Nature*, v. 537, 394-398.

Burles S., Nollett K.M., and Turner M.S., 2001. Big Bang nucleosynthesis predictions for precision cosmology. *The Astrophysical Journal*, v. 552, L1-L5.

Busso M., Gallino R., Wasserburg G.J., 1999. Nucleosynthesis in Asymptotic Giant Branch Stars: Relevance for Galactic Enrichment and Solar System Formation. *Annual Review of Astronomy and Astrophysics*, v. 37, 239-309.

Campbell A.J., and Humayun M., 1999. Microanalysis of platinum group elements in iron meteorites using laser anliation ICP-MS (abstract 1974). *Lunar and Planetary Science* XXX (CD-ROM). Lunar and Planetary Institute.

Campbell A.J., Humayun M., Krot A., Keil K., 2001. Origin of zoned metal grains in the QUE 94411 chondrite. *Geochimica et Cosmochimica Acta*, 65, 163-180.

Campbell A.J., Humayun M., Weisberg M.K. 2002. Siderophile element constraints on the formation of metal in the metal-rich chondrites, Bencubbin, Gujba, and Weatherford. *Geochimica et Cosmochimica Acta*, 66, 647-660.

Campbell A.J., Humayun M., 2003. Formation of metal in Grosvenor Mountains 95551 and comparison to ordinary chondrites. *Geochimica et Cosmochimica Acta,* v. 67, 2481-2495.

Chaisson E., and McMillan S., 1999. *Astronomy Today*, 3rd Edition, Prentice-Hall.

Choi B-G. and Wasson J.T., 2003. Microscale oxygen isotopic exchange and magnetite formation in the Ningqiang anomalous carbonaceous chondrite. *Geochimica et Cosmochimica Acta,* v. 67, 4655-4660.

Chou C.-L. 1974. Fractionation of Siderophile Element Ratios in the Earth's Upper Mantle and Lunar Samples, *Lunar and Planetary Science*, IX, (1058).

Clayton R.N., Mayeda T.K., Rubin A.E., 1984. Oxygen isotopic compositions of enstatite chondrites and aubrites. *Proc. Lunar Planet Scientific Conference 15th*, in *Journal of Geophysics Research*, 89, C245-C249.

Clayton R.N. and Mayeda T.K., 1999. Oxygen isotope studies of carbonaceous chondrites. *Geochimica et Cosmochimica Acta,* v. 63, 2089-2014.

Coc A., 2009. Big-bang nucleosynthesis: A probe of the early Universe. *Nuclear Instruments and Methods in Physics Research Section A: Accelerators, Spectrometers, Detectors and Associated Equipment*, v. 611, I. 2-3, 224-230.

Cohen A.S., Waters F.G., 1996. Separation of osmium from geological materials by solvent extraction for analysis by thermal ionization mass spectrometry. *Analytica Chimica Acta*, v. 332, 269-275.

Corder, C.A., 2015. Primitive and differentiated achondrite meteorites and partial melting in the early Solar System. Master's thesis, University of California, San Diego, 2015, Earth Sciences, UC San Diego (b8882274).

Criss R.E., Farquhar J., 2008. Abundance, notation and fractionation of light stable isotopes. *Reviews in Mineralogy and Geochemistry*, v. 68, 15-30.

Crozaz G., Floss C., Wadhwa M., 2003. Chemical alteration and REE mobilization in meteorites

from hot and cold deserts. *Geochimica et Cosmochimica Acta,* v. 67, 4727-4741.

Day J.M.D., Corder C.A., Rumble III D., Assayag N., Cartigny P., Taylor L.A., 2015. Differentiation processes in FeO-rich asteroids revealed by the achondrite Lewis Cliff 88763. *Meteoritics and Planetary Science*, v. 50, 1750-1766.

Day J.M.D., 2015. Planet formation processes revealed by meteorites. Geology Today, v. 31, 12-20.

Day J.M.D., Waters C.L., Schaefer B.F., Walker R.J., Turner S., 2016a. Use of Hydrofluoric Acid Desilicification in the Determination of Highly Siderophile Element Abundances and Re-Pt-Os Isotope Systematics in Mafic-Ultramafic Rocks. *Geostandards and Geoanalytical Research,* v. 40, 49-65.

Day J.M.D., Brandon A.D., Walker R.J., 2016b. Highly Siderophile Elements in Earth, Mars, the Moon, and Asteroids. *Reviews in Mineralogy and Geochemistry,* v. 81, 161-238.

Day J.M.D., 2016. Extraordinary world. *Nature*, v. 537, 310-311.

Day J.M.D., Corder C.A., Cartigny P., Steele A., Assayag N., Rumble III D., Taylor L.A., 2017. A carbon-rich region in Miller Range 091004 and implications for ureilite Petrogenesis. *Geochimica et Cosmochimica Acta,* v. 198, 379-395.

Dhaliwal J.K., Day J.M.D., Corder C.A., Tait K.T., Marti K., Assayag N., Cartigny P., Rumble III D., Taylor L.A., 2017. Early metal-silicate differentiation during planetesimal formation revealed by acapulcoite and lodranite meteorites. *Geochimica et Cosmochimica Acta, v.* 216, 115-140.

Endress M. and Bischoff A. 1996. Carbonates in CI chondrites: Clues to parent body evolution. *Geochimica et Cosmochimica Acta,* 60, 489-507.

Fischer-Gödde, M., Becker, H., Wombacher, F., 2010. Rhodium, gold and other highly siderophile element abundances in chondritic meteorites, *Geochimica et Cosmochimica Acta, v. 74,* 356-379.

Friedrich J.M., Wang M-S, Lipschutz M.E., 2002. Comparison of the trace element composition of Tagish Lake with other primitive carbonaceous chondrites. *Meteoritics and Planetary Science,* v. 37, 677-686

Friedrich J.M, Wang M-S., Lipschutz M.E., 2003. Chemical studies of L chondrites. V: compositional patterns for 49 trace elements in 14 L4-6 and 7 LL4-6 falls. *Geochimica et Cosmochimica Acta, v.* 67, 2467-2479.

Geiger T. and Bischoff A., 1989. (Os, Ru, Ir)S2 and other refractory siderophile element-rich particles in the metamorphosed carbonaceous chondrites Karoonda, Mulga (West) and PCA82500. *Lunar and Planetary Science Conference,* XX, 335-336.

Göpel C., Birck J-L, Galy A., Barrat JA., Zanda B., 2015. Mn-Cr systematics in primitive meteorites: Insights from mineral separation and partial dissolution. *Geochimica et Cosmochimica Acta, v.* 156, 1-24.

Hopp T. and Kleine T., 2018. Nature of late accretion to Earth inferred from mass-dependent Ru isotopic composition of chondrites and mantle peridotites. *Earth and Planetary Science Letters*, v. 494, 50-59.

Horan, M.F., Walker, R.J., Morgan, J.M., Grossman, J.N., and Rubin, A.E., 2003. Highly Siderophile elements in chondrites, *Chemical Geology,* v. 196, 5-20.

Hoyle F., 1954. On nuclear reactions occurring in very hot stars. I. The synthesis of elements from carbon to nickel. *Astrophysical Journal Supplement* 1, 121-146.

Hubble E. and Humason M.L., 1931. The velocity-distance relation among extra-galactic nebulae. *Astrophysical Journal*, v. 71, 43-80.

Huber H., Rubin A.E., Kallemeyn G.W., Wasson J.T., 2006. Siderophile-element anomalies in CK carbonaceous chondrites: Implications for parent-body aqueous alteration and terrestrial weathering of sulfides. *Geochimica et Cosmochimica Acta,* v. 70, 4019-4037.

Hyde B.C., Day J.M.D., Tait K.T., Ash R.D., Holdsworth D.W., & Moser D.E., 2014. Characterization of weathering and heterogeneous mineral phase distribution in brachinite Northwest Africa 4872. *Meteoritics & Planetary Science*, v. 49, 1141-1156.

Jacquet E., Alard O., Gounelle M., 2015. Trace element geochemistry of ordinary chondrite chondrules: The type I/type II chondrules dichotomy. *Geochimica et Cosmochimica Acta,* v. 155, 47-67.

Jarosewish E., Clarke R.S., Barrows J.N., 1987. The Allende meteorite reference sample. *Smithson Contributions, Earth Science*, v. 27, 1-49.

Jochum K.P. 1996. Rhodium and other platinum-group elements in carbonaceous chondrites. *Geochimica et Cosmochimica Acta, v.* 60, 3353-3357.

Jones R.H., McCubbin F.M., Dreeland L., Guan Y., Burger P.V., Shearer C.K., 2014. Phosphate minerals in LL chondrites: A record of the action of fluids during metamorphism on ordinary chondrite parent bodies. *Geochimica et Cosmochimica Acta,* v. 132, 120-140.

Kallemeyn G.W., Boynton W.V., Willis J., Wasson J.T., 1978. Formation of the Bencubbin polymict meteoritic breccia. *Geochimica et Cosmochimica Acta,* 42, 507-515.

Kallemeyn G.W. and Wasson J.T., 1981. The compositional classification of chondrites-I. The carbonaceous chondrite groups. *Geochimica et Cosmochimica Acta,* v. 45, 1217-1230.

Kallemeyn G.W., Rubin A.E., Wang D., Wasson J.T., 1989. Ordinary chondrites: bulk

compositions, classification, lithophile-element fractionation, and composition petrographic type relationships. *Geochimica et Cosmochimica Acta, v.* 53, 2747-2767.

Kallemeyn G.W. and Wasson J.T., 1986. Composition of enstatite (EH3, EH4,5 and EL6) chondrites: implications regarding their formation. *Geochimica et Cosmochimica Acta, v.* 50, 2153-2164.

Kallemeyn G.W., Rubin A.E., Wasson J.T., 1991. The compositional classification of chondrites: V. The Karoonda (CK) group of carbonaceous chondrites. *Geochimica et Cosmochimica Acta*, 55, 881-892.

Käppeler F., 2007. Reaction rates, nucleosynthesis, and stellar structure. *Nuclear Instruments and Methods in Physics Research Section B: Bean Interactions with Materials and Atoms,* v. 259, I.1, 663-668.

Keil K., 1968. Mineralogical and chemical relationships among enstatite chondrites. *Journal of Geophysical Research*, 73, 6945-6976.

Keller L.P., Clark J.C., Lewis C.F., Moore C.B., 1992. Maralinga, a metamorphosed carbonaceous chondrite found in Australia. *Meteoritics*, v. 27, 87-91.

Kimura K., Lewis R.S., Anders E., 1974. Distribution of gold and rhenium between nickel-iron and silicate melts: implications for the abundance of siderophile elements on the Earth and Moon, *Geochimica et Cosmochimica Acta,* v. 38, 683-701.

Krot A.N., Scott E.R.D., Zolensky M.E., 1995. Minerologic and chemical variation among CV3 chondrites and their components: Nebular and astroidal alteration. *Meteoritics*, 30, 748-775.

Krot A.N., Petaev M.I., Scott E.R.D., Choi B.-G., Zolensky M.E., Keil K., 1998. Progressive alteration in CV3 chondrites: More evidence of astrodial alteration. *Meteoritics and Planetary Science*, 33, 1065-1085.

Krot A.N., Meibom A., Weisberg M.K., and Keil K., 2002. The CR chondrite clan: Implications for early Solar System processes. *Meteoritics and Planetary Science*, 37, 1451-1490.

Krot A.N., Petaev M.I., Bland P.A., 2003. Growth of ferrous olivine in the oxidized CV chondrites during fluid-assisted thermal metamorphism (abstract). *Meteoritics and Planetary Science*, 38, A73.

Krot A.N., Keil K., Goodrich C.A., Weisberg M.K., Scott E.R.D., 2004. Classification of meteorites. A.M. Davis (Ed.), *Treatise of Geochemistry*, v. 1, Elsevier-Pergamon, 83-128.

Langanke K., Martinez-Pinedo G., Petermann I., Thielemann F.K., 2011. Nuclear quests for supernova dynamics and nucleosynthesis. *Progress in Particle and Nuclear Physics*, v. 66, I. 2, 319-328.

Lee M.R. & Bland P.A., 2004. Mechanisms of weathering of meteorites recovered from hot and cold deserts and the formation of phylosilicates. *Geochimica et Cosmochimica Acta,* v. 68, 893-916.

Lemaitre G. 1931. The expanding universe. *Monthly Notices of the Royal Astronomical Society*, v. 91, 490-501.

Leshin L.A., Rubin A.E., McKeegan K.D., 1997. The oxygen isotopic composition of olivine and pyroxene from CI chondrites. *Geochimica et Cosmochimica Acta,* 61, 835-845.

Lin Y., and El Goresy A., 2002. A comparative study of opaque phases in Qingzhen (EH3) and MacAlpine Hills 88136 (EL3): Representatives of EH and EL parent bodies. *Meteoritics and Planetary Science,* v. 37, 577-599.

Mann U., Frost D.J., Rubie D.C., Becker H., Audétat A., 2012. Partitioning of Ru, Rh, Pd, Re, Ir and Pt between liquid metal and silicate at high pressures and high temperatures – implications for the origin of highly siderophile element concentrations in the Earth's mantle. *Geochimica et Cosmochimica Acta,* v. 84, 593-613.

Marty B., 2012. The origins and concentrations of water, carbon, nitrogen and noble gases on Earth. *Earth and Planetary Science Letters,* v 313-314, 56-66.

McDonald I., Andreoli, M.A.G., Hart R.J., Tredoux M. 2001. Platinum group elements in the Morokweg impact structure, South Africa: evidence for the impact of a large ordinary chondrite projectile at the Jurassic-Cretaceous boundary. *Geochimica et Cosmochimica Acta, v.* 65, 299-309.

McKeegan K.D., Leshin L.A., 2001. Stable isotope variations in extraterrestrial materials. *Reviews in Mineralogy and Geochemistry,* v. 43, 279-318.

McSween H.Y. Jr. 1977. Petrographic variations among carbonaceous chondrites of the Vigarano type. *Geochimica et Cosmochimica Acta,* 41, 1777-1790.

McSween H.Y. Jr., 1979. Are carbonaceous chondrites primitive of processed? A review. *Reviews of Geophysics and Space Physics,* 17, 1059-1078.

McSween H.Y. Jr. and Richardson S.M., 1977. The composition of carbonaceous chondrite matrix. *Geochimica et Cosmochimica Acta,* 41, 1145-1161.

Meibom A., Petaev M.I., Krot A.N., Keil K., and Wood J.A., 2001. Growth mechanism and additional constraints on FeNi metal condensation in the solar nebula. *Journal of Geophysical Research,* 106, 32797-32801.

Meyer B.S., 1994. The r-, s- and p-processes in Nucleosynthesis. *Annual Review of Astronomy and Astrophysics,* v. 32, 153-190.

Mittlefehldt D.W., 2002. Geochemistry of the ungrouped carbonaceous chondrite Tagish Lake, the anomalous CM chondrite Bells, and comparison with CI and CM chondrites. *Meteoritics and Planetary Science*, v. 37, 703-712.

Morgan J.W., Janssens M.-J., Takahashi H., Hertogen J., Anders E., 1985. H-chondrites: trace element clues to their origin. *Geochimica et Cosmochimica Acta, v.* 49, 247-259.

Narayan C., and Goldstein J.I., 1985. A major revision of the iron meteorite cooling rates-An experimental study of the growth of the Widmanstätten pattern. *Geochimica et Cosmochimica Acta,* v. 49, 397-410.

Noguchi T., 1993. Petrology and mineralogy of the CK chondrites: Implications for the metamorphism of the CK chondrite parent body. *Proc. NIPR Symposium, Antarctic Meteorites*, v. 7, 30-41

Norman M.D. and Mittlefehldt D.W., 2001. Imapct processing of chondritic planetesimals: Siderophile and volatile element fractionation in the Chico L chondrite. *Meteoritics & Planetary Science,* v. 37, 329-344

Olive K.A., Steigman G., Walker T.P., 2000. Primordial nucleosynthesis: theory and observations. *Physics Reports,* v. 333-334, 389-407.

Pack A., Russell S.S., Shelley J.M.G., and van Zuilen M., 2007. Geo- and cosmochemistry of the twin elements yttrium and holmium. *Geochimica et Cosmochimica Acta,* v. 71, 4592-4608.

Penzias A.A. & Wilson R.W., 1965. A measurements of excess antenna temperature at 4080 Mc/S. Astrophysical Journal, v. 142, 419-421.

Petaev M.I., Meibom A., Krot A.N., Wood J.A., Keil K., 2001. The condensation origin of zoned metal grains in Queen Alexandra Range 94411: Implications for the formation of the Bencubbin-like chondrites. *Meteoritics and Planetary Science,* 36, 93-106.

Puchtel I.S., Walker R.J., James O.B., Kring D.A., 2008. Osmium isotope and highly siderophile element systematics of lunar impact melt breccias: Implications for the late accretion history of the Moon and Earth, *Geochimica et Cosmochimica Acta,* v. 72, 3022-3042.

Rubin A.E., 1990. Kamacite and olivine in ordinary chondrites: Intergroup and intragroup relationships. *Geochimica et Cosmochimica Acta,* v. 54, 1217-1232.

Rubin A.E., Huber H., Wasson J.T., 2009. Possible impact induced refractory-lithophile fractionations in EL chondrites. *Geochimica et Cosmochimica Acta,* v. 73, 1523-1537.

Rubin A.E., 2013. Secrets of Primitive Meteorites. *Scientific American,* February 2013, 37-41.

Rumble D., Farquhar J., Young E.D., Christensen C.P., 1997. In situ oxygen isotope analysis with an excimer laser using F2 and Br F5 reagents and O2 gas as analyte. *Geochimica et Cosmochimica Acta,* v. 61, 4229-4234.

Schmitz B., Yin Q.-Z., Sanborn M.E., Tassinari M., Caplam C.E., Huss G.R., 2016. A new type of solar-system material recovered from Ordovician marine limestone. Nature Communications, v. 7, 1-7.

Scott E.R.D. and Krot A.N., 2007. 1.07 – Chondrites and Their Components. *Treatise on Geochemistry*, v. 1, 1-72.

Sears D.W.G., & Dodd R.T., 1988. Overview and classification of meteorites. In *Meteorites and the Early Solar System* (J.F. Kerridge & M.S. Matthews, eds.), 3-31. University of Arizona, Tucson.

Sears D.W.G., Hasan F.A., Batchelor J.D., Lu J., 1991. Chemical and physical studies of type 3 chondrites; XI, Metamorphism, pairing, and brecciation of ordinary chondrites. *Proceedings of the Lunar and Planetary Science Conference*, v. 22, 493-512.

Seeger P.A., Fowler W.A., Clayton D.D., 1965. Nucleosynthesis of heavy elements by neutron capture. Astrophysical Journal Supplement, v.11, 121-126.

Shinotsuka K., Hidaka H., Ebihara M., 1995. Detailed abundances of rare earth elements, thorium and uranium in chondritic meteorites: an ICP-MS study. *Meteoritics & Planetary Science,* v. 30, 694-699

Shirey S.B. and Walker R.J., 1995. Carius tube digestion for low-blank rhenium-osmium analysis. *Analytica Chimica Acta*, v. 67, 2136-2141.

Smoliar M.I., Walker R.J., Morgan J.W., 1996. Re-Os ages of group IIA, IIIA, IVA, and IVB iron meteorites. *Science* 271, 1099-1102.

Stracke A., Palme H., Gellissen M., Münker C., Kleine T., Birbaum K., Günther D., Bourdon B., Zipfel J., 2012. Refractory element fractionation in the Allende meteorite: Implications for solar nebula condensation and the chondritic composition of planetary bodies. *Geochimica et Cosmochimica Acta, v.* 85, 114-141.

Swindle T.D., Kring D.A., Burkland M.K., Hill D.H., Boynton W.V., 1998. Noble gases, bulk chemistry, and petrography of olivine-rich achondrites Eagles Nest and Lewis Cliff 88763: Comparison to brachinites. *Meteoritics & Planetary Science,* v. 33, 31-48.

Sylvester P.J., Ward B.J., Grossman L. and Hutcheon I.D., 1990. Chemical compositions of siderophile element-rich opaque assemblages in an Allende inclusion. *Geochimica et Cosmochimica Acta*, v. 54, 3491-3508.

Sylvester P.J., Simon S.B. and Grossman L., 1993. Refractory inclusions from the Leoville,

Efremovka, and Vigarano C3V chondrites: major element differences between types A and B, and extraordinary refractory siderophile element compositions. *Geochimica et Cosmochimica Acta,* v. 57, 3763-3784.

Tagle R., Berlin J., 2008. A database of chondrite analyses including platinum group elements, Ni, Co, Au, and Cr: Implications for the identification of chondritic projectiles. *Meteoritics & Planetary Science,* v. 43, 541-559

Takahashi H., Janssens M.-J., Morgan J.W., Anders E., 1978. Further studies of trace elements in C3 chondrites. *Geochimica et Cosmochimica Acta,* v. 42, 97-106.

Valley J.W., Kitchen N.E., Kohn M.J., Niendorf C.R., and Spicuzza M.J., 1995. UWG-2, a garnet standard for oxygen isotope ratios: Strategies for high precision and accuracy with laser heating. *Geochimica et Cosmochimica Acta,* v. 59, 5223-5231.

Van Schmus W.R. & Wood J.A., 1967. A chemical-petrologic classification for the chondritic meteorites. *Geochimica et Cosmochimica Acta,* v. 31, 747-765.

Walker, R.J., Horan, M.F., Morgan, J.W., Becker, H., Grossman, J.N., and Rubin, A.E., 2002. Comparative Re-Os systematics of chondrites: Implications regarding early Solar System processes, *Geochimica et Cosmochimica Acta, v. 66,* 4187-4201.

Walker R.J., Bermingham K, Liu J., Puchtel I.S., Touboul M., Worsham E.A., 2015. In search of late-stage planetary building blocks. Chemical Geology, v. 411, 125-142.

Walker R.J., Yin Q-Z, and Heck P.R., 2018. Rapid effects of terrestrial alteration on highly siderophile elements in the Sutter's Mill meteorite. *Meteoritics and Planetary Science*, v. 53, 1500-1506.

Wang Z., and Becker H., 2013. Ratios of S, Se and Te in the silicate Earth require a volatile-rich late veneer. *Nature*, v. 499, 328-331.

Weisberg M.K., 2001. Sahara 00182, the first CR3 chondrite and formation of multi-layered chondrules (abstract). *Meteoritics and Planetary Science*, 36, A222-A223.

Weisberg, M.K., McCoy, T.J., Krot, A.N., 2006. Systematics and Evaluation of Meteorite Classification. In: *Meteorites and the Early Solar System II,* ed. D.S. Lauretta and H.Y. McSween, Tucson, AZ: University of Arizona Press, pp. 19-52.

White, W.M. (2014). *Geochemistry*. Chichester, West Sussex: John Wiley & Sons, Ltd.

Wolf R., Richter G.R., Woodrow A.B., Anders E., 1980. Chemical fractionations in meteorites – XI. C2 chondrites. *Geochimica et Cosmochimica Acta,* v. 44, 711-717.

Woosley S.E. and Howard, W.M., 1978. The p-process in supernovae. *Astrophysical Journal Supplement Series*, v. 35, 285-304.

Yamanobe M., Nakamura T., Nakashima D., 2018. Oxygen isotope reservoirs in the outer asteroid belt inferred from oxygen isotope systematics of chondrule olivines and isolated forsterite and olivine grains in Tagish Lake-type carbonaceous chondrites, WIS 91600 and MET 00432. *Polar Science,* v. 15, 29-38.

Yokoyama T., Walker R.J., 2016. Nucleosynthetic Isotope Variations of Siderophile and Chalcophile Elements in the Solar System. *Reviews in Mineralogy & Geochemistry*, v. 81, 107-160.

Zolensky M.E., Weisberg M.K., Buchanan P.C., Mittlefehldt D.W., 1996. Minerology of carbonaceous chondrite clasts in HED achondrites and the moon. *Meteoritics and Planetary Science,* 31, 518-537.

Zolensky M.E., Nakamura K., Gounelle M., Mikouchi T., Kasama T., Tachikawa O., Tonui, 2002. Mineralogy of Tagish Lake: an ungrouped type 2 carbonacsous chondrite. *Meteoritics and Planetary Science,* v. 37, 737-761.

Tables

Table 1. Non-analytical characteristics of the chondrite sample set from this study

Chondrite	Sample ID	Classification	Fall/ Find	Mass of original chondrite	Year	Fall Area
Carbonaceous						
NWA 5958		C2	Find	286 g	2009	Morocco
Tagish Lake		C2-ung	Fall	10 kg	2000	British Columbia, Canada
Gujba		CBa	Fall	100 kg	1984	Yobe, Nigeria
Ivuna		CI1	Fall	705 g	1938	Mbeya, Tanzania
Orgueil		CI1	Fall	14 kg	1864	Midi-Pyrenees, France
Maralinga		CK4-an	Find	3.39 kg	1974	South Australia
Banten		CM2	Fall	629 g	1933	Jawa Barat, Indonesia
Cold Bokkeveld		CM2	Fall	5.3 kg	1838	Western Cape, South Africa
Murchison	Main SIGL Mass	CM2	Fall	100 kg	1969	Victoria, Australia
	MTF 2005	CM2				
Murray		CM2	Fall	12.6 kg	1950	Kentucky, USA
Allende		CV3	Fall	2 t	1969	Chihuahua, Mexico
	USNM 3529	CV3				
GRA 06101		CV3	Find	3.56 kg	2006	Antarctica
Vigarano		CV3	Fall	15 kg	1910	Emilia-Romagna, Italy
NWA 4502		CV3	Find	100 kg	2005	Algeria
Ordinary						
Fayetteville		H4	Fall	2.36 kg	1934	Arkansas, USA
Forest City	AMNH 2421	H5	Fall	152 kg	1890	Iowa, USA
Pultusk		H5	Fall	250 kg	1868	Ostroleka, Poland
Richardton		H5	Fall	90 kg	1918	North Dakota, USA
NWA 869		L3-6	Find	2 t	2000	Northwest Africa
Khohar		L3.6	Fall	9.7 kg	1910	Madhya Pradesh, India
Saratov		L4	Fall	200 kg	1918	Saratovkaya oblast', Russia
Aïr		L6	Fall	24 kg	1925	Agadez, Niger
Kunashak	Lg Slice	L6	Fall	200 kg	1949	Chelyabinskaya oblast', Russia
	LAT	L6				
Kyle		L6	Find	7.78 kg	1965	Texas, USA
Peace River	MTF 2116, Main Mass	L6	Fall	45.76 kg	1963	Alberta, Canada
Chelyabinsk		LL5	Fall	1 t	2013	Chelyabinskaya oblast', Russia
Olivenza		LL5	Fall	150 kg	1924	Extremadura, Spain
Larkman						
Enstatite						
Atlanta		EL6	Find	5.5 kg	1938	Louisiana, USA
Eagle		EL6	Fall	10 kg	1946	Nebraska, USA
Khairpur		EL6	Fall	13.6 kg	1873	Punjab, Pakistan
LON94100		EL6	Find	1947 g	1994	Antarctica

Table 2. Characteristics of petrologic grade in chondrites. Modified from Weisberg et al. (2006).

Petrologic Type	**1**	**2**	**3**	**4**	**5**	**6**	**7**
Homogeneity of olivne compostions	—	>5% mean deviations		<5%	Homogeneous		
Chondrule-matrix intergration	No chondrules	Visable chondrule boundaries		Some chondrules visible		Poorly delineted chondrules	Primary textures non-existant
Matrix	Fine grained, opaque	Mostly fine-grained & opaque	Opaque to transparent	Transparent, recrystalized			
Sulfides: Mean Ni (wt%)	—	>0.5	<0.5				
Carbon (wt%)	3-5	0.8-2.6	0.2-1	<0.2			
Water (wt%)	18-22	2-16	0.3-3	<1.5			

After Van Schmus & Wood, (1967) with modifications by Sears & Dodd, (1988), Brearley & Jones, (1998) and Weisberg et al., (2006).

Table 3. HSE abundances (μg g^{-1}) of Chelyabinsk metals

	Metal 1		Metal 2	
n	[5]	1s	[3]	1s
Re	0.99	0.15	0.90	0.35
Os	9.48	1.70	6.40	3.56
Ir	7.40	1.03	5.54	2.90
Ru	8.50	1.81	6.35	0.88
Rh	2.60	0.45	2.47	0.63
Pt	11.84	1.97	12.13	4.14
Pd	12.10	2.24	1.47	0.35
Au	2.90	0.68	0.74	0.23

Table 4. Major-element mineral chemistry (wt.%) for the Chelyabinsk chondrite fall, February 15th, 2013

Phase	Olivine		Plagioclase		Orthoclase	Low-Ca Pyroxene		High-Ca Pyroxene		Cr-Spinel		Ilmenite		Apatite		Merrillite	
n	[128]	1s	[60]	1s	[1]	[156]	1s	[55]	1s	[35]	1s	[6]	1s	[79]	1s	[32]	1s
SiO2	37.5	0.6	65.4	0.9	64.8	54.9	0.4	53.6	0.5	0.08	0.04	0.03	0.01	0.10	0.25	0.01	0.02
TiO2	0.01	0.01			0.04	0.19	0.05	0.40	0.06	3.01	0.38	53.2	0.4				
Al2O3	0.01	0.04	21.9	0.7	19.7	0.15	0.06	0.45	0.05	5.84	0.21	0.01	0.01				
Cr2O3	0.04	0.08				0.16	0.35	0.70	0.10	56.1	1.0	0.09	0.08				
MgO	35.8	0.6	0.05	0.17	0.01	27.6	0.3	16.3	0.3	1.87	0.32	2.45	0.29	0.19		3.61	0.07
CaO	0.09	0.68	2.21	0.27	1.44	0.72	0.13	21.96	0.56	0.02	0.03	0.03	0.01	53.9	0.9	46.7	0.2
MnO	0.45	0.02			0.02	0.45	0.02	0.21	0.02	0.53	0.03	1.17	0.26				
FeO	26.1	0.6	0.49	0.31	0.18	15.8	0.2	5.3	0.4	31.8	0.4	42.5	0.6	0.38	0.38	0.64	0.26
NiO	0.01	0.02								0.02	0.02	0.04	0.01				
Na2O			8.96	0.89	1.02	0.01	0.01	0.49	0.04					0.05	0.04	2.37	0.11
K2O			0.97	0.52	14.1												
P2O5	0.03	0.05												41.4	0.6	46.2	0.4
V2O3										0.66	0.06						
Cl														5.35	0.40		
F														0.18	0.14		
SO3														0.02	0.02		
Total	**100.0**	**0.7**	**99.9**	**1.0**	**101.3**	**100.0**	**0.6**	**99.3**	**1.0**	**99.9**	**1.03**	**99.5**	**0.48**	**101.6**		**99.5**	
O=Cl														1.21	0.09		
O=F														0.07	0.06		
Fo	71.0	0.4															
Or			6	3	84												
An			11	2	7												
Ab			83	4	9												
En						74.6	0.4	46.4	0.5								
Wo						1.4	0.3	45.1	0.9								
Fs						24.0	0.4	8.5	0.9								
Mg#						76		85		9.5		9.3		82		9	
Cr#										79.5							

An = Ca/(Ca+Na+K)*100, Ab = Na/(Ca+Na+K)*100, Wo=Ca/(Ca+Mg+Fe)*100, En=Mg/(Ca+Mg+Fe)*100, Mg# = Mg/(Mg+Fe)*100, Cr# = Cr/(Cr+Al)*100

Table 4. (continued)

	Troilite [12]	1s	Kamacite	Taenite	Taenite
Si	0.01	0.00	0.01	0.01	0.00
S	36.1	0.22			0.00
Fe	62.8	0.27	92.1	50.8	72.0
Co	0.00	0.01	2.03	0.33	1.12
Ni	0.06	0.07	5.67	48.8	25.8
P	0.00	0.00			0.01
Mg	0.00	0.00	0.01		0.00
Al	0.00	0.00	0.00	0.01	0.01
Ti	0.00	0.00		0.01	0.00
Total	**99.1**	**0.5**	**99.8**	**100.0**	**99.0**
Fe	50		52	74	93
Ni			48	25	5
S	50				

Table 5. Trace-element mineral chemistry (μg g-1) for the Chelyabinsk chondrite meteorite fall, February 15th, 2013

	Fusion Crust		Chondrule		Olivine		Low-Ca Px		Plagioclase	Phosphate
n	[4]	1s	[4]	1s	[4]	1s	[8]	1s	[1]	[1]
Li	1.7	0.2	0.9	0.7	1.7	0.9	0.4	0.6	1.6	0.2
Sc	10.1	3.3	27.4	2.3	13.6	4.3	13.6	5.5	8.6	1.2
Rb	0.65	0.96	2.71	0.38	0.051	0.003	1.32	1.30	5.40	0.69
Sr	2.7	4.1	8.9	1.6	0.2	0.0	3.2	3.2	62.7	17.8
Y	0.2	0.2	1.5	0.3	0.1	0.0	0.3	0.1	9.3	209.8
Zr	4.2	5.8	17.5	3.9	0.8	0.3	4.0	3.7	39.9	1.8
Nb	0.2	0.1	1.4	0.2	0.10	0.05	0.2	0.1	0.4	0.0
Cs	0.032	0.004	0.46	0.28	0.006	0.015	0.014	0.006		0.46
Ba	1.7	2.4	3.8	1.0	0.2	0.1	1.6	1.6	13.5	0.2
La	0.16	0.22	0.15	0.06	0.010	0.015	0.096	0.124	8.21	39.6
Ce	0.31	0.41	0.86	0.59	0.024	0.030	0.188	0.148	23.38	117.7
Pr	0.05	0.05	0.08	0.04	0.003	0.004	0.020	0.015	2.16	16.4
Nd	0.14	0.19	0.40	0.24	0.009	0.009	0.150	0.222	7.10	75.5
Sm	0.04	0.04	0.16	0.03	0.005	0.005	0.019	0.020	1.64	22.8
Eu	0.01	0.01	0.06	0.01	0.003	0.004	0.025	0.031	2.72	1.0
Gd	0.04	0.03	0.17	0.02	0.006	0.007	0.031	0.033	1.69	31.6
Tb	0.01	0.00	0.03	0.01	0.002	0.001	0.008	0.007	0.30	5.4
Dy	0.04	0.03	0.34	0.07	0.010	0.010	0.036	0.016	2.76	36.0
Ho	0.01	0.01	0.06	0.01	0.002	0.000	0.013	0.004	0.59	7.6
Er	0.03	0.02	0.20	0.03	0.006	0.004	0.061	0.032	1.16	22.0
Tm	0.01	0.00	0.04	0.01	0.001	0.000	0.009	0.004	0.20	2.9
Yb	0.07	0.02	0.31	0.14	0.013	0.001	0.093	0.033	2.75	16.7
Lu	0.01	0.00	0.05	0.01	0.002	0.002	0.019	0.007	0.21	2.2
Hf	0.08	0.12	0.39	0.01	0.007	0.005	0.094	0.090	0.89	0.2
Ta	0.01	0.01	0.08	0.01	0.005	0.001	0.011	0.005	0.08	BDL
Pb	0.04	0.03	0.19	0.02	BDL	BDL	0.053	0.063	BDL	0.30
Th	0.01	0.00	0.25	0.10	0.005	0.006	0.047	0.027	BDL	0.94
U	0.01	0.02	1.02	1.40	0.001	0.003	0.013	0.012	BDL	0.22

BDL-Below detection limit.

Table 6. Bulk-rock major, minor and trace-element chemistry for the Chelyabinsk chondrite meteorite fall and other chondrites

Sample		Chelyabinsk With FC	Chelyabinsk Without FC	Saratov	NWA869	Air	Kunashak Slice	Kunashak Fragment	Larkman	Larkman	Kyle	Fayateville	Pultusk
Method		Paar Bomb (1)	Paar Bomb (1)	Teflon (2)	Teflon (2)	Teflon (2)	Paar Bomb (1)	Paar Bomb (1)	Paar Bomb (1)	Teflon (2)	Teflon (2)	Teflon (2)	Teflon (2)
Al	$\mu g\ g^{-1}$	9560	9476	9806	12964	11617	10347	10125	11820	12313	11128	11352	9956
Fe	$\mu g\ g^{-1}$	224585	168198	165208	190304	194549	163706	164993	197066	213298	191442	257740	326865
Mn	$\mu g\ g^{-1}$	2045	2234	3053	2574	2622	2300	2280	2399	2582	2467	2389	2142
Mg	$\mu g\ g^{-1}$	119124	123269	136323	148872	152740	128720	126688	134221	150904	141904	146371	126432
Ca	$\mu g\ g^{-1}$	10688	12879	16834	24863	19009	13275	12588	12871	20101	17117	17794	16078
Na	$\mu g\ g^{-1}$	5984	5978	6213	7955	7477	6341	6171	6866	8136	6131	6505	6066
Cr	$\mu g\ g^{-1}$	3343	2979	3005	2879	3302	3111	2975	3433	3476	3277	3497	3286
Co	$\mu g\ g^{-1}$	1722	483	368	168	283	346	378	521	359	370	523	868
Ni	$\mu g\ g^{-1}$	19717	14043	7943	6576	5955	7023	8501	9823	7556	7525	11679	14938
Li	$\mu g\ g^{-1}$	1.5	1.6	1.5	3.9	1.9	1.7	1.6	1.8	1.9	1.8	1.9	1.6
P	$\mu g\ g^{-1}$	1128	1442	913	1141	974	825	932	912	1187	1035	1225	1239
Sc	$\mu g\ g^{-1}$	5.7	6.4	6.2	8.7	8.1	7.4	7.0	7.6	8.0	7.7	7.7	6.8
Ti	$\mu g\ g^{-1}$	488	710	524	608	752	697	683	885	703	604	599	542
V	$\mu g\ g^{-1}$	56.7	51.7	78.6	86.6	90.4	56.0	53.9	63.9	92.2	88.2	92.0	85.5
Cu	$\mu g\ g^{-1}$	109.7	85.7	62.8	84.9	66.5	52.2	53.7	73.1	75.5	67.6	88.0	82.9
Zn	$\mu g\ g^{-1}$	46.8	38.5	49.7	44.4	49.4	29.0	28.7	36.2	36.8	53.6	153.1	42.4
Ga	$\mu g\ g^{-1}$	4.96	4.40	5.09	5.30	4.94	4.51	4.54	4.71	4.82	5.19	6.19	6.81
Ge	$\mu g\ g^{-1}$	9.25	5.01	2.10	1.99	2.15	3.27	3.64	4.90	2.28	2.38	2.88	3.63
Se	$\mu g\ g^{-1}$	0.50	0.40	0.09	0.55	0.44	0.45	0.36	0.53	0.41	0.37	0.43	0.37
Rb	$\mu g\ g^{-1}$	2.67	2.72	3.12	2.65	0.65	1.18	1.51	0.70	0.65	2.60	2.75	2.70
Sr	$\mu g\ g^{-1}$	10.1	10.0	7.9	60.0	10.4	10.8	10.5	11.9	10.8	9.1	10.2	9.0
Y	$\mu g\ g^{-1}$	2.62	3.36	1.77	1.53	1.84	1.76	2.06	1.78	1.87	2.27	2.08	1.85
Zr	$\mu g\ g^{-1}$	4.22	4.87	12.63	9.27	9.67	5.69	5.50	5.62	11.15	9.91	8.38	6.83
Nb	$\mu g\ g^{-1}$	0.28	0.41	0.31	0.40	0.55	0.40	0.38	0.48	0.51	0.43	0.41	0.36
Mo	$\mu g\ g^{-1}$	1.32	0.93	0.57	0.77	0.81	0.73	1.22	0.87	1.13	0.89	1.30	1.72
Sn	$\mu g\ g^{-1}$	0.66	0.58	0.35	0.24	0.31	0.39	0.29	0.35	0.26	0.27	1.12	0.33
Cs	$\mu g\ g^{-1}$	0.014	0.015	0.188	0.011	0.002	0.006	0.008	0.013	0.014	0.059	0.116	0.188
Ba	$\mu g\ g^{-1}$	3.36	3.56	2.96	191.92	4.03	3.63	3.79	4.14	3.83	4.19	4.83	3.17
La	$\mu g\ g^{-1}$	0.518	0.595	0.272	0.269	0.276	0.519	0.378	0.288	0.296	0.352	0.331	0.293
Ce	$\mu g\ g^{-1}$	1.36	1.69	0.71	0.70	0.73	1.40	1.03	0.77	0.76	0.94	0.88	0.77
Pr	$\mu g\ g^{-1}$	0.176	0.234	0.105	0.099	0.110	0.115	0.135	0.111	0.115	0.142	0.128	0.117
Nd	$\mu g\ g^{-1}$	0.859	1.167	0.539	0.490	0.547	0.549	0.647	0.559	0.566	0.696	0.640	0.587
Sm	$\mu g\ g^{-1}$	0.272	0.365	0.167	0.156	0.179	0.176	0.214	0.176	0.183	0.228	0.202	0.182
Eu	$\mu g\ g^{-1}$	0.073	0.080	0.066	0.121	0.079	0.076	0.075	0.082	0.083	0.082	0.079	0.071
Gd	$\mu g\ g^{-1}$	0.353	0.472	0.226	0.204	0.245	0.232	0.274	0.234	0.244	0.305	0.273	0.240
Tb	$\mu g\ g^{-1}$	0.064	0.087	0.046	0.038	0.045	0.044	0.052	0.044	0.045	0.055	0.051	0.044
Dy	$\mu g\ g^{-1}$	0.446	0.617	0.309	0.272	0.320	0.313	0.365	0.315	0.323	0.401	0.358	0.321
Ho	$\mu g\ g^{-1}$	0.096	0.132	0.067	0.060	0.069	0.068	0.080	0.069	0.070	0.085	0.077	0.070
Er	$\mu g\ g^{-1}$	0.283	0.384	0.203	0.182	0.207	0.209	0.239	0.208	0.210	0.257	0.231	0.212
Tm	$\mu g\ g^{-1}$	0.042	0.056	0.033	0.028	0.032	0.032	0.036	0.032	0.032	0.037	0.036	0.031
Yb	$\mu g\ g^{-1}$	0.264	0.351	0.206	0.199	0.223	0.217	0.241	0.211	0.220	0.253	0.233	0.210
Lu	$\mu g\ g^{-1}$	0.037	0.051	0.031	0.030	0.034	0.033	0.036	0.033	0.033	0.039	0.036	0.032
Hf	$\mu g\ g^{-1}$	0.118	0.147	0.242	0.193	0.210	0.166	0.160	0.166	0.222	0.213	0.175	0.149
Ta	$\mu g\ g^{-1}$	0.018	0.032	0.040	0.027	0.032	0.023	0.029	0.028	0.029	0.024	0.022	0.018
W	$\mu g\ g^{-1}$	0.338	0.532	0.132	0.080	0.087	0.121	0.758	0.164	0.123	0.104	0.163	0.229
Pb	$\mu g\ g^{-1}$	0.022	0.034	0.055	0.077	0.231	0.018	0.019	0.320	0.320	0.103	0.589	0.191
Th	$\mu g\ g^{-1}$	0.033	0.049	0.091	0.045	0.055	0.042	0.042	0.046	0.068	0.056	0.054	0.042
U	$\mu g\ g^{-1}$	0.085	0.121	0.010	0.092	0.015	0.140	0.111	0.135	0.013	0.009	0.014	0.011
Cd	$ng\ g^{-1}$	2.1	2.2	0.0	0.1	0.1	2.1	2.3	4.4	0.1	0.1	0.5	0.1

Published data for Allende are from Jarosewich et al. (1987) and Stracke et al. (2012), and for BHVO-1, BCR-2 and BIR-1 are from GeoREM. TPB = Total Procedural Blank. Allende UCSD 142 was previously reported in Day et al. (2015), with the exception of Ag and Cd composition.

Table 6. (continued)

Sample		Forest City	Richardton Fragment	Peace River Fragment	Tagish Lake	NWA5958	Banten	Murray	Murchison MTF 2005	Murchison Fragment	Allende UCSD 142	Allende Literature	GRA06101	Maralinga
Method		Teflon (2)	Paar Bomb (1)	Paar Bomb (1)	Teflon (2)	Teflon (2)	Teflon (2)	Teflon (2)	Paar Bomb (1)	Paar Bomb (1)	Paar Bomb (1)		Teflon (2)	Teflon (2)
Al	μg g^{-1}	11207	10917	12349	11334	11487	11417	13596	9215	12329	13627	*17359*	21746	14925
Fe	μg g^{-1}	243394	274223	174150	208951	209511	212175	192102	161608	221844	203759	*221000*	208447	229486
Mn	μg g^{-1}	2461	2276	2653	1745	2088	1664	2113.0	1264	1701	1254	*1490.0*	1925.5	1301.4
Mg	μg g^{-1}	145254	140582	149069	119430	110966	119896	112332	95844	115235	122865	*154000*	156259	141927
Ca	μg g^{-1}	17974	12924	14470	16981	13678	18239	18907	11450	14944	14684	*20000*	40165	37473
Na	μg g^{-1}	6955	6710	7218	4836	2096	4451	3062	2462	4092	3118	*3400*	5331	2934
Cr	μg g^{-1}	3338	3560	3256	2739	2547	2778	2438	2123	2959	2928	*3612*	2812	3106
Co	μg g^{-1}	457	857	387	390	404	422	398	430	582	583	*591*	398	262
Ni	μg g^{-1}	10811	18061	9046	7614	8347	8699	7904	8567	11738	11650	*13660*	8884	2707
Li	μg g^{-1}	1.9	1.7	2.0	1.7	2.2	1.6	3.01	1.3	1.6	1.5	*1.40*	1.72	1.87
P	μg g^{-1}	1263	1083	839	1043	1050	1054	1046	739	992	937	*1067*	1150	1226
Sc	μg g^{-1}	7.7	7.8	9.0	7.2	5.9	7.4	6.4	5.6	7.2	7.9	*11.0*	12.2	9.3
Ti	μg g^{-1}	607	1070	880	570	552	601	847	605	1351	570	*1000*	1143	836
V	μg g^{-1}	89.8	69.3	68.6	82.3	83.2	88.8	87.0	42.4	70.0	58.9	*82.4*	156.9	110.1
Cu	μg g^{-1}	89.9	99.8	55.1	103.1	114.7	125.0	106.4	81.7	115.2	88.9	*97.0*	70.1	51.8
Zn	μg g^{-1}	46.1	68.4	52.1	142.3	169.5	149.8	145.8	115.9	152.4	74.9	*106.0*	77.2	51.7
Ga	μg g^{-1}	5.51	6.82	4.93	8.23	7.77	8.02	7.77	5.99	8.00	4.85	*5.90*	5.08	4.46
Ge	μg g^{-1}	2.64	6.40	4.09	2.47	3.67	2.32	2.79	6.63	8.88	5.74	*17.90*	2.57	2.50
Se	μg g^{-1}	0.47	0.48	0.29	0.58	0.35	0.56	0.43	0.54	0.69	0.46		0.17	0.09
Rb	μg g^{-1}	2.88	2.81	2.79	1.57	0.77	1.74	5.05	1.30	2.33	1.16	*1.32*	1.18	0.59
Sr	μg g^{-1}	10.1	10.8	12.0	11.1	32.6	10.1	19.7	10.8	10.6	13.4	*15.7*	21.3	31.3
Y	μg g^{-1}	2.17	2.04	2.03	1.97	1.89	2.06	3.60	1.80	2.34	2.12	*2.63*	3.39	2.47
Zr	μg g^{-1}	10.72	5.79	6.55	9.97	7.23	10.46	37.09	4.20	8.05	5.60	*6.77*	19.58	10.64
Nb	μg g^{-1}	0.42	0.40	0.49	0.37	0.32	0.39	1.36	0.29	0.39	0.43	*0.57*	0.51	0.49
Mo	μg g^{-1}	1.26	1.43	0.79	1.11	1.41	1.26	1.11	0.97	1.85	1.72	*1.45*	1.51	0.67
Sn	μg g^{-1}	0.24	0.65	0.39	0.84	0.98	2.58	0.96	0.78	1.11	0.64	*0.30*	0.58	0.35
Cs	μg g^{-1}	0.101	0.056	0.008	0.129	0.075	0.136	0.290	0.104	0.128	0.076	*0.098*	0.065	0.021
Ba	μg g^{-1}	3.46	3.64	8.07	4.11	27.28	3.29	40.63	3.03	34.22	4.27	*4.74*	5.00	25.71
La	μg g^{-1}	0.334	0.302	0.301	0.317	0.386	0.368	2.358	0.441	0.345	1.097	*0.490*	0.610	0.731
Ce	μg g^{-1}	0.88	0.82	0.81	0.81	0.88	0.94	5.59	1.49	0.89	5.44	*1.24*	1.56	2.68
Pr	μg g^{-1}	0.128	0.123	0.118	0.124	0.146	0.139	0.674	0.120	0.129	0.213	*0.192*	0.243	0.240
Nd	μg g^{-1}	0.657	0.605	0.592	0.628	0.738	0.684	2.734	0.589	0.656	1.071	*0.967*	1.184	1.136
Sm	μg g^{-1}	0.220	0.199	0.193	0.204	0.217	0.213	0.632	0.179	0.203	0.281	*0.313*	0.371	0.314
Eu	μg g^{-1}	0.078	0.074	0.084	0.078	0.083	0.083	0.166	0.069	0.085	0.090	*0.115*	0.160	0.110
Gd	μg g^{-1}	0.286	0.247	0.259	0.261	0.265	0.283	0.638	0.244	0.267	0.366	*0.401*	0.496	0.377
Tb	μg g^{-1}	0.053	0.048	0.048	0.050	0.050	0.051	0.099	0.045	0.049	0.062	*0.072*	0.092	0.067
Dy	μg g^{-1}	0.373	0.342	0.345	0.359	0.342	0.357	0.632	0.313	0.347	0.411	*0.479*	0.612	0.460
Ho	μg g^{-1}	0.082	0.075	0.075	0.076	0.070	0.076	0.134	0.071	0.074	0.081	*0.100*	0.130	0.098
Er	μg g^{-1}	0.243	0.224	0.229	0.216	0.221	0.229	0.409	0.209	0.231	0.241	*0.299*	0.364	0.279
Tm	μg g^{-1}	0.037	0.033	0.035	0.033	0.034	0.036	0.063	0.031	0.034	0.044	*0.053*	0.061	0.046
Yb	μg g^{-1}	0.244	0.224	0.234	0.234	0.251	0.240	0.420	0.203	0.228	0.267	*0.319*	0.404	0.301
Lu	μg g^{-1}	0.037	0.033	0.038	0.033	0.033	0.035	0.057	0.032	0.063	0.038	*0.046*	0.059	0.044
Hf	μg g^{-1}	0.224	0.154	0.185	0.204	0.161	0.218	0.736	0.129	0.293	0.158	*0.188*	0.382	0.213
Ta	μg g^{-1}	0.023	0.027	0.091	0.022	0.017	0.021	0.082	0.021	0.033	0.027	*0.033*	0.029	0.028
W	μg g^{-1}	0.140	0.307	0.129	0.126	0.173	0.151	0.289	0.272	0.589	0.253	*0.200*	0.183	0.156
Pb	μg g^{-1}	0.095	0.347	0.327	1.582	1.709	1.964	3.347	1.376	1.681	1.286	*1.520*	1.040	0.746
Th	μg g^{-1}	0.063	0.041	0.042	0.065	0.045	0.068	0.858	0.036	0.048	0.057	*0.078*	0.134	0.121
U	μg g^{-1}	0.012	0.100	0.095	0.011	0.058	0.011	0.3025	0.081	0.123	0.012	*0.0174*	0.0130	0.0223
Cd	ng g^{-1}	0.1	3.7	24.8	1.5	1.8	1.7	1.7	154.8	121.1	79.0		0.5	0.6

Table 6. (continued)

Sample		LON91400	Eagle	Atlanta	Khaipur	BHVO-2 (n = 3)		BHVO-2 (n = 4)			BCR-2 (n = 3)		BCR-2 (n = 3)			BIR-1 (n = 3)			TPB (n = 4)	TPB (n = 3)
Method		Teflon (2) EL6	Teflon (2) EL6	Teflon (2) EL6	Teflon (2) EL6	Paar Bomb (1) Av.	RSD	Teflon (2) Av.	RSD	*Rec.*	Paar Bomb (1) Av.	RSD	Paar Bomb (1) Av.	RSD	*Rec.*	Paar Bomb (1) Av.	RSD	Rec.	Paar Bomb (1) Average	Teflon (2) Average
Al	µg g^{-1}	9456	10468	12504	7251	71654	2%	71600	1%	*71600*	71141	3%	69867	4%	*71400*	81813	6%	*82034*	112	3797
Fe	µg g^{-1}	241313	244832	166533	282833	86583	2%	86300	2%	*86300*	96387	2%	94854	4%	*96500*	80279	5%	*79036*	4290	3
Mn	µg g^{-1}	1082.1	1886.7	1677.8	1261.6	1294	2%	1290	2%	*1290*	1517	2%	1491	4%	*1520*	1320	5%	*1355*	9.6	0.3
Mg	µg g^{-1}	139166	139156	147424	121540	43513	2%	43600	2%	*43600*	21589	2%	21419	4%	*35900*	57854	5%	*58494*	87	114
Ca	µg g^{-1}	11859	8599	6912	10765	82023	2%	81700	2%	*81700*	51230	2%	50595	4%	*50900*	95234	5%	*95055*	1202	194
Na	µg g^{-1}	5571	6177	6773	5099	15947	2%	16400	2%	*16400*	22760	3%	23189	4%	*23400*	13131	6%	*13502*	360	84
Cr	µg g^{-1}	2138	1568	3129	2152	277	2%	280	2%	*280*	25	4%	19	4%	*18*	379	5%	*370*	13	0
Co	µg g^{-1}	552	602	563	658	44.4	3%	45.0	2%	*45*	31.9	3%	37.4	4%	*37.0*	52.8	6%	*52*	1.1	0.0
Ni	µg g^{-1}	10126	10895	11187	12444	120.6	3%	119.0	2%	*119*	17.8	7%	11.7	5%		167.6	6%	*170*	13.4	0.1
Li	µg g^{-1}	1.62	1.23	1.26	1.62	4.69	3%	4.80	3%	*4.80*	9.11	2%	9.78	5%	*9.00*	3.28	5%	*3.60*	0.017	0.004
P	µg g^{-1}	1395	1137	1652	1249	1168	3%	1200	7%	*1200*	1450	2%	1563	8%	*1500*	100	4%		57	41
Sc	µg g^{-1}	7.1	6.2	6.3	4.8	31.8	4%	32.0	3%	*32*	31.0	4%	32.7	5%	*33.0*	43.1	6%	*44*	0.081	0.058
Ti	µg g^{-1}	386	384	601	563	16339	5%	16300	2%	*16300*	12580	6%	12926	5%	*13500*	5573	8%		0.450	0.082
V	µg g^{-1}	53.5	38.3	63.2	56.6	317.4	6%	317.0	2%	*317*	387.3	7%	406.5	4%	*416*	318.0	9%	*310*	0.350	0.013
Cu	µg g^{-1}	83.0	52.6	63.8	84.1	128.1	5%	127.0	2%	*127.0*	19.2	7%	19.5	4%	*19.0*	115.2	8%	*125*	0.312	0.027
Zn	µg g^{-1}	4.9	164.9	50.0	12.6	104.1	5%	103.0	7%	*103.0*	122.0	5%	119.8	3%	*127.0*	66.7	8%	*70*	1.370	3.558
Ga	µg g^{-1}	12.73	13.54	12.82	14.49	22.10	5%	22.00	2%	*22.00*	21.26	5%	22.39	4%	*23.00*	15.45	7%	*16*	0.003	0.002
Ge	µg g^{-1}	2.67	3.48	2.01	3.67	1.64	6%	1.60	4%	*1.60*	1.66	8%	1.82	4%		1.22	10%		0.011	0.023
Se	µg g^{-1}	0.57	0.21	0.41	0.43	0.11	2%	0.17	11%	*0.10*	0.11	4%	0.18	8%		0.02	24%		0.043	0.012
Rb	µg g^{-1}	2.11	2.03	1.38	1.54	9.95	3%	9.11	1%	*9.11*	47.14	3%	45.23	4%	*48.00*	0.21	4%		0.005	0.005
Sr	µg g^{-1}	7.2	6.7	8.5	4.9	403.8	3%	396.0	1%	*396.0*	323.1	3%	333.7	4%	*346.0*	108.2	5%	*110*	0.021	0.211
Y	µg g^{-1}	1.27	1.24	1.87	1.05	25.83	3%	26.00	1%	*26.00*	33.04	3%	34.84	5%	*37.00*	15.2	5%	*16*	0.001	0.014
Zr	µg g^{-1}	7.99	3.72	12.96	6.06	170.3	3%	172.0	2%	*172.0*	173.7	3%	181.3	5%	*188.0*	14.6	5%	*18*	0.062	1.331
Nb	µg g^{-1}	0.20	0.11	0.26	0.20	18.03	2%	18.10	2%	*18.10*	11.49	3%	11.84	6%		0.52	5%	*0.60*	0.002	0.008
Mo	µg g^{-1}	0.95	0.90	1.17	1.05	3.71	28%	4.00	24%	*4.00*	232.36	2%	242.19	16%	*248.00*	0.038	29%		0.026	0.005
Sn	µg g^{-1}	0.39	0.86	1.10	0.82	1.84	6%	1.70	3%	*1.70*	2.30	7%	1.89	3%		0.80	4%		0.277	0.024
Cs	µg g^{-1}	0.113	0.154	0.052	0.079	0.10	3%	0.10	1%	*0.10*	1.07	2%	1.16	5%	*1.10*	0.01	4%		0.001	0.000
Ba	µg g^{-1}	1.89	2.47	4.80	1.50	139.21	2%	131.00	2%	*131.00*	653.40	2%	491.12	4%	*683.00*	6.76	4%	*7.00*	0.033	0.042
La	µg g^{-1}	0.144	0.117	0.227	0.121	15.13	2%	15.20	1%	*15.20*	22.96	1%	24.27	4%	*25.00*	0.60	0.3%	*0.63*	0.015	0.002
Ce	µg g^{-1}	0.39	0.35	0.69	0.33	37.20	2%	37.50	1%	*37.50*	48.88	1%	48.93	1%	*53.00*	1.93	1%	*1.90*	0.035	0.006
Pr	µg g^{-1}	0.061	0.058	0.108	0.055	5.33	3%	5.35	1%	*5.35*	6.33	1%	6.64	4%	*6.80*	0.36	3%		0.0008	0.0008
Nd	µg g^{-1}	0.308	0.282	0.599	0.274	24.35	3%	24.50	1%	*24.50*	26.46	1%	27.95	5%	*28.00*	2.32	4%	*2.50*	0.0028	0.0034
Sm	µg g^{-1}	0.104	0.099	0.178	0.086	6.04	3%	6.07	1%	*6.07*	6.04	1%	6.36	4%	*6.70*	1.06	4%	*1.10*	0.0001	0.0004
Eu	µg g^{-1}	0.043	0.040	0.051	0.038	2.06	3%	2.07	2%	*2.07*	1.94	2%	2.01	3%	*2.00*	0.50	5%	*0.55*	0.0001	0.0002
Gd	µg g^{-1}	0.135	0.143	0.242	0.133	6.21	2%	6.24	2%	*6.24*	6.38	2%	6.71	5%	*6.80*	1.64	4%	*1.80*	0.0005	0.0006
Tb	µg g^{-1}	0.027	0.024	0.045	0.023	0.92	3%	0.92	2%	*0.33*	0.96	2%	1.00	5%	*1.07*	0.33	4%		0.0001	0.0001
Dy	µg g^{-1}	0.189	0.197	0.317	0.174	5.29	3%	5.31	1%	*5.31*	5.92	2%	6.28	5%		2.49	4%	*4.00*	0.0002	0.0005
Ho	µg g^{-1}	0.043	0.046	0.066	0.035	0.97	3%	0.98	1%	*0.98*	1.19	1%	1.26	5%	*1.33*	0.55	4%		0.00003	0.00008
Er	µg g^{-1}	0.130	0.132	0.203	0.116	2.53	3%	2.54	2%	*2.54*	3.38	1%	3.55	4%		1.64	4%		0.0001	0.0003
Tm	µg g^{-1}	0.021	0.022	0.028	0.016	0.33	3%	0.33	2%	*0.33*	0.48	2%	0.50	6%	*0.54*	0.24	4%		0.00003	0.00006
Yb	µg g^{-1}	0.149	0.153	0.195	0.129	1.99	3%	2.00	2%	*2.00*	3.10	2%	3.26	4%	*3.50*	1.60	4%	*1.70*	0.0001	0.0001
Lu	µg g^{-1}	0.023	0.023	0.030	0.021	0.27	3%	0.27	2%	*0.27*	0.45	1%	0.48	4%	*0.51*	0.24	4%	*0.26*	0.00003	0.00003
Hf	µg g^{-1}	0.189	0.139	0.269	0.129	4.34	3%	4.36	2%	*4.36*	4.49	1%	4.64	5%	*4.80*	0.56	4%	*0.60*	0.0012	0.0248
Ta	µg g^{-1}	0.013	0.009	0.016	0.014	1.13	2%	1.14	3%	*1.14*	0.71	2%	0.72	7%		0.04	4%		0.0012	0.0001
W	µg g^{-1}	0.124	0.186	0.170	0.191	0.21	6%	0.21	3%	*0.21*	0.42	3%	0.41	6%		0.10	87%		0.070	0.014
Pb	µg g^{-1}	0.134	0.256	0.595	0.335	1.76	4%	1.60	17%	*1.60*	8.95	2%	9.50	5%	*11.00*	2.78	2%	*3.00*	0.014	0.007
Th	µg g^{-1}	0.040	0.027	0.101	0.030	1.24	5%	1.22	2%	*1.22*	5.45	1%	5.69	4%	*6.20*	0.03	1%		0.001	0.011
U	µg g^{-1}	0.0048	0.0039	0.0118	0.0037	0.41	3%	0.40	3%	*0.40*	1.51	2%	1.57	4%	*1.69*	0.10	5%		0.004	0.000
Cd	ng g^{-1}	0.1	0.8	0.1	0.1	86.2	1%	1.0	4%		235.9	6%	3.2	7%		38.5	4%		0.1	0.0

Table 7. Major-Element (wt%) and ratios

Sample	Chelyabinsk With FC	Chelyabinsk Without FC	Saratov	NWA869	Air	Kunashak Slice	Kunashak Fragment	Larkman	Larkman	Kyle	Fayateville	Pultusk	Forest City	Richardton Fragment	Peace River Fragment
Method	Paar Bomb (1)	Paar Bomb (1)	Teflon (2)	Teflon (2)	Teflon (2)	Paar Bomb (1)	Paar Bomb (1)	Paar Bomb (1)	Teflon (2)	Teflon (2)	Teflon (2)	Teflon (2)	Teflon (2)	Paar Bomb (1)	Paar Bomb (1)
SiO2	46.55	52.70	50.31	43.02	42.98	52.23	52.55	46.66	40.46	45.77	36.27	31.30	38.22	35.82	46.76
TiO2	0.08	0.12	0.09	0.10	0.13	0.12	0.11	0.15	0.12	0.10	0.10	0.09	0.10	0.18	0.15
Al2O3	1.81	1.79	1.85	2.45	2.19	1.95	1.91	2.23	2.33	2.10	2.14	1.88	2.12	2.06	2.33
FeO	28.89	21.64	21.25	24.48	25.03	21.06	21.23	25.35	27.44	24.63	33.16	42.05	31.31	35.28	22.40
MgO	19.75	20.44	22.61	24.69	25.33	21.35	21.01	22.26	25.02	23.53	24.27	20.97	24.09	23.31	24.72
MnO	0.26	0.29	0.39	0.33	0.34	0.30	0.29	0.31	0.33	0.32	0.31	0.28	0.32	0.29	0.34
CaO	1.50	1.80	2.36	3.48	2.66	1.86	1.76	1.80	2.81	2.40	2.49	2.25	2.51	1.81	2.02
Na2O	0.81	0.81	0.84	1.07	1.01	0.85	0.83	0.93	1.10	0.83	0.88	0.82	0.94	0.90	0.97
K2O	0.09	0.09	0.09	0.12	0.11	0.09	0.09	0.10	0.12	0.09	0.09	0.09	0.10	0.10	0.10
P2O5	0.26	0.33	0.21	0.26	0.22	0.19	0.21	0.21	0.27	0.24	0.28	0.28	0.29	0.25	0.19
Sum	**53.4**	**47.3**	**49.7**	**57.0**	**57.0**	**47.8**	**47.5**	**53.3**	**59.5**	**54.2**	**63.7**	**68.7**	**61.8**	**64.2**	**53.2**
Mg#	0.35	0.42	0.45	0.44	0.44	0.44	0.43	0.41	0.41	0.43	0.36	0.28	0.37	0.34	0.46
Mg/Si	0.547	0.500	0.580	0.740	0.760	0.527	0.516	0.615	0.798	0.663	0.863	0.864	0.813	0.840	0.682
Al/Mg	0.080	0.077	0.072	0.087	0.076	0.080	0.080	0.088	0.082	0.078	0.078	0.079	0.077	0.078	0.083
Ca/Al	1.118	1.359	1.717	1.918	1.636	1.283	1.243	1.089	1.632	1.538	1.568	1.615	1.604	1.184	1.172
Fe/Mg	1.885	1.364	1.212	1.278	1.274	1.272	1.302	1.468	1.413	1.349	1.761	2.585	1.676	1.951	1.168

Published data for Allende are from Jarosewich et al. (1987) and Stracke et al. (2012). Allende UCSD 142 was previously reported in Day et al. (2015), with the exception of Ag and Cd composition.

Table 7. (continued)

Sample	Tagish Lake	NWA5958	Banten	Murray	Murchison MTF 2005	Murchison Fragment	Allende UCSD 142	*Allende Literature*	GRA06101	Maralinga	LON91400	Eagle	Atlanta	Khaipur
Method	Teflon (2)	Teflon (2)	Teflon (2)	Teflon (2)	Paar Bomb (1)	Paar Bomb (1)	Paar Bomb (1)		Teflon (2)	Teflon (2)	Teflon (2)	Teflon (2)	Teflon (2)	Teflon (2)
SiO2	47.51	49.65	46.89	50.33	59.17	46.65	47.85	*38.84*	36.04	37.85	41.08	40.76	49.09	39.28
TiO2	0.10	0.09	0.10	0.14	0.10	0.23	0.10	*0.17*	0.19	0.14	0.06	0.06	0.10	0.09
Al2O3	2.14	2.17	2.16	2.57	1.74	2.33	2.57	*3.28*	4.11	2.82	1.79	1.98	2.36	1.37
FeO	26.88	26.95	27.30	24.71	20.79	28.54	26.21	*28.43*	26.82	29.52	31.04	31.50	21.42	36.39
MgO	19.80	18.40	19.88	18.63	15.89	19.11	20.37	*25.54*	25.91	23.54	23.08	23.08	24.45	20.15
MnO	0.23	0.27	0.21	0.27	0.16	0.22	0.16	*0.19*	0.25	0.17	0.14	0.24	0.22	0.16
CaO	2.38	1.91	2.55	2.65	1.60	2.09	2.05	*2.80*	5.62	5.24	1.66	1.20	0.97	1.51
Na2O	0.65	0.28	0.60	0.41	0.33	0.55	0.42	*0.46*	0.72	0.40	0.75	0.83	0.91	0.69
K2O	0.07	0.03	0.06	0.04	0.04	0.06	0.05	*0.05*	0.08	0.04	0.08	0.09	0.10	0.07
P2O5	0.24	0.24	0.24	0.24	0.17	0.23	0.21	*0.24*	0.26	0.28	0.32	0.26	0.38	0.29
Sum	**52.5**	**50.4**	**53.1**	**49.7**	**40.8**	**53.4**	**52.2**	***61.2***	**64.0**	**62.1**	**58.9**	**59.2**	**50.9**	**60.7**
Mg#	0.36	0.35	0.36	0.37	0.37	0.34	0.38	*0.41*	0.43	0.38	0.37	0.36	0.47	0.30
Mg/Si	0.538	0.478	0.547	0.477	0.347	0.528	0.549	*0.848*	0.927	0.802	0.725	0.730	0.642	0.662
Al/Mg	0.095	0.104	0.095	0.121	0.096	0.107	0.111	*0.113*	0.139	0.105	0.068	0.075	0.085	0.060
Ca/Al	1.498	1.191	1.598	1.391	1.243	1.212	1.078	*1.152*	1.847	2.511	1.254	0.821	0.553	1.485
Fe/Mg	1.750	1.888	1.770	1.710	1.686	1.925	1.658	*1.435*	1.334	1.617	1.734	1.759	1.130	2.327

Published data for Allende are from Jarosewich et al. (1987) and Stracke et al. (2012). Allende UCSD 142 was previously reported in Day et al. (2015), with the exception of Ag and Cd composition.

Table 8. Three-oxygen isotope data for Chelyabinsk and other chondrites

	$\delta^{17}O$	±2σ	$\delta^{18}O$	±2σ	$\Delta^{17}O$
Ordinary Chondrites					
Chelyabinsk	3.57	*0.03*	4.43	*0.01*	1.254
	3.65	*0.04*	4.59	*0.03*	1.253
	3.72	*0.06*	4.57	*0.02*	1.331
	3.65	*0.03*	4.63	*0.02*	1.222
AVG:	**3.65**		**4.55**		**1.265**
	0.06		**0.09**		**0.046**
Kunashak	3.29	*0.02*	4.01	*0.02*	1.190
	3.26	*0.01*	4.02	*0.02*	1.154
	3.45	*0.12*	4.15	*0.02*	1.284
	3.29	*0.06*	4.12	*0.03*	1.132
AVG:	**3.32**		**4.07**		**1.190**
	0.09		**0.07**		**0.067**
Kunashak	2.52	*0.03*	3.75	*0.01*	0.559
	2.52	*0.03*	3.79	*0.01*	0.538
AVG:	**2.52**		**3.77**		**0.549**
	0.00		**0.03**		**0.015**
Richardton	3.11	*0.04*	4.04	*0.01*	0.997
	2.87	*0.03*	3.66	*0.02*	0.957
	2.76	*0.03*	3.73	*0.02*	0.811
AVG:	**2.92**		**3.81**		**0.922**
	0.18		**0.21**		**0.098**
Peace River	3.78	*0.17*	4.32	*0.02*	1.524
	3.50	*0.02*	4.29	*0.01*	1.253
	3.60	*0.07*	4.15	*0.04*	1.434
	3.42	*0.07*	4.15	*0.02*	1.241
AVG:	**3.58**		**4.23**		**1.363**
	0.16		**0.09**		**0.139**
Larkman Chondrite	3.20	*0.07*	3.75	*0.04*	1.235
	3.12	*0.03*	3.76	*0.03*	1.149
	3.29	*0.04*	3.93	*0.02*	1.238
AVG:	**3.20**		**3.81**		**1.207**
	0.09		**0.10**		**0.051**
NWA 869	3.80	*0.05*	4.56	*0.01*	1.415
Carbonaceous Chondrites					
Allende	-5.49	*0.02*	-1.95	*0.02*	-4.465
	-5.78	*0.02*	-3.04	*0.04*	-4.180
	-5.85	*0.05*	-2.98	*0.03*	-4.287
AVG:	**-5.70**		**-2.66**		**-4.311**
	0.19		**0.61**		**0.144**
Murchison	-3.47	*0.05*	1.42	*0.20*	-4.211
	-3.57	*0.07*	1.40	*0.05*	-4.309
AVG:	**-3.52**		**1.41**		**-4.260**
	0.07		**0.01**		**0.069**

Table 9. Rhenium-osmium isotope and highly-siderophile element abundances for Chelyabinsk and other chondrite meteorites

Sample		Mass (g)	Os	Ir	Ru	Pt	Pd	Re	$^{187}Re/^{188}Os$	±2σ	$^{187}Os/^{188}Os$	±2σ	$^{187}Os/^{188}Os_i$	±2σ	DOs[1]
Ordinary															
Chelyabinsk	LL5	0.0328	655.4	614.5	961.9	1344.6	1237.5	65.9	0.485	0.033	0.13269	0.00013	0.0944	0.0038	-8
		0.0322	351.7	343.2	463.7	633.5	398.0	28.0	0.383	0.018	0.12457	0.00017	0.0943	0.0021	-9
		0.049	503.7	441.3	715.4	816.7	504.0	39.5	0.378	0.025	0.12526	0.00008	0.0954	0.0029	2
Chelyabinsk (with FC)	LL5	0.094	445.9	445.9	727.4	907.9	588.4	38.7	0.418	0.022	0.12835	0.00007	0.0953	0.0026	2
Saratov	L4	0.027	647.6	632.3	954.4	1507.2	786.8	66.1	0.493	0.032	0.13312	0.00012	0.0942	0.0037	-10
NWA869	L3-6	0.028	551.8	548.1	748.4	990.4	610.6	101.8	0.889	0.028	0.12672	0.00011	0.0564	0.0034	-386
Khohar	L3-6	0.007	743.0	751.8	1097.9	1479.5	874.1	66.6	0.432	0.037	0.12844	0.00013	0.0943	0.0042	-9
Aïr	L6	0.030	730.7	676.4	1049.0	1467.5	849.0	70.9	0.468	0.037	0.12997	0.00007	0.0930	0.0042	-22
Kunashak	L6	0.100	440.6	414.7	693.3	925.8	447.1	37.0	0.404	0.022	0.12567	0.00007	0.0937	0.0026	-15
Kunashak	L6	0.100	499.6	499.0	856.0	1160.1	546.6	40.3	0.388	0.025	0.12572	0.00006	0.0950	0.0029	-1
Peace River	L6	0.097	570.4	507.6	926.9	1220.8	494.2	49.5	0.418	0.029	0.12836	0.00009	0.0953	0.0033	2
Kyle	L6	0.095	451.2	438.9	620.6	835.4	531.2	43.0	0.459	0.023	0.12749	0.00009	0.0912	0.0026	-40
Fayetteville	H4	0.094	763.4	726.3	1062.8	1459.2	809.2	66.0	0.417	0.038	0.12880	0.00003	0.0958	0.0043	7
Pultusk	H5	0.029	1069.5	1045.0	1482.8	2081.6	1188.2	100.8	0.455	0.053	0.13177	0.00013	0.0958	0.0060	7
Forest City	H5	0.030	842.7	1023.2	808.3	1489.5	770.8	74.1	0.424	0.042	0.12765	0.00013	0.0942	0.0048	-10
Richardton	H5	0.055	1114.0	1009.5	1769.9	2180.2	958.7	105.1	0.455	0.056	0.12829	0.00009	0.0923	0.0063	-28

[1]DOs (after Fischer-Gödde et al. 2010) refers to the combined deviation in the determined $^{187}Os/^{188}Os$ and $^{187}Re/^{188}Os$ for a given chondrite sample from the IIIA iron meteorite reference isochron, DOs = 104 ($^{187}Os/^{188}O_{chondrite}$ (0.09524 + 0.07887 × $^{187}Re/^{188}O_{chondrite}$)), $^{187}Os/^{188}O_{chondrite}$ and $^{187}Re/^{188}O_{chondrite}$ are the values determined for chondrites, 0.09524 is the initial $^{187}Os/^{188}Os$ and 0.07887 is the slope of the IIIA iron meteorite isochron (Smoliar et al., 1996).

2a = [ID CT/HPA] Fischer-Gödde et al. (2010); b = [ID CT] Becker et al. (2006); c = [ID CT] Brandon et al. (2005); d = [ID CT] Walker et al. (2002) and Horan et al. (2003); e = [Spark source mass spectrometry] Jochum et al. (1996); f = [NiS] Tagle & Berlin (2008); g = [RNAA] Takahashi et al., 1978; h = [Recommended Values] Jarosewich et al. (1987); i = [Average NAA] Swindle et al. (1998).

Table 9. (continued)

Sample		Mass (g)	Os	Ir	Ru	Pt	Pd	Re	$^{187}Re/^{188}Os$	±2σ	$^{187}Os/^{188}Os$	±2σ	$^{187}Os/^{188}Os_i$	±2σ	DOs[1]
Carbonaceous															
Ivuna	CI	0.002	434.0	453.1	625.0	774.4	568.8	40.5	0.450	0.022	0.12632	0.00012	0.0907	0.0025	-44
Orgueil	CI	0.007	472.6	500.9	689.2	940.2	637.5	40.3	0.411	0.024	0.12654	0.00011	0.0940	0.0027	-11
Tagish Lake	C2-ug	0.030	548.9	572.4	845.3	1083.0	624.5	41.7	0.366	0.027	0.12630	0.00012	0.0974	0.0031	22
		0.029	533.6	571.5	774.5	1006.5	622.3	43.0	0.388	0.027	0.12669	0.00009	0.0960	0.0031	8
		0.131	566.1	578.2	837.1	1106.7	592.6	46.9	0.400	0.028	0.12803	0.00017	0.0964	0.0032	13
NWA 5958	C2	0.025	482.7	575.8	703.8	510.2	540.1	18.8	0.188	0.024	0.12985	0.00014	0.1150	0.0027	198
Gujba	CBa	0.024	3337.0	3059.5	5040.3	6647.7	3363.1	295.0	0.426	0.167	0.12566	0.00014	0.0920	0.0187	-32
Banten	CM2	0.092	616.8	615.0	845.5	1062.5	654.2	55.2	0.432	0.031	0.12697	0.00007	0.0928	0.0035	-23
Cold Bokkeveld	CM2	0.009	556.0	572.0	829.7	1117.1	685.2	45.8	0.397	0.028	0.12549	0.00029	0.0941	0.0032	-10
Murray	CM2	0.120	525.6	553.3	773.7	1023.6	615.9	42.9	0.393	0.026	0.12691	0.00036	0.0958	0.0030	7
Murchison MTF	CM2	0.101	557.9	570.9	990.1	1265.8	600.1	48.1	0.416	0.028	0.12649	0.00007	0.0936	0.0032	-15
Murchison SIGL	CM2	0.119	572.4	525.2	847.1	1134.9	537.8	85.8	0.722	0.029	0.12484	0.00006	0.0677	0.0034	-274
Allende	CV3	0.101	737.6	717.7	1030.9	1502.7	637.7	64.3	0.420	0.037	0.12586	0.00007	0.0926	0.0042	-25
		0.101	666.4	657.4	994.9	1384.7	627.2	55.4	0.400	0.033	0.12588	0.00007	0.0942	0.0038	-9
		0.100	711.3	723.6	1032.8	1378.0	758.4	63.5	0.430	0.036	0.12643	0.00014	0.0924	0.0040	-27
		0.100	871.0	698.0	1016.8	1344.1	738.7	75.7	0.419	0.044	0.12540	0.00017	0.0923	0.0049	-29
		0.101	701.4	663.2	1025.8	1354.0	739.3	60.3	0.414	0.035	0.12631	0.00033	0.0935	0.0040	-16
		0.034	764.3	762.7	1090.6	1446.6	593.3	64.3	0.406	0.038	0.12659	0.00009	0.0945	0.0043	-7
Graves Nunataks 06101	CV3	0.018	847.8	937.6	1321.5	1680.9	805.6	74.6	0.424	0.042	0.12795	0.00009	0.0944	0.0048	-8
NWA 4502	CV3	0.030	880.9	941.8	1214.9	1487.1	888.7	47.5	0.260	0.044	0.12565	0.00016	0.1051	0.0049	99
Maralinga	CK4-a	0.031	692.1	710.4	920.4	1576.0	98.7	21.8	0.152	0.035	0.11351	0.00007	0.1015	0.0039	63

[1]DOs (after Fischer-Gödde et al. 2010) refers to the combined deviation in the determined $^{187}Os/^{188}Os$ and $^{187}Re/^{188}Os$ for a given chondrite sample from the IIIA iron meteorite reference isochron, DOs = 104 ($^{187}Os/^{188}Os_{chondrite}$ (0.09524 + 0.07887 × $^{187}Re/^{188}Os_{chondrite}$)), $^{187}Os/^{188}Os_{chondrite}$ and $^{187}Re/^{188}Os_{chondrite}$ are the values determined for chondrites, 0.09524 is the initial $^{187}Os/^{188}Os$ and 0.07887 is the slope of the IIIA iron meteorite isochron (Smoliar et al., 1996).

2a = [ID CT/HPA] Fischer-Gödde et al. (2010); b = [ID CT] Becker et al. (2006); c = [ID CT] Brandon et al. (2005); d = [ID CT] Walker et al. (2002) and Horan et al. (2003); e = [Spark source mass spectrometry] Jochum et al. (1996); f = [NiS] Tagle & Berlin (2008); g = [RNAA] Takahashi et al., 1978; h = [Recommended Values] Jarosewich et al. (1987); i = [Average NAA] Swindle et al. (1998).

Table 9. (continued)

Sample		Mass (g)	Os	Ir	Ru	Pt	Pd	Re	$^{187}Re/^{188}Os$	±2σ	$^{187}Os/^{188}Os$	±2σ	$^{187}Os/^{188}Os_i$	±2σ	DOs[1]
Enstatite															
Eagle	EL6	0.030	940.3	904.0	1131.3	1551.2	1228.5	75.9	0.389	0.047	0.12522	0.00010	0.0945	0.0053	-7
Atlanta	EL6	0.030	663.9	653.9	930.4	1253.9	708.3	64.6	0.469	0.033	0.12767	0.00010	0.0906	0.0038	-46
LON91400	EL6	0.030	788.1	765.7	1060.4	1481.7	921.2	70.9	0.434	0.039	0.12782	0.00011	0.0935	0.0045	-16
Khairpur	EL6	0.010	1257.2	1177.8	1659.9	2322.6	1388.5	110.7	0.424	0.063	0.12808	0.00012	0.0945	0.0071	-6
Literature data[2]															
Allende[a]			729	684	1007	1357	674	60.5	0.393		0.12595				-3
Allende[b]			763	700	1140	1379	786	61.2	0.386		0.12638				7
Allende[c]			785	720	1118	1421	682	63.5	0.390		0.12596				0
Allende[d]			758	712	1016	1348	674	60.9	0.387		0.12615				4
Allende[e]			746	730	843	1290		60.2							
Allende[f]				694	1058	1395	598								
Allende[g]			833	776			705	68.4							
Allende[h]				740											
Murchison[d]			580	558	741	1043	629	46.0	0.393		0.12526				-10
Murchison[a]			572	569	843	1127	151	46.7	0.382		0.12609				7

[1]DOs (after Fischer-Gödde et al. 2010) refers to the combined deviation in the determined $^{187}Os/^{188}Os$ and $^{187}Re/^{188}Os$ for a given chondrite sample from the IIIA iron meteorite reference isochron, DOs = 104 ($^{187}Os/^{188}Os_{chondrite}$ (0.09524 + 0.07887 × $^{187}Re/^{188}Os_{chondrite}$)), $^{187}Os/^{188}Os_{chondrite}$ and $^{187}Re/^{188}Os_{chondrite}$ are the values determined for chondrites, 0.09524 is the initial $^{187}Os/^{188}Os$ and 0.07887 is the slope of the IIIA iron meteorite isochron (Smoliar et al., 1996).

2a = [ID CT/HPA] Fischer-Gödde et al. (2010); b = [ID CT] Becker et al. (2006); c = [ID CT] Brandon et al. (2005); d = [ID CT] Walker et al. (2002) and Horan et al. (2003); e = [Spark source mass spectrometry] Jochum et al. (1996); f = [NiS] Tagle & Berlin (2008); g = [RNAA] Takahashi et al., 1978; h = [Recommended Values] Jarosewich et al. (1987); i = [Average NAA] Swindle et al. (1998).